Sheffield Hallam University

A Sheffield Hallam University thesis

REFERENCE

Highlighting Dissimilarity in Medical Images Using Hierarchical Clustering Based Segmentation (HCS)

A.D. Arul Nirai Selvan

A thesis submitted in partial fulfilment of the requirements of
Sheffield Hallam University
for the degree of Master of Philosophy

August 2007

Declaration

This is to certify that I am responsible for the work submitted in the thesis, that the original work is my own except in acknowledgements, and that neither the thesis nor the original work contained therein has been submitted to this or any institution for a higher degree.

Signature   :

Name   :   A.D. Arul Nirai Selvan

Date   :   15 August 2007

Abstract

Highlighting Dissimilarity in Medical Images Using Hierarchical Clustering Based Segmentation (HCS)

Tissue abnormality in a medical image is usually related to a dissimilar part of an otherwise homogeneous image. The dissimilarity may be subtle or strong depending on the medical modality and the type of abnormal tissue. Dissimilarity within an otherwise homogeneous area of an image may not always be due to tissue abnormality. It might be due to image noise or due to variability within the same tissue type. Given this situation it is almost impossible to design and implement a generic segmentation process that will consistently give a single appropriate solution under all conditions. Hence a dissimilarity highlighting process that yields a hierarchy of segmentation results is more useful. This would benefit from high level human interaction to select the appropriate image segmentation for a particular application, because one of the capabilities of the human vision process when visualising images is its ability to visualise them at different levels of details.

The purpose of this thesis is to design and implement a segmentation procedure to resemble the capability of the human vision system's ability to generate multiple solutions of varying resolutions. To this end, the main objectives for this study were :
  (i) to design a segmentation process that would be unsupervised and completely data driven.
  (ii) to design a segmentation process that would automatically and consistently generate a hierarchy of segmentation results.

In order to achieve these objectives a hierarchical clustering based segmentation (HCS) process was designed and implemented. The developed HCS process partitioned the images into their constituent regions at hierarchical levels of allowable dissimilarity between the different spatially adjacent or disjoint regions. At any particular level in the hierarchy the segmentation process clustered together all the pixels and/or regions that had dissimilarity among them which was less than or equal to the dissimilarity allowed for that level. The clustering process was designed in such a way that the merging of the clusters did not depend on the order in which the clusters were evaluated.

The HCS process developed was used to process images of different medical modalities and the results obtained are summarised below :
  (i) It was successfully used to highlight hard to visualise stroke affected areas in T2 weighted MR images confirmed by the diffusion weighted scans of the same areas of the brain.
  (ii) It was used to highlight dissimilarities in the MRI, CT and ultrasound images and the results were validated by the radiologists.

It processed medical image data and consistently produced a hierarchy of segmentation results but did not give a diagnosis. This was left for the experts to make use of the results and incorporate these with their own knowledge to arrive upon a diagnosis. Thus the process acts as an effective computer aided detection (CAD) tool.

The unique features of the designed and implemented HCS process are :
  (i)   The segmentation process is unsupervised, completely data driven and can be applied to any medical modality, with equal success, without any prior information about the image data.
  (ii) The merging routines can evaluate and merge spatially adjacent and disjoint similar regions and consistently give a hierarchy of segmentation results.
  (iii) The designed merging process can yield crisp border delineation between the regions.

Acknowledgements

Publication

1. Selvan, A.N.; Saatchi, R.; Amavasai, B.P.; Travis, J.R. "A Dissimilarity Visualisation System for CT: Pilot Study" The International Conference on Computer as a Tool, EUROCON 2005, Volume: 2, Pages: 1007- 1010.

Table of Contents

List of Figures

List of Tables

List of Equations

List of Abbreviations

ACR	American College of Radiology
CAD	Computer Aided Diagnostic
CBF	Cerebral Blood Flow
CBV	Cerebral Blood Volume
CPU	Central Processing Unit
CSF	Cerebrospinal Fluid
CT	Computed Tomography
DICOM	Digital Imaging and Communications
DWI	Diffusion Weighted Images
FCM	Fuzzy-C-Means
FLC	Fuzzy Logic Classification
GTD	Gray Tone Distribution
GUI	Graphical User Interface
HCS	Hierarchical Clustering based Segmentation
HSEG	Hierarchical Segmentation
HSWO	Hierarchical Stepwise Optimisation
HU	Hounsfield Unit
LBP	Local Binary Pattern
LBP-C	Local Binary Pattern and Contrast
MR	Magnetic Resonance
MRI	Magnetic Resonance Imaging
NASA	National Aeronautics and Space Administration
NEMA	National Electrical Manufacturers Association
NIH	National Institutes of Health
PD	Proton Density
PET	Positron Emission Tomography
PWI	Perfusion Weighted Imaging
RAM	Random Access Memory
RHSEG	Recursive Hierarchical Segmentation
ROI	Region of Interest
rtPA	Recombinant Tissue Plasminogen Activator
SPECT	Single Positron Emission Computer Tomography
T2-WI	T2 Weighted Images
US	Ultrasound

Chapter 1

Introduction and Objectives for this Study

1.1 Introduction

The field of medical imaging has experienced an explosive growth in recent years due to the availability of several imaging modalities, such as X-Ray, Computed Tomography (CT), Magnetic Resonance (MR) imaging, Positron Emission Tomography (PET), Single Positron Emission Computer Tomography (SPECT) and Ultrasound. The digital revolution and the increased processing power in computers in combination with these imaging modalities has improved the understanding of the complex human anatomy and its behaviour to a great extent [Suri *et al.*, 2002].

Image segmentation, defined as the separation of an image into regions, is one of the first steps leading to image analysis and interpretation [Sonka and Fitzpatrick, 2000]. Image segmentation is essentially a process of pixel classification, wherein similar pixels are segmented into a common set [Suri *et al.*, 2002].

The goal of medical image segmentation is to separate the image into regions that are meaningful for a specific task. This task may, for instance, involve the detection of specific section of organs such as the heart, the liver, or the lungs using MR or CT images. Other applications may require the quantification of white and Grey matter volumes in MR brain images, the labelling of deep brain structures such as the thalamus or hippocampus, or quantitative measurements made from ultrasound images [Sonka and Fitzpatrick, 2000].

1.2 Medical Image Segmentation an Illustration

Medical image segmentation is a difficult task because of issues such as spatial resolution, poor contrast, ill-defined boundaries, noise, or acquisition artefacts [Sonka and Fitzpatrick, 2000]. The medical images in the Figures 1.1 and 1.2 illustrate the difficulty faced even by an expert to accurately delineate the boundaries of the different regions.

Figure 1.1 shows a CT image of a section of the brain. The image area within the region of interest (rectangular area outlined in black) is made up of three different types of regions viz. Grey matter, White matter and the stroke affected area. The stroke affected area has been outlined in white by an expert.

Figure 1.2 shows the segmentation result obtained by Hierarchical Segmentation (HSEG) [Tilton, 2003]. HSEG is chosen as an illustration since it is one of the very few studies with an approach that is similar to the one developed in the current study.

Figure 1.2 illustrates the difficulties faced by segmentation processes to segment medical images. Although the image pixels within the region of interest (ROI), have been segmented into three classes colour coded as red (the diseased area), green (white matter) and blue (grey matter) it has misclassified some of the pixels not belonging to the diseased area as being diseased as well. This can be seen by the presence of red coloured pixels at the other end of the ROI *i.e.* outside the area outlined by the expert.
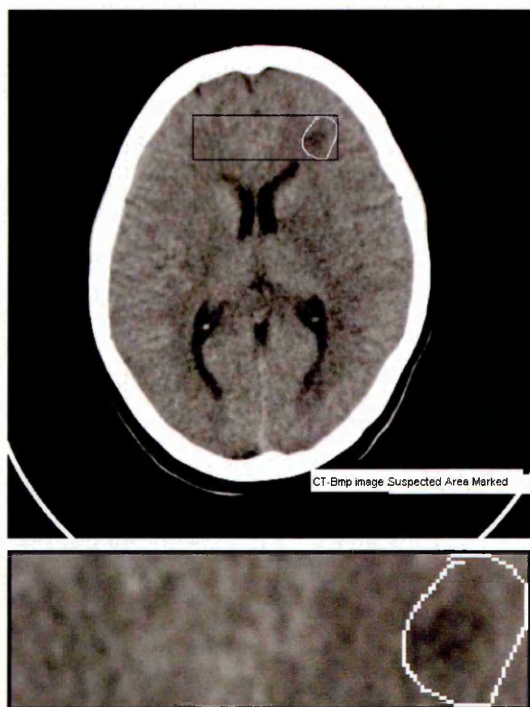
Figure 1.1 - CT image showing the suspected area outlined in white by a neuroradiologist.
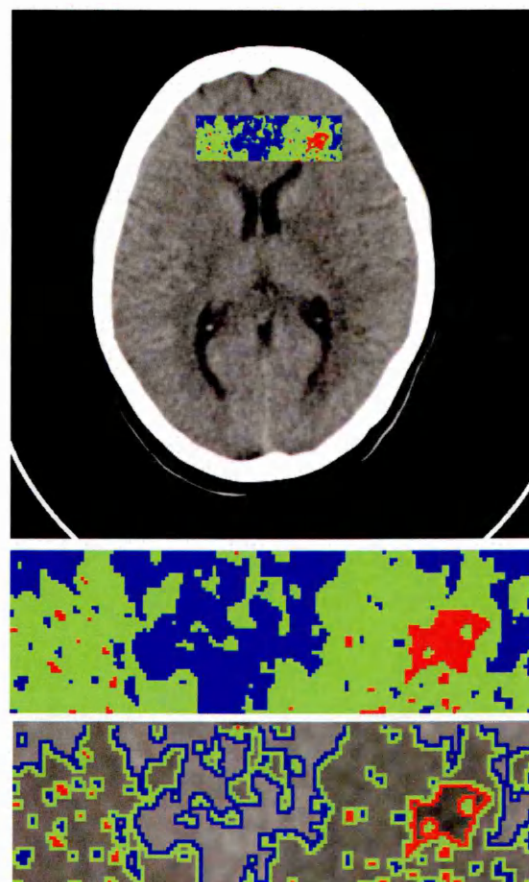
Figure 1.2 - Segmentation of the Grey matter, White matter and Stroke affected regions and their boundaries by HSEG

Figure 1.3 shows the segmentation result based on the new segmentation process viz. Hierarchical Clustering based Segmentation (HCS) process developed in this study. In this case the process has successfully delineated the three different types of regions viz. Grey matter, White matter and the stroke affected area indeed. The HCS process delineation of the stroke affected area is much more precise than that of visual inspection by an expert. This is evident from Figure 1.3, from where it could be seen that the expert's outline of the diseased area (white outline) is only very approximate, which includes substantial part of the healthy part of the image.

Comparing the segmentation results of Figures 1.2 and 1.3 it can be seen that the HSEG process segmentation is suboptimal. In subsequent chapters (See Chapter 6 Section 6.5) it will be explained in detail how the HCS process developed in this study is able to achieve such a smooth segmentation shown in Figure 1.3.
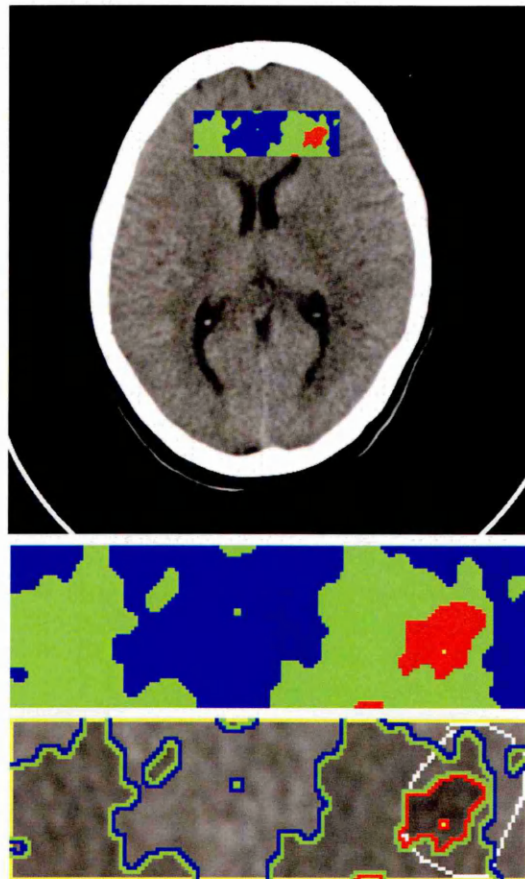
Figure 1.3 - Segmentation of the Grey matter, White matter and Stroke affected regions and their boundaries by HCS.

1.3 Objectives for the Current Study

The problem of segmentation is an important research field and many segmentation methods have been proposed in the literature. Over the years the different segmentation processes developed have been surveyed and evaluated [Haralick and Shapiro, 1985], [Pal and Pal, 1993], [Freixenet *et al.,* 2002]. The common factor amongst all the segmentation processes developed so far is that they each yield a single segmentation result.

Segmentation processes which give a one-off solution force the user into a take-it-or-leave-it situation. It will be much more appropriate if the user is given an option to choose the segmentation result depending upon a quantifiable measure chosen by the user. This allows the user to select the result best suited for a given situation. Since the human vision system has the ability to generate multiple solutions of varying resolutions. For example, given the anatomical image of the cross-section of a skull, at a low resolution a radiologist can classify the image as regions belonging to soft tissues and the skull bone. At a fine resolution different types of soft tissues are also identified. At a finer resolution still, the radiologist will also be able to distinguish the dissimilar regions within the same tissue type.

Again tissue abnormality in medical images is related to the part of the image being dissimilar from an otherwise homogeneous area representing the healthy part of the same tissue type. The dissimilarity may be subtle or strong depending on the medical modality and the type of tissue abnormality. But dissimilarity, within an otherwise homogeneous area of the image may not always be due to tissue abnormality. It might be due to image noise or due to variability within the same tissue type. For example MRI images contain various noise artefacts, such as intra-tissue noise, inter-tissue intensity contrast reduction, partial-volume effects and others [Macovski, 1996]. The intra variability of the intensity feature within a tissue is mainly due to artefacts of the imaging process. Hence a human expert is needed to decide what is significant.

Given the above situation, it is almost impossible to design and implement a generic segmentation process which will always give a single appropriate solution under all conditions. There have been very few earlier segmentation methods which are designed to yield a hierarchy of segmentation results [Beaulieu and Goldberg, 1989] [Tilton, 2003].

4

The purpose of this study is to design and implement a segmentation procedure to mimic the capability of the human vision system ability to generate multiple solutions of varying resolutions. To this end, the original contributions and the main objectives of this thesis are as follows :

- To design a segmentation process which will be unsupervised and be completely data driven.

  This objective ensures that the segmentation process can be applied to any medical image modality without any prior information or training with equal success.

- To design a segmentation process which will automatically generate a hierarchy of segmentation results.

  Satisfying this objective will ensure that at any particular level in the hierarchy, the designed segmentation process will automatically cluster together all the pixels and/or regions that have dissimilarity among them less are equal to the dissimilarity allowed for that level. And the end result will be a hierarchy of segmentation results

- The merging (*i.e.* Iterative clustering) of the most similar regions should not depend on the order in which the regions are evaluated for merging.

  This objective will ensure that the segmentation process will consistently yield the same set of regions for any particular level in the hierarchy.

- To implement a merging process that will be independent of the type of similarity measure used to compare the different regions in the image.

  This objective will ensure that the segmentation procedure is modular and can be used to segment any type of images whether textural or tonal just by using the most appropriate similarity measure.

- To design and implement a graphical user interface (GUI) based on good human computer interface principles, to display the hierarchy of segmentation results. The GUI will display the segmentation results based on the merge tree generated by the HCS process.

  The GUI, will aid the user to inspect how the merging process evolves and associate the unique regions at any level with the different types of patterns present in the image.

In addition to the above listed, main objectives, the following two objectives should also be achieved. The following objectives are crucial if the HCS process is to be used for the segmentation and analysis of medical images.

- To design a merging process that can evaluate and merge spatially disjoint similar regions.

  This objective is important for medical images because in medical images regions having similar properties can be spatially disjoint.

- To design a merging process which will yield crisp border delineation between the regions.

  This objective is crucial for segmenting medical images since the separate regions in medical images can be very small, hardly couple of pixels wide.

The most crucial objectives are the first two, of the main objectives, viz. Unsupervised segmentation and Hierarchical clustering based segmentation yielding a hierarchy of segmentation results. The last two, additional objectives, are critical if the application domain is a medical image segmentation.

1.4 Thesis Outline

The different chapters and their purpose are as follows :

- Chapter 2 discusses previous related studies and discusses some of the earlier studies which have satisfied at the least one of the two crucial objective.
- Chapter 3 discusses the theoretical background of the study and discusses the theoretical details of different types of segmentation and the Hierarchical Clustering based Segmentation (HCS) method developed in this study.
- Chapter 4 discusses the methodology adopted by this study and gives the design details of the HCS method developed in this study.
- Chapter 5 discusses the implementation details of the HCS.
- Chapter 6 discusses the performance of the HCS process.
- Chapter 7 discusses the application of the HCS process. In this chapter the performance of the HCS process in segmenting medical images is discussed in detail.
- Chapter 8 discusses how the HCS process could be improved upon and where it could be further applied.

Chapter 2

Previous Studies

2.1 Introduction

The main objectives for the current study is to design a segmentation process to achieve the following four crucial objectives :

- unsupervised segmentation.
- hierarchical clustering based segmentation yielding a hierarchy of segmentation results.
- merging process which can evaluate and merge spatially disjoint similar regions.
- merging process which will yield a crisp border delineation between the regions.

In this chapter some of the previous related image segmentation studies will be described. The discussion in this chapter will highlight the need and necessity to design a segmentation process to achieve all the objectives listed in chapter 1 (See Section 1.3).

2.2 Related Studies

There is no reported single previous study which satisfies all of the main objectives listed in section 1.3, but a number of them have incorporated some of the objectives. In this section five such studies will be highlighted.

2.2.1 Unsupervised Texture Segmentation Using Local and Global Spatial Statistics

Kervrann and Heitz [1995] designed an unsupervised segmentation method for textured images that had the following prominent features :

- it was unsupervised.
- it performed region segmentation.
- it used feature distribution to compare the similarity between different regions.
- it iterated by splitting mixed regions into smaller regions and merging smaller regions that had similar properties into one homogeneous region.

The relevant areas which this study did not satisfy are :

- The method started with one region encompassing the whole image and as it iterated it subdivided the region into smaller regions.

7

- Until the whole iterative process of splitting and merging was complete the resulting segmentation could not be taken as an intermediate result.
- Thus the method gave a one-off solution of segmentation that was suitable for applications where one needs to segment *blotches* having similar properties.

2.2.2 Multi-scale Image Segmentation

Tabb and Ahuja [1997] designed an unsupervised method to segment tonal images at different scales.

The salient features of the method were :
- The method was unsupervised.
- Instead of representing the whole image at different scales, the method identified homogeneous structures within the image at different scales.
- The method incorporated both region properties (using grey level similarity) and edge information to detect homogeneous regions at different scales.

The major areas in which this study did not satisfy were :
- The study detected boundaries rather than regions. Hence it was not suitable in applications where one needs to segment regions of similarity rather than boundaries of homogeneous regions.
- The scaling measures adopted were spatial as well as the homogeneity of the regions. Spatial scaling is not suitable in applications where similar homogeneous regions might occur across the image with differing shapes and sizes.

  Since the study detected boundaries rather than marking regions of similarity, the spatial scaling was not an issue for it. Because regions of smaller size were merged with bigger regions enclosing the smaller regions and the boundary of the bigger region was demarcated.

2.2.3 Texture Segmentation Returning Multiple Solutions

Nickels and Hutchinson [1997] used an approach which gave a range of possible partitions of the image with an associated probability distribution with each partitioning. Almost all the current approaches discussed in the literature arrive at a single partition of an image at the end of a segmentation process. This study for the first

time departed from the traditional approaches; but since their approach was a supervised technique it did not satisfy the main objective.

2.2.4 Unsupervised Texture Segmentation Using Feature Segmentation

Ojala and Pietikäinen [1999] designed an unsupervised texture segmentation method which used distributions of texture features to measure similarity of regions in the image.

The major steps involved in their method were :

- The input image was divided into square blocks of equal size (say 64×64).
- Each square block was further subdivided into smaller square blocks if the larger square block was found to be not homogeneous. The procedure was repeated recursively on each sub-block until a predetermined minimum block size (16x16) was reached. This step was referred by the authors as hierarchical splitting.
- Once the image had been roughly splat into blocks of roughly uniform texture, adjacent regions of similar homogeneity were merged until a stopping criteria was satisfied.
- To further improve the localisation of the boundaries, the pixels found on the boundary of different regions were further reclassified by comparing the similarity of a small circular region (of radius 10) around the pixel with that of the regions bordering the pixel.

The major areas in which this study did not satisfy were :

- This study measured the similarity of adjacent image regions hence it could not be used in a situation where similar regions were found across the image and not bordering one another.
- By the very nature of the approach by which segmentation was done, the smallest region delineated in the image could never be smaller than 16×16 square block.
- The results published in their paper could not be entirely reproduced. This could be explained as follows :

  The first step in their procedure was to splat the original image into homogeneous square blocks. In one of their reported sample images, it so happened that the border of the square blocks correlated with the actual border

9

between the various texture patches. If the initial square blocks, into which the original image was splat, straddled the different texture patches border, there would be many misclassification.

2.2.5 NASA's Hierarchical Segmentation Algorithm and its Recursive Formulation

NASA's hierarchical segmentation algorithm (referred to as HSEG) and its recursive formulation (referred to as RHSEG) [Tilton, 2003] is the closest to our study.
Its salient features are :

- a hierarchical set of segmentation results.
- a GUI to display the segmentation results.

The method however has a major limitation. In order to avoid the combinatorial problem of having to compare all possible combinations of the regions, which are currently in the image, the method, firstly compares and merge spatially adjacent regions. And then only subsequently non-spatially adjacent regions are compared and merged if found similar [Tilton, 2003].

2.3 Summary

In this chapter studies which are closely related to this study were discussed. Of all the studies discussed, NASA's hierarchical segmentation algorithm is the only one that satisfies the major objectives of this study. However the current work provides a better performance and this will be identified by exhaustive comparison with the NASA HSEG technique.

Chapter 3

Theoretical Background

3.1 Introduction

Image segmentation is the process of partitioning an image into regions where the elements that comprise the regions are more similar to each other when compared to those of other regions. Segmentation is based on producing a higher *intra-region* similarity than *inter-region* similarity. The segmentation process associates a region with a unique label to differentiate it from the other regions. Depending upon the level of homogeneity within the constituent regions, the level of segmentation might be termed as fine or coarse. If the constituent regions are made up of highly homogeneous elements, with minimal variation of properties, then the image is finely segmented. i.e. the segmentation is very fine. If there are large variations in the *intra-region* homogeneity then the segmentation is coarse. Depending upon the application domain and the type of image data the user might prefer fine or coarse segmentation. Segmentation of digital images is the first step towards evolving a higher level image processing such as object recognition and classification.

3.2 Segmentation Process

Segmentation methods can be divided into three groups according to the dominant processes used. The three most common are global knowledge (*e.g.* using histogram of image features like gray-level), edge information and region information [Sonka, 1993]. Most image segmentation approaches therefore can be placed in one of three categories namely, characteristic feature thresholding or clustering, boundary detection and region growing [Fu, 1981].

Gray level thresholding is the simplest segmentation process. In many applications of image processing, the gray levels of pixels belonging to the object are substantially different from the gray levels of the pixels belonging to the background. Thresholding then becomes a simple but effective tool to separate objects from the background. Thresholding is computationally inexpensive and fast and can easily be done in real time using specialized hardware. Sankur and Sezgin (2004) have categorized the thresholding methods in six groups according to the information they are exploiting.

11

Characteristic feature thresholding or clustering does not exploit spatial information, and thus ignores information that could be used to enhance the segmentation results [Tilton, 2003].

Edge-based segmentation represents a large group of methods based on information about edges in the image. Edge-based segmentations rely on edges found in an image by edge detecting operators, these edges mark image locations of discontinuities in gray level, colour, texture, *etc.* [Sonka, 1993]. While boundary detection does exploit spatial information by examining local edges found throughout the image data, however it does not necessarily produce closed connected region boundaries. For simple noise-free data, detection of edges usually results in straightforward region boundary delineation. However, edge detection on noisy, complex image data often produces missing edges and extra edges that result in detected boundaries not always forming a set of close connected curves that surround connected regions [Tilton, 2003].

While edge-based segmentation locates the borders between regions, region-based segmentation directly constructs regions. Homogeneity of regions is used as the main segmentation criterion in region growing. The criteria for homogeneity could be gray level, colour, texture, shape, model *etc.* Region growing techniques are generally better in noisy images where edges are extremely difficult to detect [Sonka, 1993]. Although regions can be constructed from the borders and borders can be estimated from regions, segmentations resulting from edge-based methods and region growing methods are not usually exactly the same [Sonka, 1993]. With the aim of improving the segmentation process, a large number of new algorithms, which integrate region and boundary information, have been proposed over the last few years [Freixenet, 2002]. Region growing approaches are preferred because they exploit spatial information and guarantees the formation of closed, connected regions [Tilton, 2003]. The type of spatial information exploited for region merging is detailed in the methodology chapter (See Section 4.3.4.1 Factors considered for region merging).

3.3 Region Based Segmentation

Tilton [2003] [NASA Case No. GSC 14,328] outlines the various approaches which can be used for region based segmentation as follows :

    (i) A classic definition of image segmentation

    (ii) Hierarchical Stepwise Optimization (HSWO)

    (iii)Hierarchical image segmentation (HSEG)

    (iv)An ideal definition of image segmentation

3.3.1 Classic Definition Of Image Segmentation

As discussed by Tilton [2003], the most commonly used approach to image segmentation by region growing is based on a general definition of image segmentation using four conditions that can be summarized [Zucker, 1976] as follows: (i) Every picture element (pixel) must be in a region, (ii) each region must be connected, (*i.e.* composed of contiguous image pixels), (iii) all image pixels in a region must satisfy a specified property to be considered similar enough to be in the same region (*e.g.*, a vector norm between each pixel and the region mean must be less than a specified threshold), and (iv) in the final segmentation result, further merging of any adjacent regions cannot be done without violating the third condition.

The classic definition of image segmentation can be expressed using symbolic notation as follows [Horowitz *et al.*, 1974] :

Let **X** be a two-dimensional array representing an image. A segmentation of **X** can be defined as a partition of **X** into disjoint subsets X_1, X_2, ..., X_N, such that

    (i) $\displaystyle\bigcup_{i=1}^{N} X_i = X$

    (ii) X_i , $i = 1, 2, ..., N$ is connected.

    (iii) $P(X_i) = TRUE$ for i = 1, 2, ..., N and

    (iv) $P(X_i \cup X_j) = FALSE$ for $i \neq j$, where X_i and X_j are adjacent.

$P(X_i)$ is a logical predicate which assigns the value TRUE or FALSE to X_i, depending on the image data values in X_i. The logical predicate could be for example the condition that the vector norm between each pixel and the region mean must be less than a specified threshold. The logical predicate used for this study is detailed in the methodology chapter (See Section 4.3.4.1 Factors considered for region merging).

The first condition requires that every picture element (pixel) to be in a unique region. The second condition requires that each region to be connected, *i.e.* composed of contiguous image pixels. The third condition determines what kind of properties each region must satisfy, *i.e.* what properties the image pixels must satisfy to be considered similar enough to be in the same region. The fourth condition specifies that, in the final segmentation result, any merging of any adjacent regions would violate the third condition [Tilton, 2003].

A problem with this classic definition of image segmentation is that the segmentation so defined is not unique. The number, (N), and shape of the partitions, (X_1, X_2, ..., X_N,) depend on the order in which the image pixels are processed and in addition, it does not contain any concept of optimality. Thus all partitions that satisfy the conditions represent equally good or valid segmentations of the image [Tilton, 2003].

3.3.2 Hierarchical Stepwise Optimization (HSWO)

A less commonly used approach is the Hierarchical Stepwise Optimization (HSWO) algorithm of Beaulieu and Goldberg [1989]. HSWO is best described iteratively: Start with an image and a segmentation of that image into N regions in which (i) every picture element (pixel) is in a unique region, (ii) and each region is connected, (*i.e.* composed of contiguous image pixels). Then compare all spatially adjacent regions with each other (*e.g.*, compute a vector norm between the region means of the spatially adjacent regions). Merge the most similar pair of spatially adjacent regions. Continue to compare spatially adjacent regions and merge the most similar pair of spatially adjacent regions until either a specified number of regions are reached or the dissimilarity between the most similar pair of spatially adjacent regions reaches a given threshold. The initial partition may assign each image pixel to a separate region. Alternatively an over-segmented result from region growing based on the classic definition given above (*i.e.*, classic region growing segmentation with a low threshold value) could be used [Tilton, 2003].

14

3.3.3 Hierarchical Image Segmentation (HSEG)

HSEG normally begins by assuming every pixel in the hyperspectral data cube is a separate region. Then, a dissimilarity criteria is computed between spectra in neighbouring regions, the minimum dissimilarity criterion is found over all pairs of neighbouring region, and all pairs of neighbouring regions with this minimum dissimilarity criterion value are merged. Optionally, this spatial clustering step is followed by a spectral clustering step in which a dissimilarity criterion is computed between spectra of all spatially non-adjacent regions and all pairs of such regions with dissimilarity less than or equal to the minimum dissimilarity value found in the spatial clustering step are merged [Tilton, 2003]. A high-level description of the HSEG algorithm is shown in Figure 3.1.

Tilton's [2003] hierarchical image segmentation (HSEG) algorithm is identical to that employed by Beaulieu and Goldberg's [1989] HSWO algorithm except that HSEG optionally alternates spectral clustering iterations with region growing iterations. In the spectral clustering iterations, non-adjacent regions are merged [Tilton, 2003]. The spectral clustering step is either skipped or not, based on the value of the flag *spclust_wght* (spectral clustering weight). The segmentation iteration is continued until the number of regions in the image are more than the pre-set value *chk_nregions* (*i.e. chk_nregions* is the threshold number of regions).

'HSEG is a high quality but computationally intensive image segmentation approach. HSEG cannot be performed in a reasonable amount of time (less than a day) on moderately sized data sets, even with the most powerful (single processor) computer currently available. For example, for a 6-spectral band Landsat TM image, a 128×128 pixel section takes about 25 minutes to process on a 1.2 Ghz single processor computer. A 256×256 pixel section of the same image takes over 7.5 hours to process on the same computer. By extrapolation, a 512×512 pixel section of the same image would easily take several days.' [Tiltton, 1999].

(i) Give each data point a regional label and set the global criterion value, *critval*, equal to zero. If a pre-segmentation is provided, label each data point according to the pre-segmentation. Otherwise, label each data point as a separate region.

(ii) Calculate the dissimilarity criterion value, *dissim_val* (dissimilarity value), between each spatially adjacent region.

(iii) Find the smallest *dissim_val* and set *thresh_val* (threshold value) equal to it. Then merge all pairs of spatially adjacent regions with *dissim_val* *thresh_val*.

(iv) If *spclust_wght* = 0.0, go to step 6. Otherwise, calculate the *dissim_val* between all pairs of non-spatially adjacent regions.

(v) Merge all pairs of non-spatially adjacent regions with *dissim_val* *spclust_wght* × *thresh_val*.

(vi) If the number of regions remaining is less than the pre-set value *chk_nregions*, go to step 7. Otherwise, go to step 2.

(vii) Store the current global criterion value as previous critical value. *i.e.* let *prevcritval* = *critval*. Calculate the current global criterion value and set *critval* equal to this value. If *prevcritval* = *zero*, go to step 2. Otherwise calculate *cvratio* = *critval/prevcritval*. If *cvratio* is greater than the pre-set threshold *convfact*, save the region label map from the previous iteration as a "raw" segmentation result. Also, store the region number of pixels list, region mean vector list and region criterion value list for this previous iteration. (Note: The region criterion value is the portion of the global criterion value contributed by the data points covered by the region.) If the number of regions remaining is two or less, save the region information from the current iteration as the coarsest instance of the final hierarchical segmentation result and stop. Otherwise, go to step 2.

Figure 3.1 - A high-level description of the HSEG algorithm [Tilton, 2003].

3.3.4 Ideal Definition Of Image Segmentation

An ideal definition of image segmentation would be as follows [Tilton NASA Case No. GSC 14,328]:

Let X be a two-dimensional array representing an image. A segmentation of X into N regions can be defined as a partition of X into disjoint subsets X_1, X_2, ..., X_N, such that

(i) $$\bigcup_{i=1}^{N} X_i = X$$

(ii) X_i , $i = 1, 2, ..., N$ is connected.

(iii) $$\sum_{i=1}^{N} G(X_i) = MINIMUM$$ over all partitions into N regions and

(iv) $G(X_i \cup X_j) > G(X_i) + G(X_j)$ for $i \neq j$, where X_i and X_j are adjacent.

$G(X_i)$ is a function that assigns a cost to partition X_i, depending on the image data values in X_i. The cost function could be, for example, the condition that the vector norm between each pixel and the region mean must be less than a specified threshold. The cost function used for this study is detailed in the methodology chapter (See Section 4.3.4.1 Factors considered for region merging).

The above conditions can be summarised as follows: The first condition requires that every picture element (pixel) must be in one of N regions. The second condition requires that each region must be connected, *i.e.* composed of contiguous image pixels. The third condition states that the partition must produce a minimum cost (dissimilarity say) aggregated over all N regions. The fourth condition specifies that, in the final segmentation result, any merging of adjacent regions increases the minimum cost obtained in the third condition [Tilton NASA Case No. GSC 14,328].

Using the above method, the order dependence problem of the classic definition of image segmentation is eliminated because it ensures that a global minimum solution is found and this solution is the optimal solution.

In practice, this ideal image segmentation is difficult, if not impossible, to achieve. This is because the third condition implies that all possible image partitions consisting of N

regions must be searched to find the minimum cost. Further, the question of the proper value for N is left undetermined [Tilton NASA Case No. GSC 14,328].

3.4 Hierarchical Clustering Based Segmentation (HCS)

The segmentation algorithm developed in this thesis is region based. The algorithm is named as Hierarchical Clustering based Segmentation (HCS). HCS combines the best features of the HSEG process and the ideal segmentation process described above.

Following is a high-level description of the HCS process implemented in this study (See Figure 4.4 for a flow chart representation) :

(i) Give each pixel in the image a region label as follows.

If an initial segmentation of the image is available label each pixel according to this pre-segmentation. The initial segmentation can be obtained by prior class information (for *e.g.* based on Hounsfield value in the case of CT images). The initial segmentation can also be obtained by clustering the most similar neighbouring pixels (Refer Section 4.3.3.2)

If no initial segmentation is available label each pixel as a separate region.

Set the current dissimilarity allowed between regions equal to zero.

(ii) Calculate the dissimilarity value between all pairs of regions in the image.

Set threshold value equal to the smallest dissimilarity value.

(iii) If the threshold value found, in step 2, is less or equal to the current allowable dissimilarity value, then merge all regions having dissimilarity value, between them, less or equal to the threshold value.

Otherwise go to step 6.

(iv) If the number of regions merged in step 3 is greater than 0, then reclassify the pixels on the border of the merged regions with the rest of the regions until no more reclassification is possible. After all the possible border pixels are reclassified, among the merged regions, store the region information for this iteration as an intermediate segmentation and go to step 2.

Otherwise, if the number of regions merged in step 3 is equal to 0 then, go to step 5.

(v) If the current number of regions in the image is less than a pre-set value, say 1, then go to step 7. Otherwise, go to step 6.

(vi) If the current value of allowable dissimilarity, between regions, is less than the

maximum possible value then increase it by an incremental value and go to step 2.

Otherwise go to step 7.

(vii) Save the region information from the current iteration as the coarsest instance of the final hierarchical segmentation result and stop.

The above steps ensures that the segmentation of the image into its constituent regions is always unique irrespective of the order in which the image pixels are processed. But the computational cost of the HCS is very high. To illustrate the computational cost of the HCS process, for example, to process a 140×140 pixel section HCS takes about a month on a 1.6 GHz dual processor computer having a 16 Gigabyte of main memory.

3.4.1 Comparison of HCS with HSEG

The HCS process designed in this study is very similar to that of Tilton's [2003] hierarchical image segmentation (HSEG) algorithm with the following exceptions.

(i) In the HCS process, to merge the image regions, which are most similar with one another, all the current regions in the image are compared.

But the HSEG process optionally alternates between spectral clustering iterations and region growing iterations. In the spectral clustering iterations, a dissimilarity criterion is computed between spectra of all spatially non-adjacent regions and all pairs of such regions with dissimilarity less than or equal to the minimum dissimilarity value found in the spatial clustering step are merged while in the region growing iterations, only spatially adjacent regions are compared for merging [Tilton, 2003].

(ii) In the HCS process after every merging of the most similar regions, the pixels on the border of the merged regions are reclassified with any of the other regions if found suitable. This border pixel reclassification operation attempts to evaluate all possible image partitions consisting of the current number of regions to find the partition which consist of regions having the most similar pixels within them. The HSEG process does not have this operation viz. border pixel reclassification. The necessity of border pixel classification operation, for medical image segmentation, is demonstrated in Section 6.4.3.

3.4.2 Comparison of HCS with Ideal Definition of Segmentation

The HCS segmentation corresponds with the ideal definition of image segmentation process with the following exceptions :

(i) In the HCS process, to merge the image regions, which are most similar with one another, all the current regions in the image are compared and those regions which are most similar are merged. This operation may result in regions composed of pixels that are not contiguous.

But in the ideal definition of the segmentation process each region must be connected, i.e. composed of contiguous image pixels.

(ii) In the HCS process after every merging of the most similar regions, the border pixels of the merged regions are reclassified with any of the other regions if found suitable. This border pixel reclassification operation results in evaluating a subset of all possible image partitions consisting of the current number of regions in order to find the best possible partition of the image.

In the ideal definition of the segmentation process all possible image partitions consisting of N regions must be searched to find the best partition that has the smallest cost.

3.5 Hierarchical Clustering Based Segmentation Process Components

The implementation of the HCS process developed in this study has the following major logical components :

- Feature measurement
- Similarity measurement
- Clustering and region merging

The design details, and its implications, of the major logical components of the HCS process are discussed in the following Sections 3.5.1 to 3.5.3.

3.5.1 Feature Measurement

The distinguishing properties of an area surrounding a pixel, in an image, are obtained by feature measurement. The size of this area is application dependent. Feature measure is the most crucial and important part of any segmentation process. The success or failure of any subsequent clustering and/or merging process depends on the way the

properties of the smallest part of the image are evaluated and extracted. Since the designed segmentation procedure aims for multiple solutions, the feature extraction process involves the calculation of the distribution of the properties within a region (surrounding a pixel) rather than finding a single value of the property for that region. So, by comparing the distribution of the properties of two regions, the probabilistic value of similarity or dissimilarity between the two regions can be evaluated. Any suitable feature extraction method which gives a similarity measure may be used for this purpose.

Many medical image analysis studies that used Computed-Tomography (CT) and Magnetic-Resonance-Imaging (MRI) have treated the images as purely tonal and only pixel values were used for their analysis [Brandt *et al.*, 1994]. More recent studies have also captured the textural property of such images as well [Mir, 1995] [Chabat *et al.*, 2003]

Gray-tone (Pixel value) distribution is a unique feature which has been exclusively designed for the current work. Gray-tone-distribution uses the actual distribution of the pixel values in a region surrounding a pixel. This technique may be considered to work in a way similar to the human visual system where features for texture (region) segmentation are not consciously computed [Bhattacharya, 1997]. The results indicate that the gray-tone distribution feature is well suited for the segmentation of images which are primarily tonal rather than textural. Since the technique compares the distribution of the pixel values, rather than just comparing two pixel values, it is possible to capture the micro-textural property of the image.

Medical images like CT and MRI are primarily tonal and have minimal textural content (Micro-Texture). Thus they can be successfully segmented using this method. It will be shown that in medical images like CT and MRI, the gray-tone distribution feature has been successfully used for delineating dissimilar regions barely two pixels wide. The details of the gray-tone distribution feature extraction method is explained in detail in section 4.3.1 of this report.

It should be noted that gray-tone distribution feature measure is not suitable for segmenting images which are primarily textural. To segment images which are textural a texture feature measure such as Local-Binary-Pattern and Contrast (Appendix 2) needs to be used.

3.5.2 Similarity Measurement

Pixel pair similarity measurement involves calculation of the similarity between two small areas surrounding two individual pixels in the image. This is achieved by finding the similarity between the feature distributions around each pixel being compared. For the gray-tone distribution feature, this is the distribution of the gray tone values within the small region around the pixel.

To find the feature distribution around a pixel, it is a usual practice to consider a small region around the pixel of fixed window size with the pixel at the very centre of the window. This practice works well for segmenting large sections of different types of regions found within an image. Because in the cases of images having large areas of similarity, misclassification along the border of the different regions could be tolerated for a couple of pixels depth. But in situations where the image regions are only a few pixels wide, for example in some medical images, such misclassification is unacceptable.
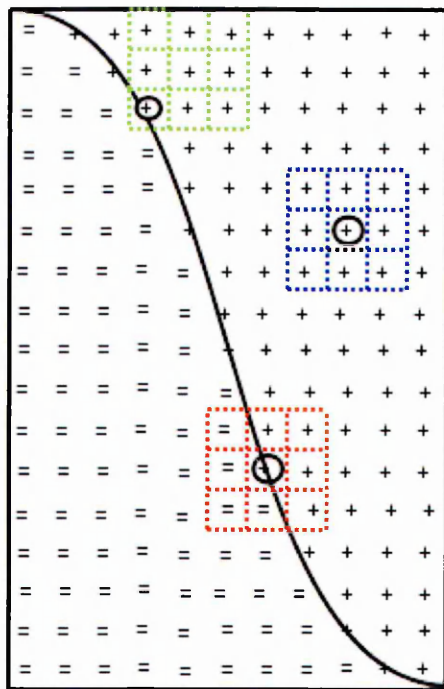
Figure 3.2 - Finding the feature
distribution within a 3×3
neighbourhood of a pixel.

In the HCS process, developed in this study, boundary pixels are localised providing a more accurate boundary delineation. This is achieved by finding the feature distributions around a pixel with the pixel at different locations within the window and then comparing the different distributions to get the best possible comparison. Figure 3.2 illustrates how the feature distribution within a region in the neighbourhood of a pixel could be found either by positioning a 3×3 size window centred around the pixel (red and blue masks) or with the pixel at different locations within the 3×3 size window (green mask).

From Figure 3.2 it can be seen why the feature distribution, within a 3×3 neighbourhood of a pixel, needs to be found by positioning the 3×3 windows differently depending on the location of the pixel. For example the red and blue masks are positioned with the pixel at the centre, and the green mask is positioned with the pixel at the bottom left corner of the mask. If the pixel is an interior pixel, which is the case in the blue mask, locating the pixel at the centre of the mask is acceptable. But if the pixel is at the border of two different regions, as it is the case of the red and green masks, locating the mask with the pixel at the centre is not acceptable. This is because, if the feature distribution is found by positioning the mask with the pixel at the centre of the mask, the feature distribution will include pixel values from the other region as well (red mask in Figure 3.2). But by positioning the mask similar to the green mask with the pixel on the border, the feature distribution will include only the pixel values from the region to which the pixel belongs.

In actual practice since it is unknown as to whether a pixel is a border pixel or an interior pixel, feature distributions for all possible orientations are found. Figure 4.6 shows the nine possible orientations of a 3×3 mask.

The images shown in Figures 3.3 - 3.5 illustrate the effect of positioning the window to find the feature distribution, in the neighbourhood of a pixel, in the border pixel classification of a real image. The image in Figure 3.3 is a tonal image comprising of a light background with two squares of the same darker tone embedded within it. Figures 3.4 and 3.5 show the segmentation results after initial clustering of the most similar neighbouring pixels (see Section 4.3.3 for details).

The image in Figure 3.4 shows the border pixels classification using a 3×3 mask centred around the pixel and the single feature distribution for each pixel being compared to each other. This shows that the pixels on the boundary of the small darker regions were marked as regions belonging neither to the background nor to the small squares (The different regions are pseudo coloured).

The image in Figure 3.5 shows the crisp border pixel classification when using the 3×3 window with the pixel at different locations within the window rather than centred only around the pixel.

Figure 3.5 shows that the gray background of the original image, shown in Figure 3.3, has been segmented as one region (pseudo coloured as cyan) and the two darker squares were segmented as two different regions (pseudo coloured as green and red). The two darker regions were segmented as two different regions, because during initial clustering only the most similar neighbouring pixels were compared for possible clustering (see Section 4.3.3 for details). Since the pixels belonging to the two darker regions were not neighbours, they were not compared and hence were not clustered together even though they were similar. But on the subsequent region merging stage, the two regions would be merged as one region, because during the region merging stage all pairs of regions (spatially adjacent or disjoint) currently in the image were compared and merged if found similar (see Section 4.3.4 for details).

3.5.3 Clustering And Region Merging

Clustering based merging of regions is achieved by comparing their properties in the image and merging together similar regions. The region merging process adopts an agglomerative type of hierarchical clustering procedure [Legendre and Legendre, 2003]. In this procedure, pairs of regions are compared and the most similar pairs of regions are marked. If the dissimilarity between the most similar pairs of regions is less than the currently allowed dissimilarity then the regions are merged into a single region. The most similar regions, for the current allowable dissimilarity, may be found either by comparing only those regions adjacent to each other, or by comparing all the regions currently in the image.
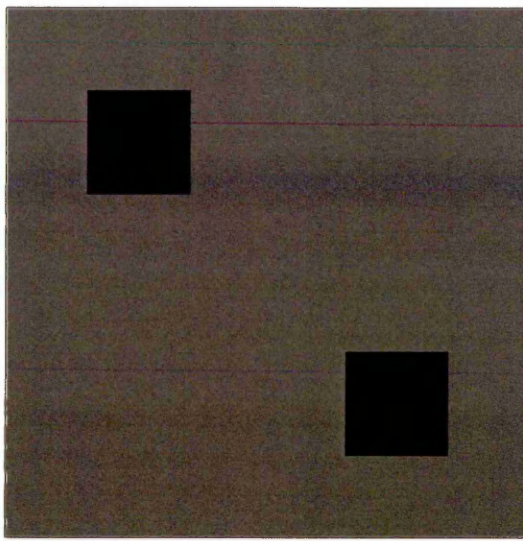
Figure 3.3 - A tonal image
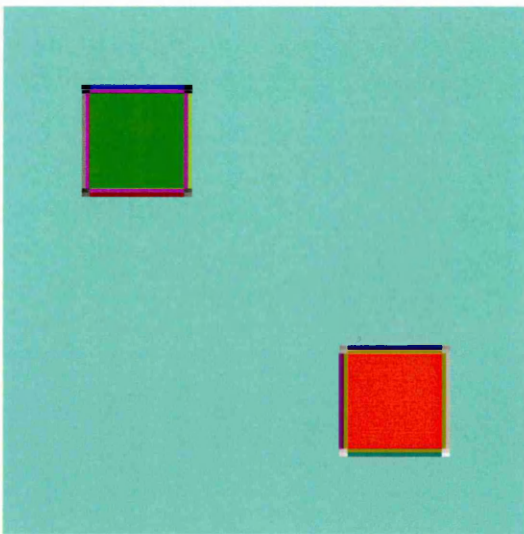
Figure 3.4 - Image segmentation result when single mask orientation was used for comparing different locations. The pixels bordering the regions were not classified properly
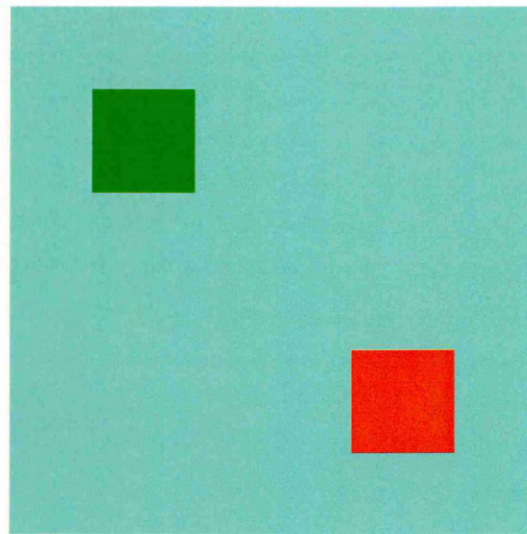
Figure 3.5 - Image segmentation result when multiple mask orientations were used for comparing different locations. The pixels bordering the regions were properly classified. The image segmentation shows crisp border delineation.

3.5.3.1 Agglomerative Clustering Algorithms

There are many different agglomerative algorithms for producing hierarchical clustering. They differ in the way the dissimilarity between the clusters is evaluated. The Lance-Williams recurrence formula [Webb, 2002] expresses the dissimilarity $d_{i+j,k}$ between a cluster k and the cluster formed by joining clusters i and j as

$$d_{i+j,k} = a_i d_{ik} + a_j d_{jk} + b d_{ij} + c |d_{ik} - d_{jk}|$$ [3.1]

25

where a_i, b and c are parameters that, if chosen appropriately, will give a specific agglomerative algorithm method as indicated in Table 3.1.

Table 3.1
Values of the parameters for different agglomerative methods

Agglomerative method	a_i	b	c
Single link	0.5	0	-0.5
Complete link	0.5	0	0.5
Group average link	$\dfrac{n_i}{n_i+n_j}$	0	0

The single-link method seeks isolated clusters and is useful in circumstances if the clusters are not homogeneous. The complete-link method and group average-link methodology tend to concentrate on internal cohesion, producing homogeneous, compact groups.

3.5.3.1.1 Single-Link Method

In the single-link method at each stage of the agglomerative algorithm the closest groups are fused to form a new group, where the distance, d_{AB}, between two groups, A and B, is the distance between their closest members, *i.e.,*

$$d_{AB} = \min_{i \in A,\, j \in B} d_{ij} .$$

[3.2]

The single-link method is alternatively known as *nearest-neighbour* method. The drawback of the single link method is that the grouping can become elongated, with some distant points, having little in common, being grouped together because there is a chain of intermediate objects [Webb, 2002].

3.5.3.1.2 Complete-Link Method

In this method, at each stage of the agglomerative algorithm the closest groups are fused to form a new group, where the distance, d_{AB}, between two groups, A and B, is the distance between their farthest members, *i.e.,*

$$d_{AB} = \max_{i \in A, j \in B} d_{ij} \ .$$

[3.3]

Complete-link method is alternatively known as *furthest-neighbour* method [Webb, 2002].

3.5.3.1.3 Group Average Link Method

In this method, at each stage of the agglomerative algorithm the closest groups are fused to form a new group, where the distance, d_{AB}, between two groups, A and B, is defined to be the average of the dissimilarities between all pairs of individuals, one from each group [Webb, 2002]., *i.e.,*

$$d_{AB} = \frac{1}{n_i n_j} \sum_{i \in A, j \in B} d_{ij}$$

[3.4]

3.5.3.2 Agglomerative Clustering Difficulties

Agglomerative hierarchical clustering is also known as the bottom-up method. The bottom-up method described in the literature usually suffers from a distorting phenomena, in which the cluster structures depend on the order in which the regions are considered for merging. This is because the most similar pairs of regions are found by comparing only those regions adjacent to one another. The same problem occurs in the classic definition of image segmentation, *i.e.* the number and the shape of the merged regions obtained depend on the order in which the image pixels are processed.

Nadler and Smith [1993] illustrate how the merged regions are different when the order of the merging process is changed (Figures 3.6 - 3.8) [Nadler and Smith, 1993]. Figure 3.6 shows the pixel values of an 8x8 image.

Figure 3.6 - Pixel values of a 8x8 image
[Nadler and Smith, 1993]

Figure 3.7 - Merged regions and their average pixel values when merging is initiated from the corner locations **A** and **C** of the image shown in Figure 3.5 [Nadler and Smith, 1993].

Figure 3.7 shows the average pixel values of the merged regions when merging was performed starting from the corner location A and C of the image. Figure 3.8 shows the average pixel values of the merged regions when merging is done starting from the corner locations B and D of the image. It can be seen from the Figures 3.7 and 3.8 that the merged results obtained are quite different for different starting points of the merging process.

It will be shown in Chapter 4 (Section 4.4.1) that the clustering and region merging methods designed in this study consistently yields the same results irrespective of the order of merging.

28
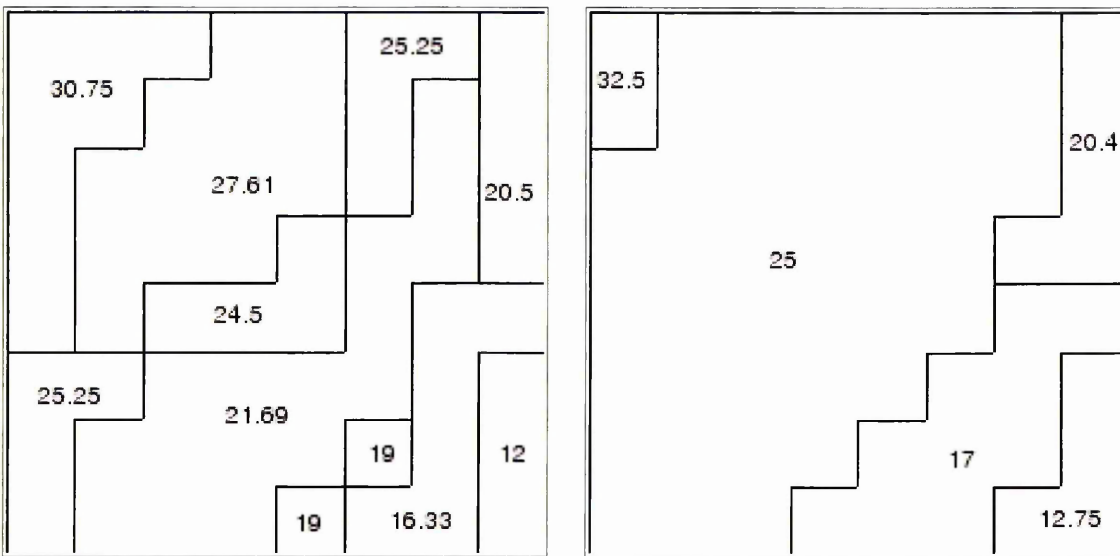
Figure 3.8 - Merged regions and their average pixel values when merging is initiated from corner locations **B** and **D** of the image shown in Figure 3.5 [Nadler and Smith, 1993].

3.6 Summary

In this chapter the theoretical background behind the design and implementation of the hierarchical clustering based segmentation (HCS) process, developed in this study, has been discussed in detail.

First the following different types of region based segmentation were discussed :

- Classic definition of image segmentation
- Hierarchical stepwise optimisation (HSWO)
- Hierarchical image segmentation (HSEG)
- Ideal definition of image segmentation

Second the design of the HCS process, developed in this study, was discussed in detail :

- The steps involved in the HCS algorithm were discussed
- The HCS process algorithm was compared and contrasted with the two other region based segmentation methods viz. HSEG and the ideal definition of image segmentation.

Third the major logical components of the HCS process were discussed :

- The design details of the major logical components.
- The implications of the design of the major logical components.

29

Chapter 4

Methodology

4.1 Introduction

Any segmentation method involves two primary steps: feature extraction and clustering/merging of pixels and regions having similar properties or features. Feature extraction is the operation to extract various image features for identifying or interpreting meaningful physical objects from images. Features are classified into three types *viz*. Spectral features, Geometric features and Textural features. Colour and Tone are examples of Spectral features, edges and linements are examples of Geometric features, pattern and homogeneity are examples of Textural features.

To ensure that the method developed was modular, the feature extraction part and the clustering/merging parts were made independent of each other. Thus initially, depending upon the type of the image under investigation, the properties of a part of the image was found using tonal measurements or textural measurements. Subsequent merging of pixels/regions having similar properties could follow the same procedural steps. The procedural steps adopted to combine similar pixels or merge similar regions are not dependent on the way the similarity is measured. The current study attaches far more importance in determining the optimum way to combine similar pixels or merge similar regions. Ways of justifying the best features to measure the property of a part of the image could vary from one type of image to another. However the success of using those properties to subsequently classify the image into different regions is largely dependent upon the efficiency of the classification/merging process.

The success of any classification process is evaluated by comparing the results with those of a human classifier. The classification process designed by the current study tries to mimic the human vision process in classifying an input image. One of the capabilities of the human vision process is the ability to classify an image and establishing multiple solutions of varying resolutions. For example given the anatomical image of the cross-section of a skull, at a coarser level a radiologist can classify the image as regions belonging to soft tissue and the skull bone. At a finer level the radiologists can also classify the different types of the soft tissue. At still a finer level, the radiologist can also distinguish the dissimilar regions within the same tissue type.

The major unique contribution of the current study is that it designed a procedural method that generates a range of segmentation solutions, for the user to select from. The images shown in Figures 4.1 - 4.3 illustrate this unique feature of the current study. The Computed Tomography (CT) image, shown in Figure 4.1, of the skull is initially segmented into many varied regions and subsequently consolidated into a few major regions. The image shown in Figure 4.2 shows the segmentation at a fine level. The image shown in Figure 4.3 shows the different regions in the segmented image at a coarse level of segmentation. The segmentation shown in Figure 4.3 is obtained by merging the different regions in the finer level of segmentation, shown in Figure 4.2, by allowing higher threshold of dissimilarity between the different regions. The regions in the image are displayed by giving unique colours for the different regions in the image.
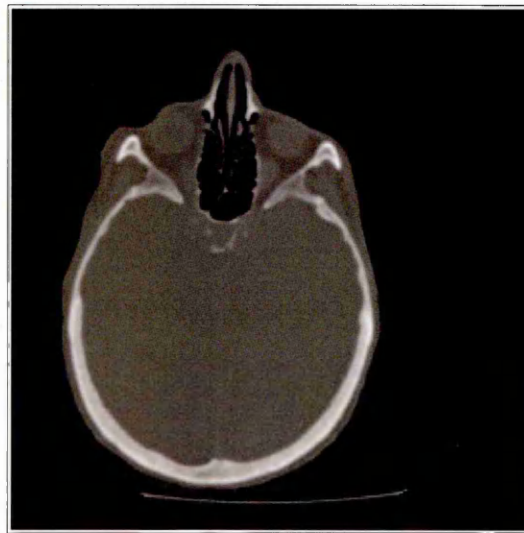
Figure 4.1 - Computer Tomography (CT)
image slice
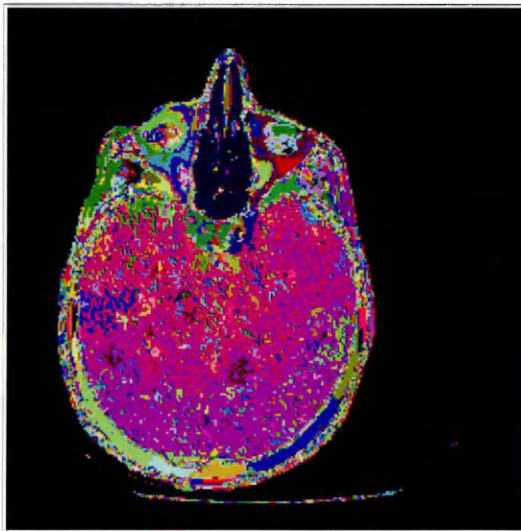
Figure 4.2 - Segmentation at a finer level
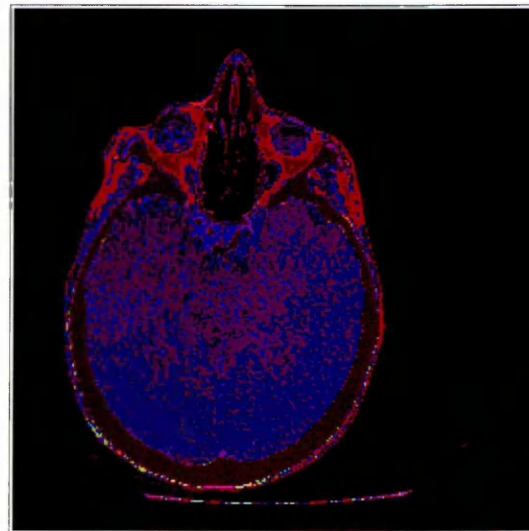
Figure 4.3 - Segmentation at a coarser
level

31

4.2 Overview of the Hierarchical Clustering based Segmentation (HCS) Process

The hierarchical clustering based segmentation (HCS) process, implemented in this study, partitioned an image into its constituent regions at hierarchical levels of allowable dissimilarity between the different regions. At any particular level, in the hierarchy, the segmentation process clustered together all the pixels and/or regions that had dissimilarity among them less than or equal to the dissimilarity allowed for that level. The clustering process was designed in such a way that the merging of the clusters did not depend on the order in which the clusters were evaluated for merging. This ensured that the clustering process consistently yielded the same set of regions for any particular level in the hierarchy. Figure 4.4 illustrates the overall operation of the HCS process developed and implemented in this study.
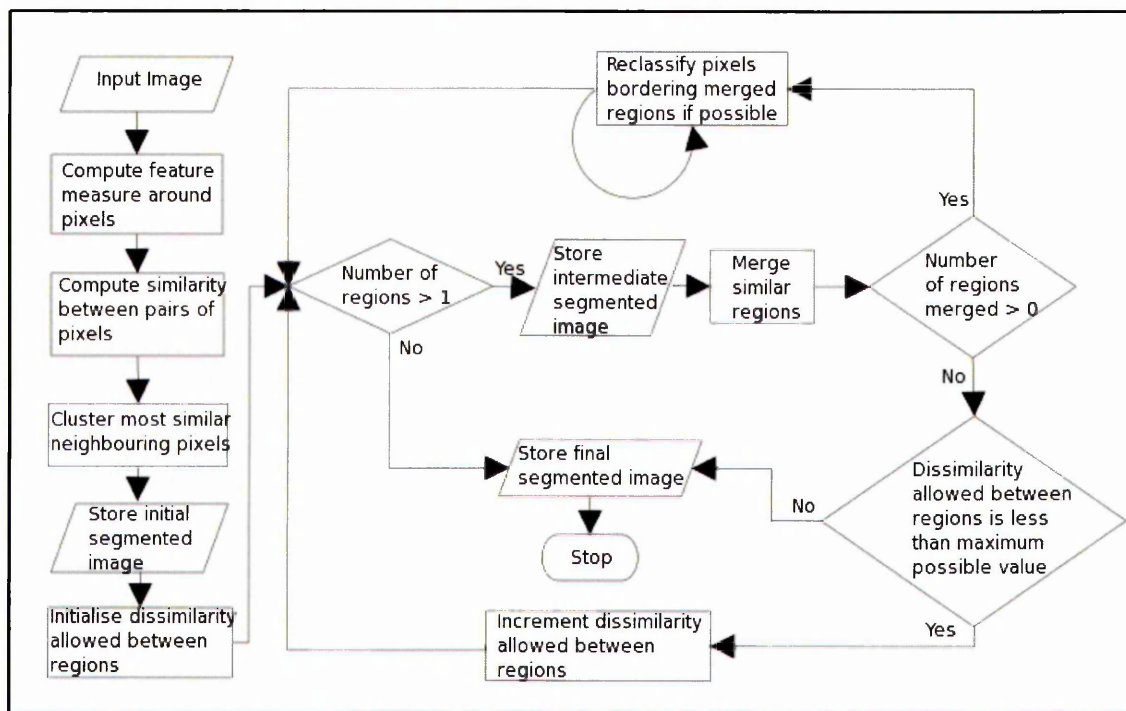
Figure 4.4 - Flow chart illustrating the different operations of the HCS process developed and implemented in this study.

During the segmentation process each constituent region was labelled with a unique number. The HCS process yielded a merge tree. Based on the merge tree, a graphical user interface (GUI) displayed the hierarchy of merges. Making use of the GUI, the user can inspect how the merging process evolves and associates the unique regions at any level with the different types of patterns present in the image. It should be noted that the time consuming aspect was in the production of the merge tree. Once the merge tree was got, the hierarchy of segmentations could be displayed by the GUI instantaneously.

32

4.3 Detailed description of HCS

The HCS process, developed in this study, delineated the regions in the input image at a hierarchical levels of dissimilarity. The five major modules of the HCS process are outlined below (also see the flow chart given in Figure 4.4) :

(i) Feature measurement :

This involved the calculation and extraction of the distinguishing properties within a neighbourhood of the individual pixels in the image. In the flow chart (Figure 4.4) this corresponds to the processing step "Compute feature measure around pixels".

(ii)Pixel pair similarity measurement :

This involved the calculation of the similarity between the feature measurement found within the neighbourhood surrounding two pixel locations. In the flow chart (Figure 4.4) this corresponds to the processing step "Compute similarity between pairs of pixels".

(iii)Initial clustering of the most similar neighbouring pixels :

Initial clustering was performed by comparing the feature distribution around each pixel in the image and the most similar neighbouring pixels were clustered to form the initial set of regions. In the flow chart (Figure 4.4) this corresponds to the processing step "Cluster most similar neighbouring pixels".

(iv)Regions merging :

Region merging was performed by comparing the properties of the different regions in the image and regions having similar properties within the allowed dissimilarity threshold at that stage were merged. In the flow chart (Figure 4.4) this corresponds to the processing step "Merge similar regions".

(v)Border pixels reclassification :

After the merging of similar regions, the pixels bordering the regions that were merged (with other similar regions) and their bordering regions, were re-evaluated to determine exactly which region they (the bordering pixels) actually belonged. In the flow chart (Figure 4.4) this corresponds to the processing step "Reclassify pixels bordering merged regions if possible".

The methodologies adopted to implement these major modules of the HCS process are discussed in detail in Sections 4.3.1 to 4.3.5.

4.3.1 Feature Measurement

Since feature measurement is a critical part of any segmentation process, many studies were conducted to design the best feature measurement method. A study by Randen and Husoy [1999] gives an excellent comparative study of different feature measurements used for texture classification. A more recent study by Zhang and Tan [2002] evaluates texture analysis approaches whose performances are not affected by translation, rotation, affine, and perspective transform.

For the current study, the subsequent merging and clustering steps required a similarity measure between two locations in an image. So any suitable feature extraction method which gives a similarity measure could have been used to extract the property of part of the image. For the subsequent classification, since the aim was to obtain multiple solutions, the feature measurement process should calculate the distribution of the properties within the neighbourhood of a pixel rather than finding a single value. Thus by comparing the distribution of the properties of two locations the probabilistic value of similarity or dissimilarity between the two locations can be evaluated.

Texture refers to spatial/statistical distribution of the tones, so it is fundamentally different from tone, which is defined at one location (pixel) while texture occurs over some finite area and hence requires some finite number of pixels to represent it. It is generally believed that one of the main visual cues is texture and differences in textural properties between regions. Textural features contain information about the spatial variation of gray tones in a neighbourhood where the neighbourhood is small compared to the region.

Gray-tone (Pixel value) distribution is a unique feature which has been exclusively designed for the current study. Gray-tone-distribution uses the actual distribution of the pixel values in a region surrounding a pixel. This technique may be a considered to work in a way similar to the human visual system where features for texture segmentation are not consciously computed [Bhattacharya, 1997].

The feature extraction method used in this study was based on gray-tone distribution. The gray-tone distribution feature was found as follows. A small mask of fixed size is placed around the pixel of interest. The gray-tone values within the mask, moving from

34

the top left corner of the mask to the bottom right corner of the mask, were taken as the distribution of the gray tone feature for the pixel. Figure 4.5 illustrates the method. Given the observations of gray-tone values from two different locations in the image and a certain level of significance, the aim was to determine whether they belonged to the same distribution. The commonly used test for difference between binned distributions is the Chi-Squared test [Press *et al.,* 2002].

4.3.2 Pixel Pair Similarity Measurement

The similarity between a pair of pixels, were found by comparing the gray-tone distribution around each pixel. To ensure precise border delineation, the mask was placed at different orientations around the pixel, as illustrated in Figure 4.6. All possible combinations of feature distributions between the two pixels were compared to find the best possible similarity value.

The comparison of the feature distribution for all possible mask orientations is highly process intensive. This is because, as the mask size increases, the number of comparisons increases exponentially. However to accurately localise the border between two dissimilar regions the exhaustive comparisons of feature distributions, for all possible mask orientations, becomes an absolute necessity.

Section 3.5.2 describes in detail why the feature distribution, within a neighbourhood of a pixel, needs to be found by positioning the mask differently depending on the location of the pixel (on the border or interior). In actual practice since one does not know whether a pixel is a border pixel or an interior pixel, feature distributions for all possible orientations are found.

In segmenting medical images, the current study employs a mask size of 3×3 pixels for finding the feature distribution around pixels. There will be nine possible orientations for a 3×3 mask size as illustrated in Figure 4.6. This corresponds to nine different feature distributions. Each feature distribution found for the pair of pixels is compared with the others and the largest similarity value is then taken as the similarity measure between the two pixels. For a 3× 3 mask size and nine different mask orientations there will be eighty one combinations. Their evaluation was found to be computationally feasible.

35
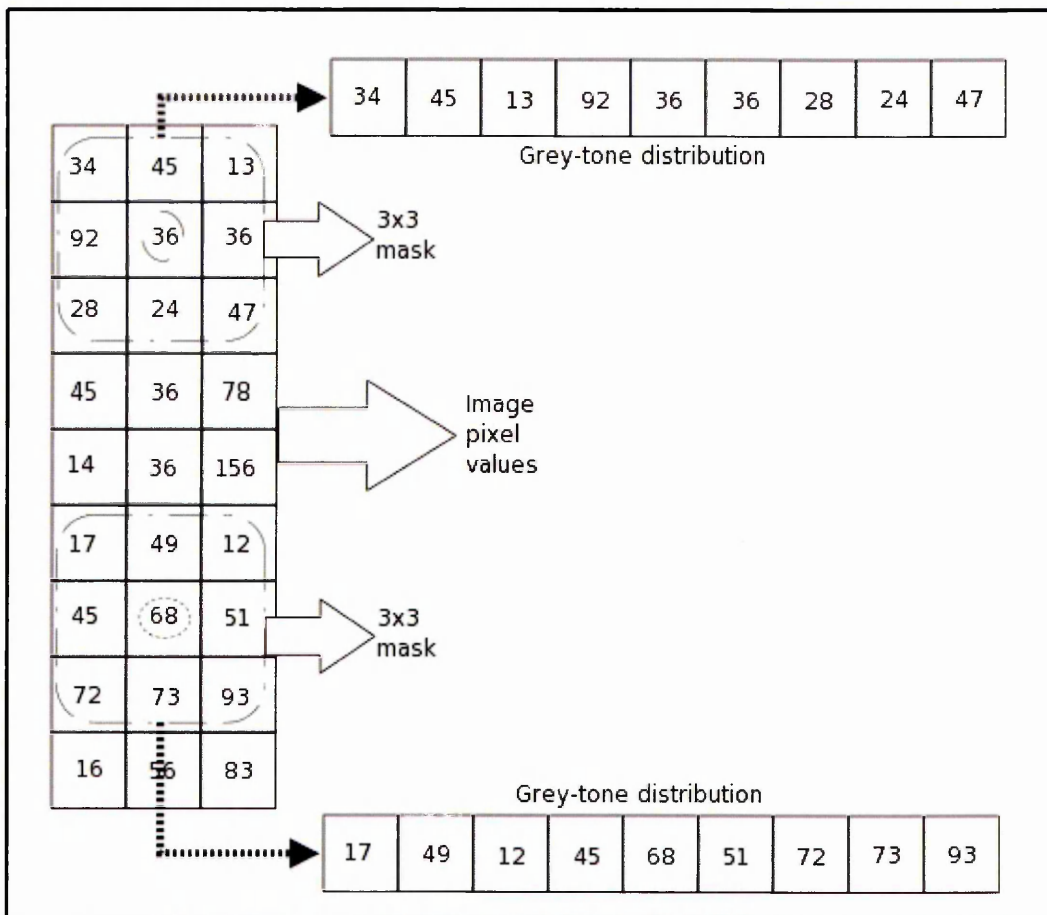
Figure 4.5 - Gray-tone distribution feature representation

4.3.3 Initial Clustering Of The Most Similar Neighbouring Pixels

Initial clustering of the most similar neighbouring pixels was necessary to form the initial set of regions in the image. If the image consists of homogeneous regions, then the initial clustering will give a proper segmentation and will need only a single merging of similar regions (not bordering each other) at the subsequent region merging stage.

Initial clustering was achieved by comparing the feature distribution around each of the pixels in the image and the most similar neighbouring pixels were clustered together to form the initial set of regions. In the current method, the initial segmentation will always be the same given a chosen threshold and it will result in the best possible solution since all possible comparisons of the pixels in the neighbourhood were considered and the best possible combination determined. This is achieved by the process described below.

36

The grid of pixel values (repeated for all nine mask orientations):

14	61	51	30	73	51	86
81	34	36	56	13	45	64
45	63	45	10	31	61	56
93	16	53	92	39	27	87
67	82	67	72	89	66	78
75	63	85	20	42	79	21
73	82	63	57	41	33	17

Nine possible orientations of a 3x3 mask with the pixel of interest at different locations within the mask
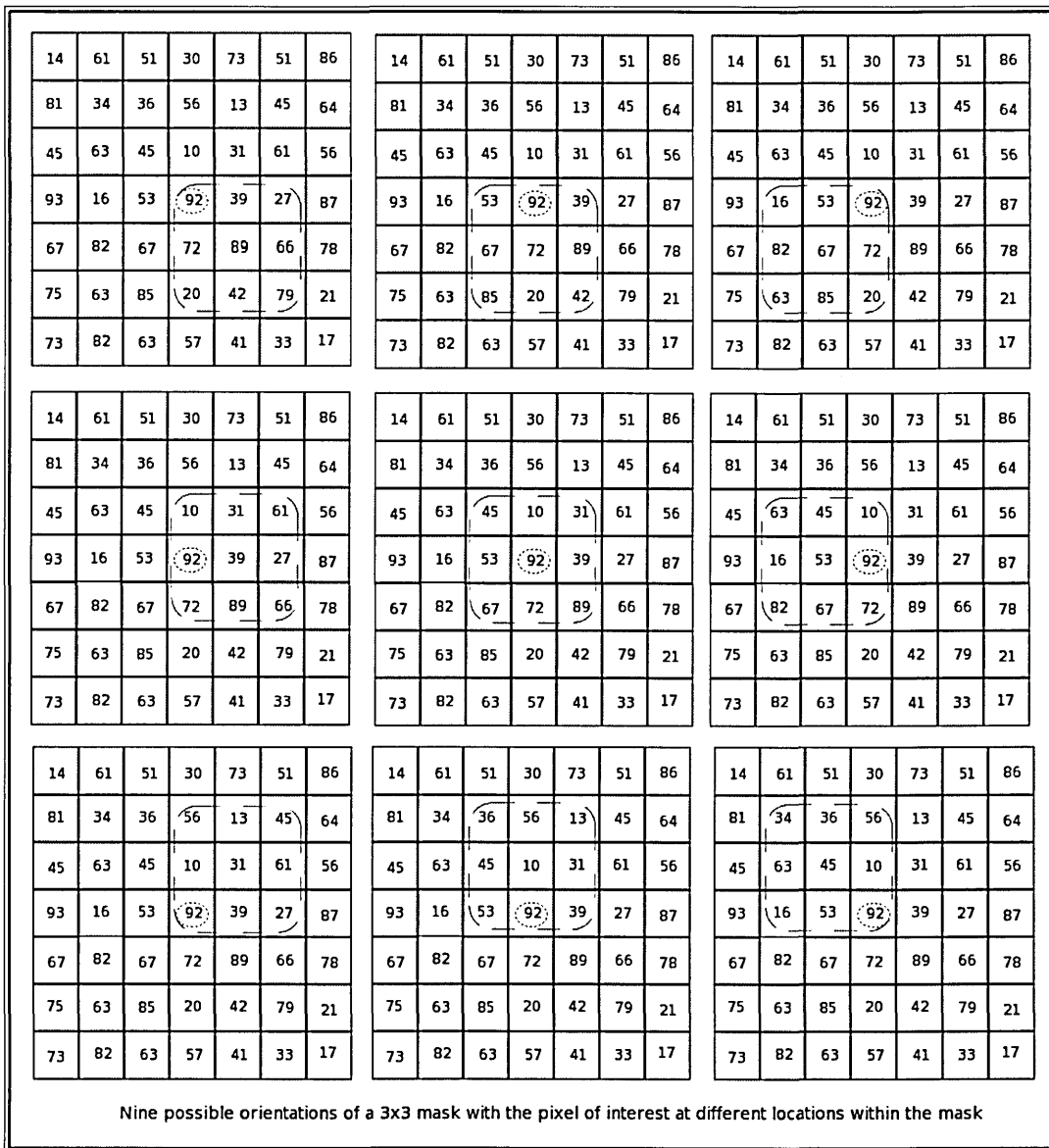
Figure 4.6 - Nine different orientations of a 3×3 mask window around a pixel

The initial clustering involved the following two steps. :

(i) Compare the feature measures of all the pixels in the image to find the most similar neighbouring pixel and/or pixels.

(ii) Cluster the most similar neighbouring pixels in the image to form the initial regions.

These two steps are now explained in detail in Sections 4.3.3.1 and 4.3.3.2.

4.3.3.1 Finding the most similar neighbouring pixel or pixels

For each pixel in the image the similarity measure between the pixel and each of its neighbours was found. The number of neighbours for each pixel will depend on the allowable distance up to which the pixels were considered as neighbours. For example, if the distance allowed was one then the number of neighbours compared with each of the pixel would be eight.

A neighbouring pixel was considered similar to the pixel under consideration if the similarity measure between the pixels was above the given threshold value. A list of the most similar neighbouring pixels to the current pixel was formed. This list could be either all the similar neighbouring pixels found above the given threshold value or only those similar neighbouring pixels which had the largest similarity measure above the given threshold value. The value of the similarity threshold chosen could be high if one wants a very fine initial segmentation or small if the initial segmentation need to be coarse.

Forming a list of the most similar neighbouring pixels, which had the largest similarity measure above the given threshold value, gives a consistent and best possible initial merging solution. This is because all possible combinations of pixels, in the neighbourhood, have been considered and only the best possible pixel pairs chosen.

Figure 4.7 illustrates the process of finding the list of the most similar neighbouring pixels. Note that a pixel could have a number of most similar neighbours.

4.3.3.2 Clustering The Most Similar Neighbouring Pixel or Pixels

The set of the most similar neighbouring pixels (found as described in Section 4.3.3.1) were clustered together to form the initial set of homogeneous regions in the image. The clustering could be done in either of the two ways outlined below :

- A pair of neighbouring pixels were clustered together even if only one in the pair is found to be the most similar to the other. The other pixel in the pair may be similar to another neighbour of it rather than this pixel.
- Only neighbouring pixels which were most similar to each other were clustered together.
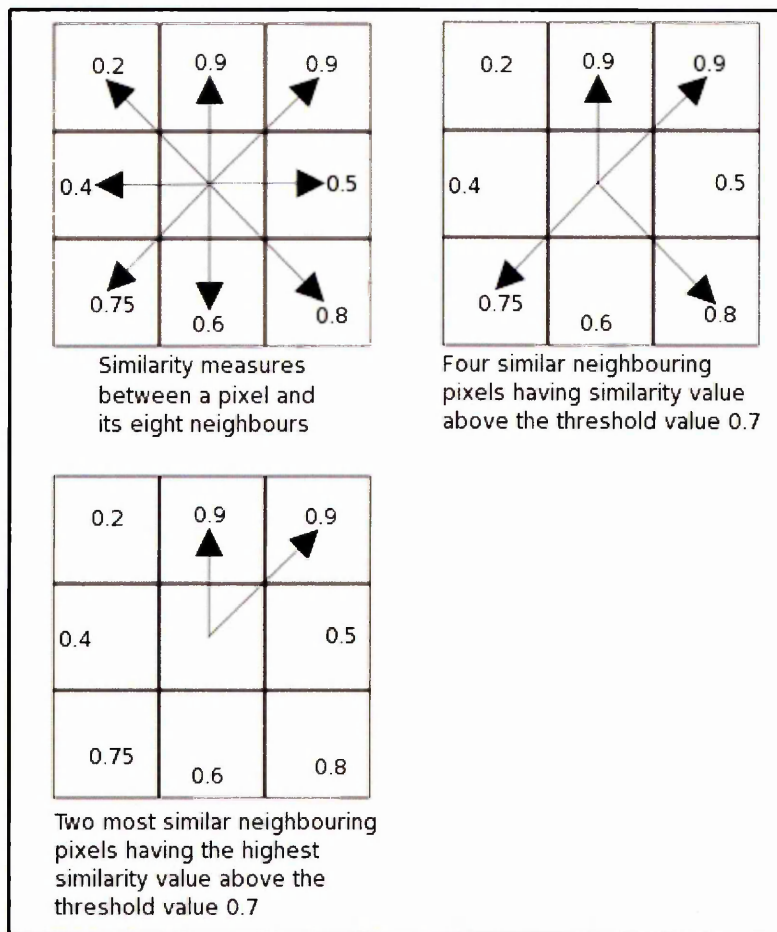
Figure 4.7 - Finding the most similar neighbouring pixels

These two different ways of initial clustering, are illustrated in Figure 4.8 (each of the different regions found is given a unique colour). Here it can be seen that the regions formed were homogeneous and were compact (smaller and unique) when only neighbouring pixels which were most similar to each other were clustered together.

To ensure that the initial segmentation will always be the same for a given threshold and also to get the best possible consistent initial segmentation, the following conditions were applied :

- When finding the most similar neighbouring pixels, the lists of the most similar neighbouring pixels were formed, by listing those neighbours which had the largest similarity measure above the pre-specified threshold value.

- When clustering the most similar neighbouring pixels in the image, to form the initial regions, only pixels which were the most similar to each other were clustered together.

- Note that the initial segmentation may produce regions of a single pixel.

39

For a practical illustration of the above scheme, which aims to achieve a consistent best possible initial segmentation, refer to Section 4.4.1 HCS Region Merging Consistency Validation.

The arrow heads point to the most similar neighbouring pixel for each of the pixels

Initial pixel clustering when all similar neighbouring pixels are clustered together, even if only one is found to be similar to the other.

Initial pixel clustering when only those pixels which are most similar to each other are clustered together.
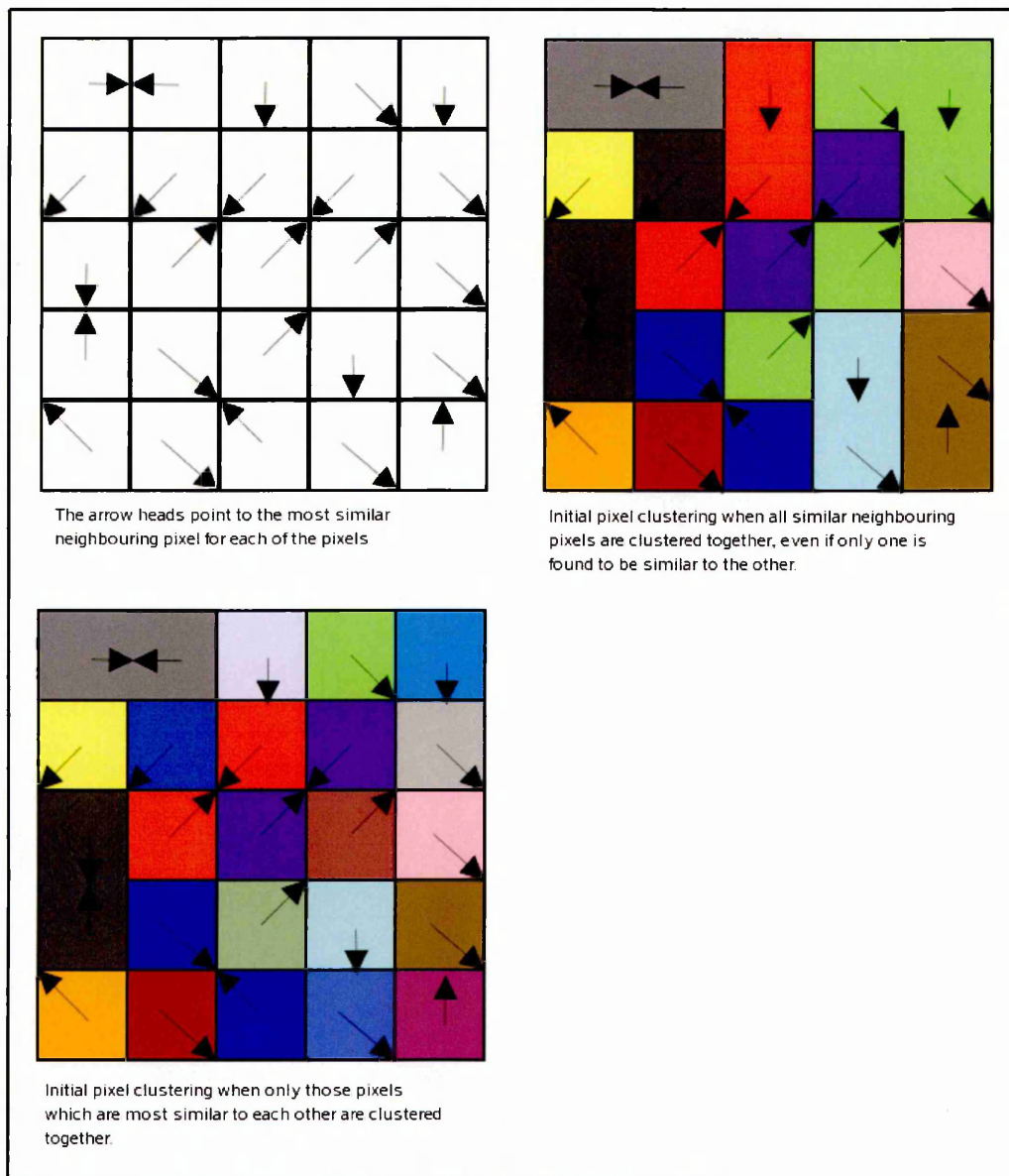
Figure 4.8 - An illustration of the two different ways of initial pixels clustering.

4.3.4 Region Merging

Region merging was accomplished using the agglomerative type of hierarchical clustering process also known as the bottom-up method. A hierarchy of segmentation results was obtained by adopting a dynamic threshold for the allowable dissimilarity measure between merging regions. The merging was carried forward until no more merging was possible for the current allowable dissimilarity between regions.

For possible merging of two regions, both regions should be closest to each other among all other possible regions which were candidates for merging. In addition, the dissimilarity measure between the two regions should be the lowest below the current allowable dissimilarity measure.

The distorting problem associated with the bottom-up method [Nadler and Smith, 1993] was avoided by comparing all pairs of regions currently in the image to find the most similar regions for merging. This ensured that the designed process always yielded the same segmentation for any given dissimilarity threshold. For a practical example, refer to Section 4.4.1.

Comparing all the possible combinations of regions, in an image, is CPU process intensive. However this was necessary in the medical image domain since similar tissue types could occur across the image interspersed by different tissue types.

4.3.4.1 Factors Considered For Region Merging

For a human observer, two regions in an image look similar if their components are similar. In a digital image, the components which constitute a region are the individual pixels. Hence it is hypothesised that the overall similarity between the individual components of the two regions could be measured, then that measure will represent the similarity of the two regions itself.

Thus to find the similarity between two regions the following factors were taken into account :
- Similarity between individual pixels of the two regions.
- Similarity between the pixels bordering the two regions.
- Similarity between the combined feature property of all the pixels in the two regions.

Intuitively the above three factors are appropriate considering the fact that a human observer considers the same three measures while visualising the different regions in an image. The above hypothesis will also be experimentally validated by showing how the accuracy of the segmentation improves by taking into account all the above factors (See Chapter 6 Section 6.3.2).

4.3.4.1.1 Individual Pixels Similarity Measurement

One of the tasks involved in evaluating the similarity between two regions is to determine the similarity between the individual pixels within the regions. A human observer could very easily assert the similarity of the set of pixels which comprise two regions. To mimic the human observer, we hypothesise that one needs to find the similarity between all the possible pairings of pixels within the two regions. The list of similarities thus obtained will be used to evaluate the distance (similarity) between the two regions using an agglomerative method, *i.e.* single-link, complete-link and group average-link.

Thus to measure the similarity of individual pixels between two clusters, the following expression was evaluated :

Pixel_Similarity_Measure = Pixel_Maximum_Similarity + Pixel_Minimum_Similarity + Pixel_Average_Similarity [4.1]

Where :

- *Pixel_Maximum_Similarity* is the maximum similarity obtained by finding the similarity between each and every pixel of one region with each of the pixels of the other regions. This is in fact the complete-link agglomerative algorithm defined by the expression (3.3) $d_{AB} = \max_{i \in A, j \in B} d_{ij}$

- *Pixel_Minimum_Similarity* is the minimum similarity obtained by finding the similarity between each and every pixel of one region with each of the pixels of the other regions. This is in fact the single-link agglomerative algorithm defined by the expression (3.2) $d_{AB} = \min_{i \in A, j \in B} d_{ij}$

- *Pixel_Average_Similarity* is the average similarity obtained by finding the similarity between each and every pixel of one region with each of the pixels of the other regions. This is in fact the group average-link agglomerative algorithm defined by the expression (3.4) $d_{AB} = \dfrac{1}{n_i n_j} \sum_{i \in A, j \in B} d_{ij}$

42

4.3.4.1.2 Border Pixels Similarity Measurement

A human observer takes into account the similarity between the regions' borders in an image for its segmentation. To be consistent in the way the similarity was measured, the similarity of pixels bordering the two clusters was evaluated using the following expression :

Border_Pixel_Similarity_Measure = Border_Pixel_Maximum_Similarity +

Border_Pixel_Minimum_Similarity +

Border_Pixel_Average_Similarity   [4.2]

Where :

- *Border_Pixel_Maximum_Similarity* was the maximum similarity obtained by finding the similarity between each and every border pixel of one region with each of the border pixels of the other regions.

- *Border_Pixel_Minimum_Similarity* was the minimum similarity obtained by finding the similarity between each and every border pixel of one region with each of the border pixels of the other regions.

- *Border_Pixel_Average_Similarity* was the average similarity obtained by finding the similarity between each and every border pixel of one region with each of the border pixels of the other regions.

4.3.4.1.3 Combined Feature Similarity Measurement

A human observer not only compares the individual pixels and the border pixels of a pair of regions for evaluating similarity, but also considers the combined effect of all pixels in each of the regions. This combined similarity measure feature between a pair of clusters was obtained as follows :

- First, a combined feature vector distribution for each region was obtained by constructing a normalised histogram of the feature values considering the feature vectors of all individual pixels in the region.

- Then the similarity between the combined feature vector of the two regions was found using Bhattacharya measure [Aherne *et al.*, 1997].

The Bhattacharya measure was used to compare the combined feature vector of two regions because it may be a sparse histogram and the method gives a more robust measure of similarity than either Chi-Square statistic or the G statistic [Aherne *et al.*, 1997] .

The Bhattacharya measure was found as follows :

If A_i is the frequency coded quantity in bin i (frequency coded in the sense that $\sum_i A_i = 1$ i.e. Normalised histogram), for the first region's feature histogram and B_i a similar quantity for the second region's histogram. Then A_i and B_i can be assumed to be Poisson distributed random variable. The Bhattacharaya measure $\sum_i \sqrt{A_i}\sqrt{B_i}$ is proposed as a measure of similarity between the two histograms. For the case of identical histograms, $\sum_i \sqrt{A_i}\sqrt{B_i} = 1$ indicates a perfect match.

4.3.5 Border Pixels Reclassification

After the merging of similar regions, the border pixels of the regions that had merged and their bordering regions were further evaluated to allocate them to the most suitable region.

Border pixel reclassification is necessary because the merging process starts with individual pixels and the pixels are merged to form regions and subsequently regions are merged to form bigger regions and so on. During the initial merging of neighbouring pixels and neighbouring small regions, pixels belonging to different regions might get merged. This could happen, for example when comparing pixels over a small neighbourhood, where the dissimilarity between pixels belonging to different regions might be smaller than the dissimilarity between pixels belonging to the same region because of the local in-homogeneity (arising due to inadequate scaling factor in measuring the repetitive pattern constituting the texture). However as the regions grow those pixels which have been merged as a result of comparison with neighbouring pixels might subsequently be reclassified by properly comparing them with the rest of the pixels from a larger neighbourhood.

In a textured image a larger region might be able to properly capture the repetitive texture pattern because of the larger region size. This hypothesis was investigated by improving the misclassification error while segmenting medical images [See Chapter 6, Section 6.4.3].

Border pixel reclassification was considered only for those pixels on the boundary of the clusters which had been merged with other clusters. These boundary pixels were removed one at a time from their original clusters. The pixel removed was considered as a region of its own and the similarity between the one pixel region and the regions bordering it (which included the original cluster to which it belonged) were found and the single pixel region was merged with the most similar bordering region. During this process the pixel could possibly be re-classified to one of the neighbouring regions rather than the region to which it originally belonged.

4.4 Hierarchical Clustering based Segmentation process Validation

The performance and the usefulness of the designed HCS process will be discussed in detail in Chapters 6 and 7. In this section it is demonstrated how HCS is not affected by the order dependence problem and how it is able to solve a typical problem which most other clustering algorithms find difficult to solve.

4.4.1 HCS region merging consistency validation

In the region merging process, it should be ensured that the merging result arrived upon does not depend upon the order in which the merging of the regions are considered. As discussed in Section 3.5.3.2, the region merging method described in the literature usually suffers from the distorting phenomena resulting from the order dependence of selecting regions for merging.

In the HCS method developed in this study, this problem was avoided by evaluating all possible combinations of clustering and merging only those regions which were found most similar. This merging consistency by the HCS method is demonstrated by the following clustering example processed using HCS.

Figure 4.9 - Pixel values in a image

33	30	30	29	28	27	25	22
32	30	29	28	26	25	23	21
31	29	28	27	27	24	22	20
30	28	27	26	25	23	20	19
30	27	25	24	24	22	18	15
27	25	21	23	22	20	16	13
25	23	22	21	20	19	17	12
24	23	22	20	19	17	15	11

(Corners: C top-left, B top-right, D bottom-left, A bottom-right)

Figure 4.10a - Average pixel values within the thirty eight regions after initial clustering

32.5	30.0	29.0	28.0	27.0	25.0	22.0
		29.0	28.0	26.0	25.0	23.0	21.0
31.0	29.0	28.0	27.0	24.0	22.0	20.0
30.0	28.0	27.0	26.0	25.0	23.0	20.0	19.0
	27.0	25.0	24.0	22.0	18.0	15.0
27.0	25.0	21.0	23.0	22.0	20.0	16.0	13.0
25.0	23.0	22.0	21.0	20.0	19.0	17.0	12.0
24.0			20.0	19.0	17.0	15.0	11.0

Figure 4.9 shows the pixel value of an 8×8 image. This image is the same as that, shown in Figure 3.6, and referred to in Section 3.5.3.2. Initial clustering of the most similar neighbouring pixels were done as described in Section 4.3.3.2. Figure 4.10a shows the average pixel value of the thirty eight clusters after the initial clustering.

Each of the thirty eight initial clusters was tagged with a unique index. Figures 4.10b and 4.10c show the thirty eight clusters locations, when they were given the indices sequentially (left to right top to bottom) and randomly respectively.

Figure 4.10b - Region indices when the initial regions were tagged sequentially.

0	1	2	3	4	5	6
		2	3	7	5	8	9
10	2	3	11	12	13	14
15	3	11	16	17	18	14	19
	11	20	21	22	23	24
11	20	25	26	22	27	28	29
20	30	31	25	27	32	33	34
35			27	32	33	36	37

Figure 4.10c - Region indices when the initial regions were tagged randomly.

37	35	33	32	31	26	15
		33	32	28	26	20	12
36	33	32	30	22	14	10
34	32	30	29	27	19	10	9
	30	25	23	17	7	3
30	25	13	21	17	11	5	2
25	18	16	13	11	8	6	1
24			11	8	6	4	0

46
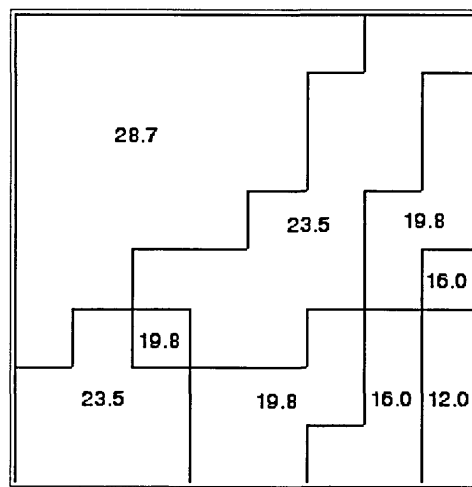
Figure 4.11a - Merging in the intermediate stage showing average
pixel values within the segmented regions.
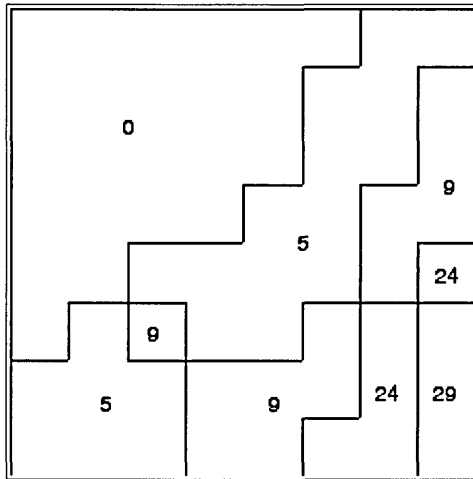
Figure 4.11b - The region indices
when the sequentially tagged initial
regions were merged.
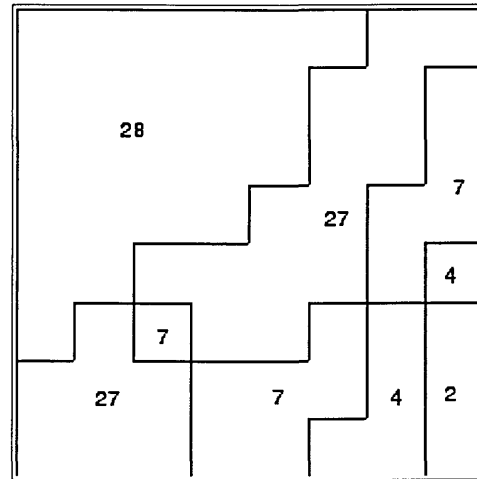
Figure 4.11c - The region indices
when the randomly tagged initial
regions were merged.

The initial set of thirty eight clusters were merged using the HCS process developed in
this study. Figure 4.11a shows the average pixel values of the nine clusters present in the
image during an intermediate clustering stage.

Figure 4.11b shows the nine cluster indices when the HCS merging was done using the
sequentially assigned initial cluster indices of Figure 4.10b and Figure 4.11c shows the
nine cluster indices when the HCS merging was done using the randomly assigned
initial cluster indices of Figure 4.10c.

From Figure 4.11b and Figure 4.11c it can be seen that whatever the order of merging
(sequentially or randomly), the HCS algorithm arrives at the same set of clusters. Hence
the HCS method consistently gives the only possible best solution. This consistency in
segmentation is illustrated by the segmentation example illustrated in Figures 4.9 - 4.11.

47
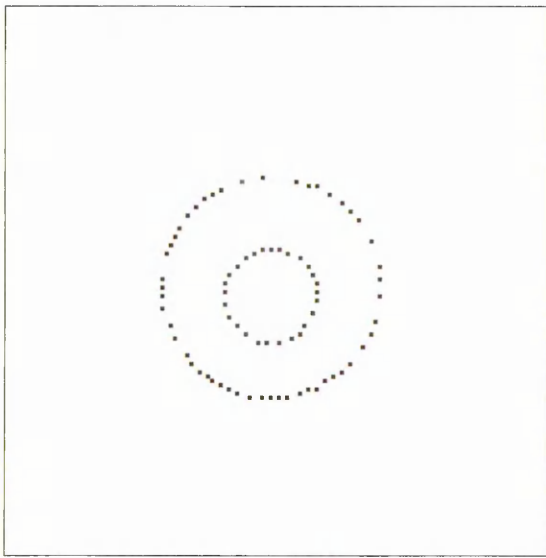
Figure 4.12 - Two clusters of points.
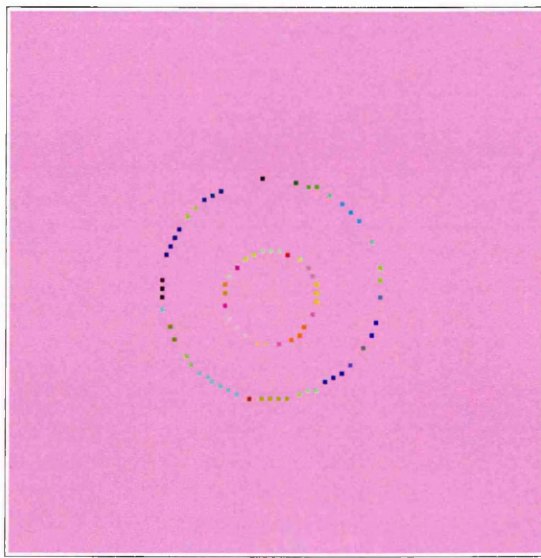
Figure 4.13 - Initial clustering by the HCS process.
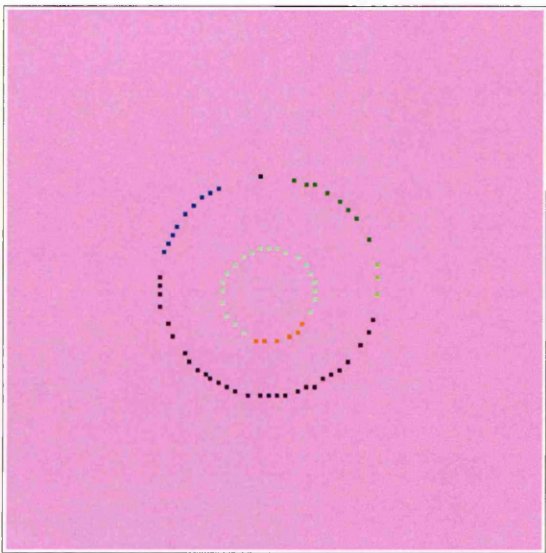
Figure 4.14 - Intermediate clustering during HCS process.
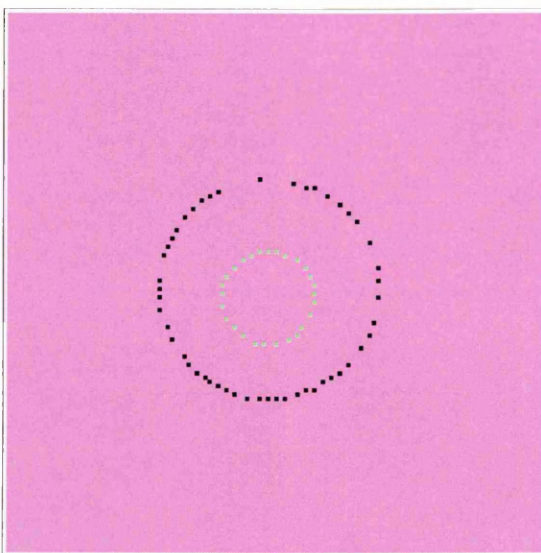
Figure 4.15 - Final clustering by the HCS process.

4.4.2 HCS Clustering Validation

The clustering performance of the HCS merging process could be validated further by trying to merge the points in the image, shown in the Figure 4.12, into two different clusters. For a human observer it is very easy to identify the two clusters of points (inner and outer circles). But many clustering methods given in the literature fail to come up with the solution identical to that arrived upon by the human observer [Gokcay and Principe, 2002].

When the HCS process is applied to this problem the solution obtained is shown in Figures 4.13-4.15. The feature measure used was the spatial distance between points Figure 4.13 shows the initial clustering of similar points. Figure 4.14 shows the intermediate clustering result during the merging process and Figure 4.15 shows the final merging with two clustered region of points.

The HCS process succeeds because, to evaluate the similarity between clusters, the similarity between the individual members of the clusters were taken into account. This is same as the Single-link method discussed in section 3.5.3.1.1.

4.5 Summary

In this chapter the details of the methodology adopted to implement the HCS process, developed in this study, was described.

First the logical flow chart of the of the HCS process was discussed.

Second the detailed description of the methodology adopted to implement the following five modules of the HCS process were discussed :

- Feature measurement
- Pixel pair similarity measurement
- Initial clustering of the most similar neighbouring pixels
- Regions merging
- Border pixels reclassification

Finally the validity of the regions found by the HCS process was demonstrated.

Chapter 5

Implementation

5.1 Introduction

The hierarchical clustering based segmentation (HCS), developed in this study, performs exhaustive search to merge regions having the least dissimilarity between them. The process, is a combinatorial problem and it is both CPU processing and memory intensive and hence time consuming. The challenge of efficiently implementing the process has led to the development of novel ways to optimise performance. This chapter will discuss in detail the different optimising techniques used for the search process and hence reduce the time to arrive upon the hierarchy of segmentation results.

The output of the HCS process is a hierarchy of segmentation results corresponding to a set of dissimilarity values. The nature of the HCS procedure is such that a large amount of visual information is produced. A graphical user interface (GUI) was designed to present the segmentation output in an informative way for the user to interpret. This chapter will also discuss in detail the functionality of the GUI.

5.2 Optimisation Techniques

As discussed in chapter 4 (Section 4.3.4), to find regions that are similar to each other, the HCS process not only compares regions bordering one another but also regions which are spatially apart. Such a task can easily overwhelm the computing power currently available and a number of optimisation methods were devised as part of implementing the HCS process.

One of these was to reduce the combinatorial problem itself. This was achieved by reducing the number of regions that needed to be compared. This was achieved with prior knowledge about the input data. If the different classes of regions contained in the image are known, the program only needs to compare those within the different classes. This largely reduces the combinatorial problem.

If no prior information is available then, through experience the user can specify an region of interest (ROI) defining the limit of the segmentation process borders.
Other optimisation techniques implemented and used were as follows :

- Since the calculations of the dissimilarity between the regions are independent of each other they can be performed in parallel.
- If adequate memory is available the information which does not change can be estimated once and can be stored for subsequent use.

The different methods of optimisation will be discussed in more detail in Sections 5.2.1 - 5.2.5.

5.2.1 Class Information for Computed Tomography (CT) Images

Figure 5.1 shows a CT image consisting of 256×256 pixels. If one needs to segment the image using the HCS process the number of start up clusters will be equal to 65,536. The number of combinations, to compare each of the 65,536 clusters with the rest, can be obtained by the following expression :

$$[N \times (N-1)] \div 2 \hspace{4cm} [5.1]$$

Where N is the number of clusters to be compared.

Hence for 65,536 clusters the number of combinations is given by

$$[65536 \times (65536-1)] \div 2 = 2,147,450,880 \ .$$

In a CT image the digital value ascribed to each pixel is called the Hounsfield value (HU). HU lies on a scale where pure water has a value 0, bone has a value of the order of +1000 and air has a value of -1000 [Albertyn and Brown, 1996]. To reduce the number of combinations, for CT images, Hounsfield values can be used as class information to achieve an initial classification. The HCS process can be provided the prior information about the different tissue types present in the image based on the Hounsfield unit (HU) values (Refer to Table 5.1). Figure 5.1 shows a CT image of a skull and Figure 5.2 shows the pseudo coloured image showing the nine different classes in the image based on the HU values from Table 5.1.

Table 5.1
The Hounsfield values for the different tissue types

Classes (Colour codes)	Hounsfield values range	Number of pixels	Percentage of total volume
Air (Black)	-1117 To -201	41907	63.95
Fat (Magenta)	-200 To -65	752	1.15
Water (Aqua)	-64 To +5	1549	2.36
Cerebral Spinal Fluid (Yellow)	+6 To +15	463	0.71
White matter (Green)	+16 To +30	1423	2.17
Grey matter (Blue)	+31 To +50	7356	11.22
Blood (Red)	+51 To +89	7508	11.46
Calcification (Silver)	+90 To +120	392	0.60
Bone (White)	+121 To +2248	4186	6.39
Total		65536	100
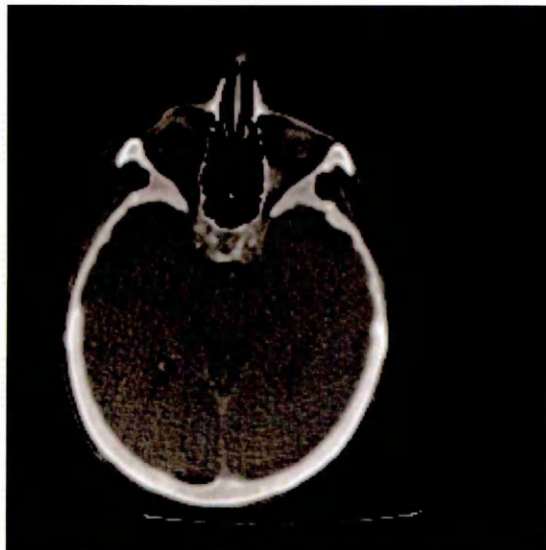
Figure 5.1 - A CT image
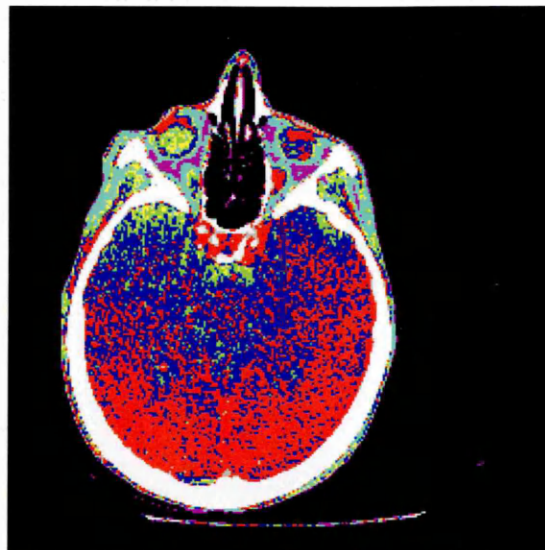
Figure 5.2 - The colour coded image showing the nine different classes in the CT image based on the HU values and colour codes listed in Table 5.1.

If the HCS process is restricted to perform the clustering of regions within a tissue type, the combinatorial problem can be avoided. Discarding the pixels corresponding to class Air, the largest tissue classes are Blood and Grey matter. Hence the largest combination of clusters that needs to be evaluated substantially reduces to $[7508 \times (7508 - 1)] \div 2 = 2,818,127$.

5.2.2 Class Information For MRI Images

A major drawback of Magnetic Resonance Imaging (MRI) is the lack of a standard and quantifiable interpretation of image intensities. Unlike X-ray and Computerised Tomography (CT), MRI images taken for the same patient using the same scanner at different times may appear different from each other due to a variety of scanner-dependent variations and, therefore, the absolute intensity values do not have a fixed meaning [László *et al.,* 2000]. Hence it is not possible to get an initial segmentation of the different classes in an MRI image based on the specific pixel value range alone.

Proton density (PD) and transverse relaxation time (T2) are two of the pulse sequences used to generate MRI images. When reviewing an MR image, the easiest way to determine which pulse sequence was used, or the "weighting" of the image, is to look at the Cerebro-Spinal Fluid (CSF). If the CSF is bright (high signal), then it must be a T2-weighted imaged. If the CSF is dark, it is a PD-weighted image. [Suri *et al.,* 2002]. Refer Appendix 1 for further details.
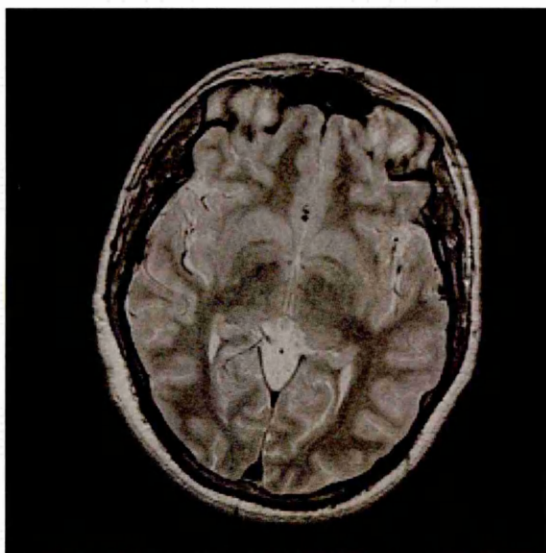
Figure 5.3 – PD Image slice I0000659   Figure 5.4 – T2 Image slice I0000660
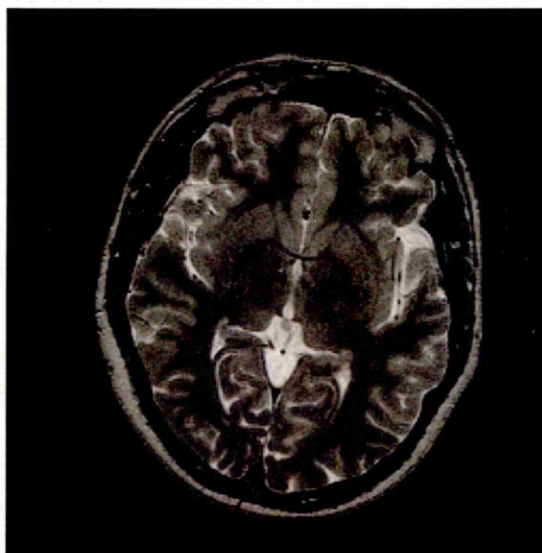
The images shown in Figures 5.3 - 5.6 show four sample image slices labelled as I0000659, I0000660, I0000661 and I00006662. They are the 30th and the 31st anatomical slice out of 60 slices of a single patient. From the four slices it could be inferred that all odd numbered slices are of the same anatomical region with PD weighted and all the even numbered slices are of the same anatomical region with T2 weighted.
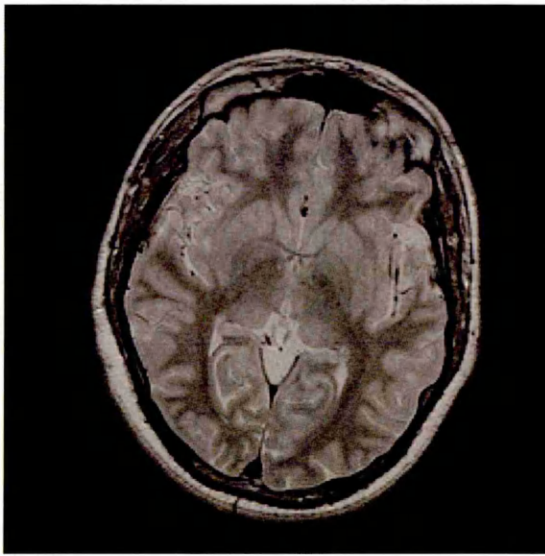
Figure 5.5 – PD Image slice I0000661   Figure 5.6 – T2 Image slice I0000662
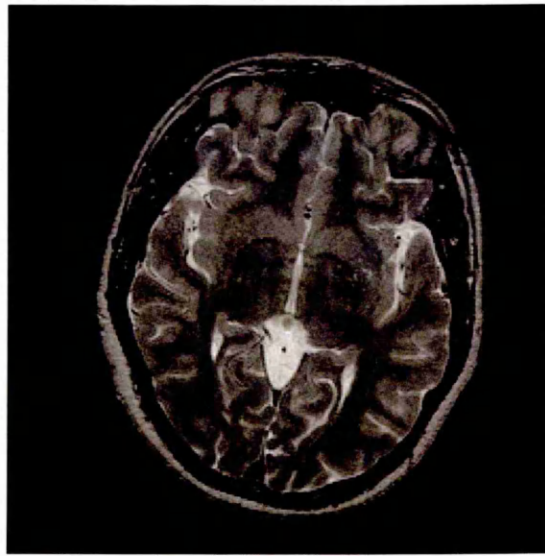
5.2.2.1 Fuzzy C-Means Clustering Based Multi-Spectral Segmentation

The T2 weighted MRI image gives a high contrast between Cerebral Spinal Fluid (CSF) and brain parenchyma. On the other hand Multiple sclerosis (MS) lesions appear bright on the proton density-weighted images while CSF (Cerebral Spinal Fluid) appears somewhat isointense with the rest of the brain parenchyma (see Appendix 1). Multi-spectral segmentation techniques based on multiple image sets (T2, PD) exploit the above powerful multi-parametric nature of MRI. The Multi-spectral segmentation technique is generally more robust since it combines information from multiple image sets with different contrasts for tissue classification [Suri *et al.*, 2002].

In MRI images, the initial classification, can be estimated by using a clustering technique such as the Fuzzy-C-Means (FCM). This technique has been previously used to estimate the CSF, White and Grey matter volumes in MRI images [Brandt *et al.*, 1994].

The main idea behind fuzzy logic classification (FLC) is that an object can belong simultaneously to more than a single group and does so to a varying degree. In "hard" classification procedures (such as the C-means clustering algorithm), each entity must belong exclusively to only one group and does not admit varying degrees of membership. In the case of MRI images, gray scale pixel values in an image can arise from more than one tissue type, such as a combination of gray and white matter. This

54

volume averaging of tissue poses problems for hard classification of image volume elements (voxels). The FCM is one of many "soft" classification procedures that allow sub-classification of individual MR image voxels into two or more groups. For example, a given voxel in an image could be classified as 0.4 (40%) Grey matter and 0.6 (60%) White matter. The FCM algorithm is a fuzzy generalisation of the traditional C-means "hard" clustering algorithm. Both the FCM algorithm and the C-means algorithm are unsupervised classification procedures: they are not dependent on the use of training regimens for cluster separation [Brandt et al., 1994].

The procedure basically consists of three computations, distance, cluster membership, and cluster centroid location. The algorithm operates in an iterative fashion eventually ending at a solution in the least mean squares sense. Clustering is performed using a, multi-spectral, 2-D pixel-value feature space with the dimensions representing the pixel-value intensity values of the PD and T2 weighted images (respectively) for a given slice. Thus each non-zero pixel image location consists of two pixel-value values one from the PD-weighted image and one from the T2-weighted image of the same slice. Each location's two pixel-value sets make up a "pixel vector" [Brandt et al., 1994].

To start the clustering operation, an initial estimate of the pixel-value sets representing the prototypical centroid for each cluster needs to be provided for each of the PD and T2 weighted images. The final solution is independent of the choice of initial cluster centroids. If the initially chosen centroid values are far (in PD, T2 Euclidian space) from the final solution values, then more iterations will be required. To identify the centroids of the different classes in the image following strategy was used : the distributions of the pixel values of the PD and T2 weighted images were plotted (Figures 5.7 and 5.8). From the plots, four different ranges of pixel values were identified corresponding with the four classes in the image i.e.. Air, White Matter, Grey matter and CSF. The midpoint of each of these four ranges for each of PD and T2 weighted images was then chosen to represent the initial pixel-value estimate for the cluster centroid values. The clustering procedure is then executed with the steps expanded below. The process described below was successfully used by Brandt et al. to estimate CSF, White and Grey matter in MR images [Brandt et al., 1994] and hence it has been adopted without any further modifications in our study.

FCM clustering procedural steps [Brandt *et al.*, 1994] :

   (i) Initialise the number of clusters and their centroid locations.

   (ii)For each image pixel vector, the squared Euclidean distance to each cluster centroid vector was computed as :

$$\| \mathbf{x}_k - \mathbf{v}_i \|^2 \qquad\qquad [5.2]$$

where $\mathbf{x}_k$ refers to each of the n pixel vectors in the slice, and $\mathbf{v}_i$ refers to each of the N_c cluster centroid vectors.

Thus

k value ranges from 1 to n, where n is the number of pixels in the image.

i value ranges from 1 to N_c. where N_c is the number clusters.

   (iii)Using the inverse squared distances calculated from equation 5.1, a fractional membership value between 0 and 1 was computed for each image pixel vector and for each cluster :

$$\mu_{i,k} = \frac{\left(\dfrac{1}{\|x_k - v_i\|^2}\right)^{\frac{1}{(m-1)}}}{\displaystyle\sum_{j=1}^{N_c} \left(\dfrac{1}{\|x_k - v_j\|^2}\right)^{\frac{1}{(m-1)}}} \quad \text{for } i = 1,2,.....,N_c \text{ and } k = 1,2,....n \qquad [5.3]$$

where m is the fuzziness parameter that determines the amount of overlap between clusters.

The value chosen for m is mathematically arbitrary within the range $1.0 < m < \infty$. Therefore, the choice of this parameter is determined empirically based on the actual problem domain. Note that use of $m = 1$ reduces the algorithm to the classical C-means hard clustering procedure in which objects are assigned 100% membership to the nearest cluster centroid.

Brandt *et al.* [1994] had experimentally found that a value of 1.3 for m yielded consistent results across different images and subjects. Hence in this study the value of m was chosen to be 1.3.

The membership values, $\mu_{i,k}$ are such that they satisfy the following three conditions:

$0 \leq \mu_{i,k} \leq 1$ for all i, k

$\displaystyle\sum_{i=1}^{N_c} \mu_{i,k} = 1$ for all k

and

$$0 < \sum_{k=1}^{n} \mu_{i,k} < n \quad \text{for all } i.$$

(iv)New cluster centroid vectors were recalculated based on pixel vector membership values as :

$$v_i = \left(\frac{1}{\sum\limits_{k=1}^{n} (\mu_{i,k})^m} \right) \sum_{k=1}^{n} (\mu_{i,k})^m x_k \qquad \text{for } i = 1, 2, \ldots, N_c \qquad [5.4]$$

Where v_i is the clusters' centroid value and m is the fuzziness parameter as in expression 5.3.

(v)The absolute difference (Euclidean distance) between cluster centroid values computed in the previous iteration and those in the current iteration were computed. Repeat procedure from step 2 above if :

$$\max \left(\left| v_{i,\alpha} - v_{i,\alpha-1} \right| \right) > \epsilon \quad \text{for } i = 1, 2, \ldots, N_c \qquad [5.5]$$

where $v_{i,\alpha}$ is the location of cluster centroid i computed during iteration α

Otherwise, convergence in the least mean squares sense has been achieved.

Brandt *et al.* [1994] had chosen the value of ϵ as 0.1 which was retained in this study as well.

5.2.2.2 Extracting Class Information For MRI Images Using Fuzzy C-Means Based Clustering

The original pixel values of the PD weighted (Figure 5.3) and the T2 weighted (Figure 5.4) images were plotted as shown in Figures 5.7 and 5.8. These plots will be used to estimate the number of possible clusters in the image and their initial centroid locations. The method of doing this is hereby discussed.

The original pixel values of the image section I0000659 (PD weighted) (Figure 5.3) ranged from a minimum value of 0 to a maximum value of 1094. The distribution of the original image pixel data is shown in Figure 5.7. Even though the maximum pixel value is 1094, the count of pixel values larger than 830 are all single digit and many of them have a count zero. Hence the plot was curtailed to pixel values up to 830 only.
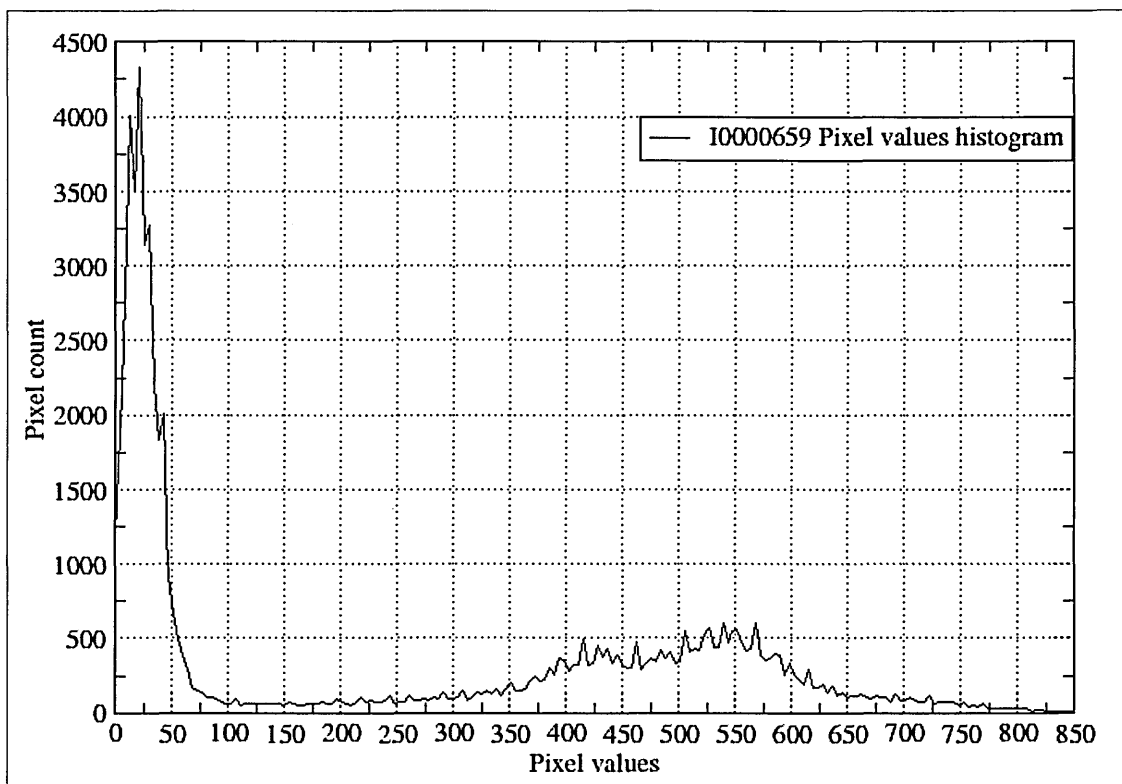
Figure 5.7 - The distribution of the pixel values of the MRI image slice I0000659 (PD weighted)
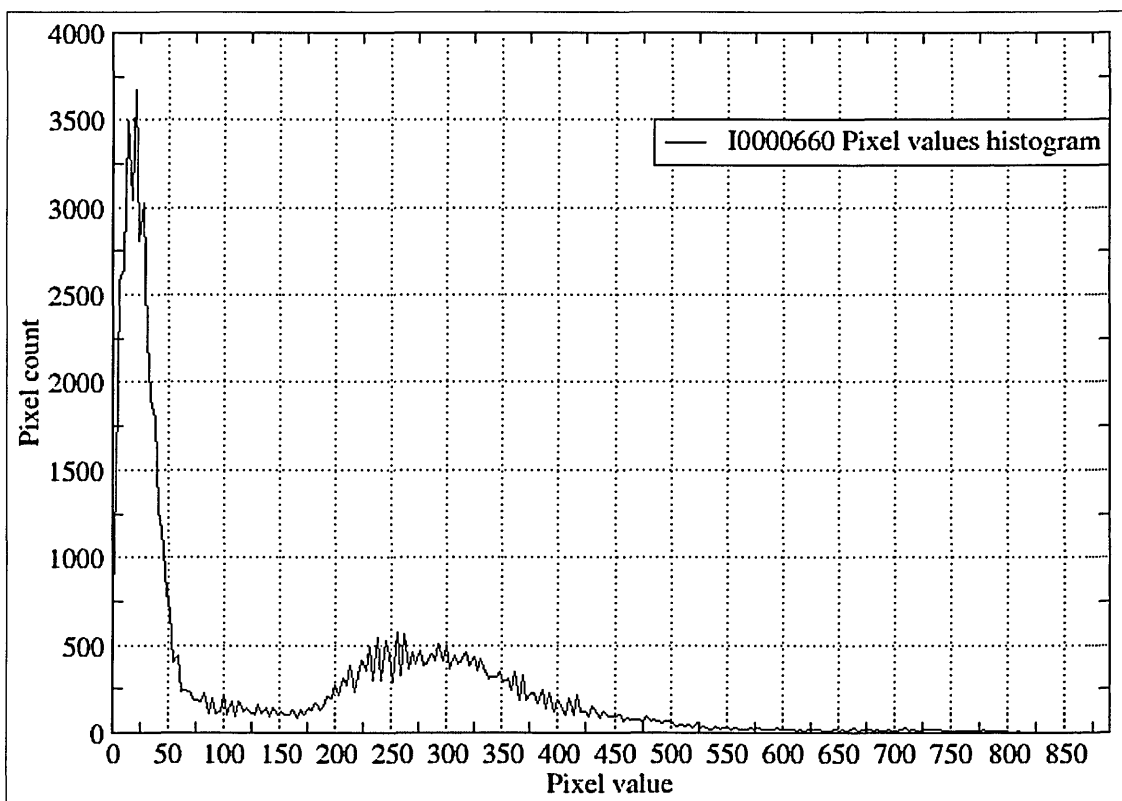
Figure 5.8 - The distribution of the pixel values of the MRI image slice I0000660 (T2 weighted)

The original pixel values of the image section I0000660 (T2 weighted) (Figure 5.4) range from a minimum value of 0 to a maximum value of 881. The distribution of the original image pixel data is shown in Figure 5.8.

Healthy brain tissue can generally be classified into three broad tissue types on the basis of an MR image. These are Grey matter (GM), White matter (WM) and Cerebral Spinal Fluid (CSF) [Frackowiak *et al.* 2003]

From the plots in Figures 5.7 and 5.8 it could be visualised that there are four distinct parts of range of pixel values. For the plot in Figure 5.7 the four parts could be roughly estimated as 0 to100, 100 to 350, 350 to 650 and 650 to 830. From the plot in Figure 5.8 the four parts could be roughly estimated as 0 to 50, 50 to 175, 175 to 450 and 450 to 880.

Table 5.2
Initial estimate of the distribution of the pixel count for the four classes, for the PD weighted MRI image slice of Figure 5.3.

Classes	Pixel value range	Number of pixels	Percentage of total volume
Air	0 to 100	33,775	51.54
CSF	100 to 350	5,147	7.85
White matter	350 to 650	23,816	36.34
Grey matter	650 to 830	2,798	4.27
Total		65,536	100.00

Table 5.3
Initial estimate of the distribution of the pixel count for the four classes, for the T2 weighted MRI image slice of Figure 5.4.

Classes	Pixel value range	Number of pixels	Percentage of total volume
Air	0 to 50	33,302	50.81
CSF	50 to 175	5,869	8.96
White matter	175 to 450	23,498	35.86
Grey matter	450 to 880	2,867	4.37
Total		65,536	100.00

From the four different range of pixel values, it was estimated that there are four distinct classes in the images. Based on the pixel values and their spatial location in the images the four different classes were taken as Air, Cerebral Spinal Fluid (CSF), White matter and Grey matter. Tables 5.2 and 5.3 show the initial estimate of the distribution of the pixel count for the four classes for the PD (Figure 5.3) and T2 (Figure 5.4) weighted MRI image slices respectively.

To begin the clustering procedure, an initial estimate of the gray scale values representing the prototypical centroid for each cluster must be provided for each of the two images. The final solution has been observed in repeated tests to be independent of the choice of initial cluster centroids. If the initially chosen centroid values are far (in PD, T2 Euclidean space) from the final solution values, then more iterations will be required to arrive at a solution. The following arbitrary strategy was used: the range of gray scale values in each image histogram was divided into three parts (for the three clusters of White matter, Grey matter, and CSF). The midpoint of each of these three parts for each image was then chosen to represent the initial gray scale estimate for the cluster centroid values' [Brandt, *et al.* 1994].

In this study the midpoint of each of the four parts, for each of PD and T2 weighted images, was chosen from the pixel value plots. These four pixel value pairs are considered as the initial estimate representing the prototypical centroid for the four classes of air, White matter, Grey matter and CSF and were used to initiate the FCM based clustering.

Tables 5.4 and 5.5 give the details of the initial estimate of the cluster centroid values, for each of the four classes, for the image sections PD weighted I0000659 (Figure 5.3) and T2 weighted I0000660 (Figure 5.4) respectively.

Table 5.4
Details of the initial estimate of the four classes' centroids for the PD weighted image slice I0000659

	Air	CSF	White matter	Grey matter
Pixel Value	61	320	496	730
Pixel Location	225, 220	211, 100	168, 138	191, 106

60

Table 5.5
Details of the initial estimate of the four classes' centroids for the T2 weighted image slice I0000660

	Air	CSF	White matter	Grey matter
Pixel Value	17	127	258	689
Pixel Location	225, 220	207, 106	168, 138	129, 167

In Figures 5.9 and 5.10, one of the locations which has the same pixel value as that of the initial cluster centroid pixel value, for the four classes, *i.e.* Air (Red), CSF (Green), White matter (Blue) and Grey matter (Magenta), are marked in colour for the image sections that are PD weighted (image slice I0000659) and T2 weighted (image slice I0000660) respectively.

Figure 5.9 - Start-up class centroid locations marked PD weighted image slice I0000659
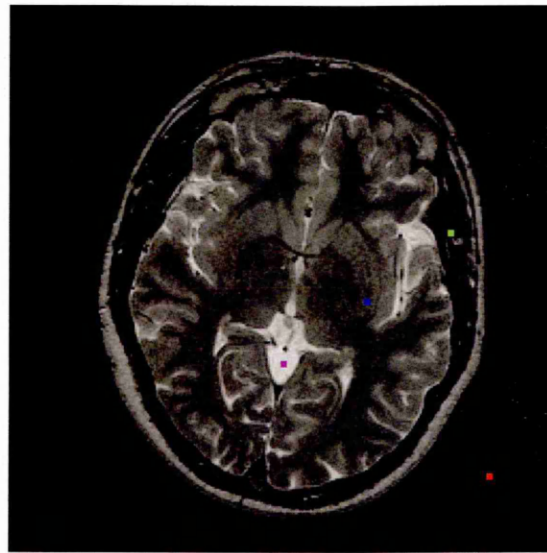
Figure 5.10 - Start-up class centroid locations marked T2 weighted image slice I0000660

Using the FCM based clustering method, the images were segmented into four different regions (Air, CSF, White_Matter and Gray_Matter). To have a robust segmentation, the original pixel values of both the PD weighted (image slice I0000659) and T2 weighted (image slice I0000660) images were used as a "pixel vector".

The fuzzy clustering iterates through Steps 2 to 6 (Outlined in Section 5.2.2.1). At the end of each iteration the the absolute difference (Euclidean distance) between cluster centroid values computed in the previous iteration and those in the current iteration were

computed. The maximum absolute difference between the four cluster centroid values computed in the previous iteration and those in the current iteration was evaluated as given by the expression 5.5. The iteration was continued until the value given by the expression 5.5 was greater than 0.1, otherwise, it was assumed that the convergence in the least mean squares sense had been achieved.
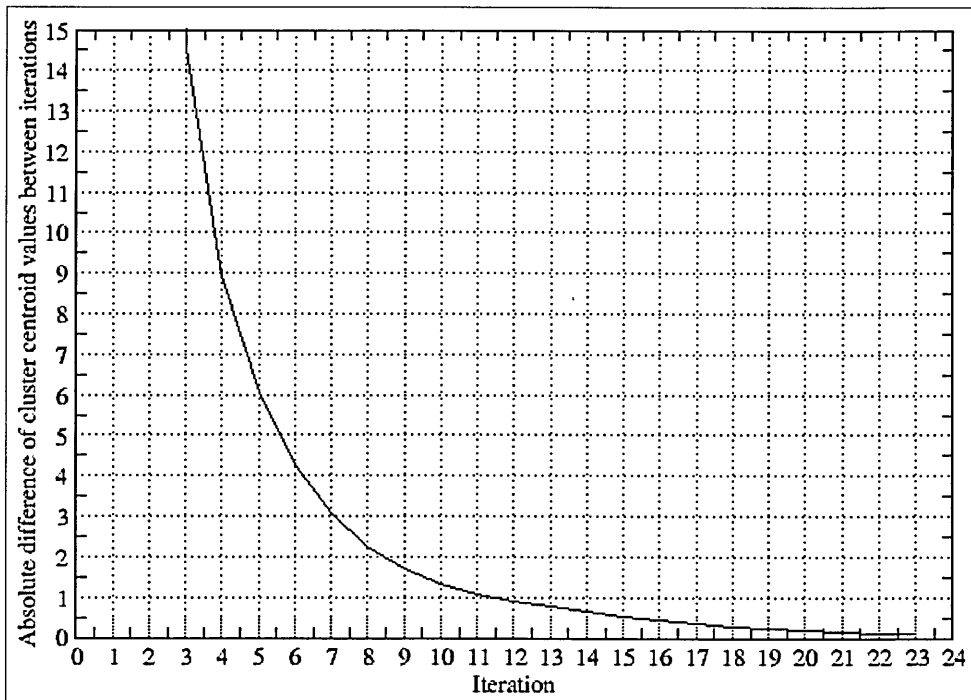
Figure 5.11 - Plot showing the maximum value of the absolute difference (Euclidean distance) between cluster centroid values computed in the previous iteration and those in the current iteration (expression 5.5), for the different iterations.

The plot in Figure 5.11 shows the value, for the expression 5.5, for different iterations. For the iterations one and two the values, which are not shown in the plot, were 888.325 and 36.5311 respectively. From the plot in figure 5.11 it can be seen that it took twenty three iterations for the process to attain a value of 0.0907436 for the expression 5.5.

Table 5.6 lists the final estimate of the centroid values for the four different classes in the two image slices PD weighted I0000659 and T2 weighted I0000660. Figures 5.12 and 5.13 show how the centroid values for the four different classes converge from the initial values (Table 5.4 and Table 5.5) to the final set of values (Table 5.6) for the two image slices PD weighted I0000659 and T2 weighted I0000660.

Table 5.6
Details of the final estimate of the four classes' centroids for the image slices PD
weighted I0000659 and T2 weighted I0000660

	Air	CSF	White matter	Grey matter
PD I0000659	33.5298	377.073	534.085	675.328
T2 I0000660	27.7616	193.59	318.39	511.429

From the plots in Figures 5.12 and 5.13 it can be seen that the values of the centroids, for the four classes in the two images, had converged almost to their respective final values after the eleventh iteration. This is also evident from the plot in Figure 5.11 where the value given by the expression 5.5 has fallen below 1.0 after the eleventh iteration.

The FCM clustering process segmented the MRI image sections, shown in Figure 5.9 and 5.10, into four different regions. The segmentation result is shown in Figure 5.14. In the Figure 5.14 each of the four different regions is given a unique pseudo colour.
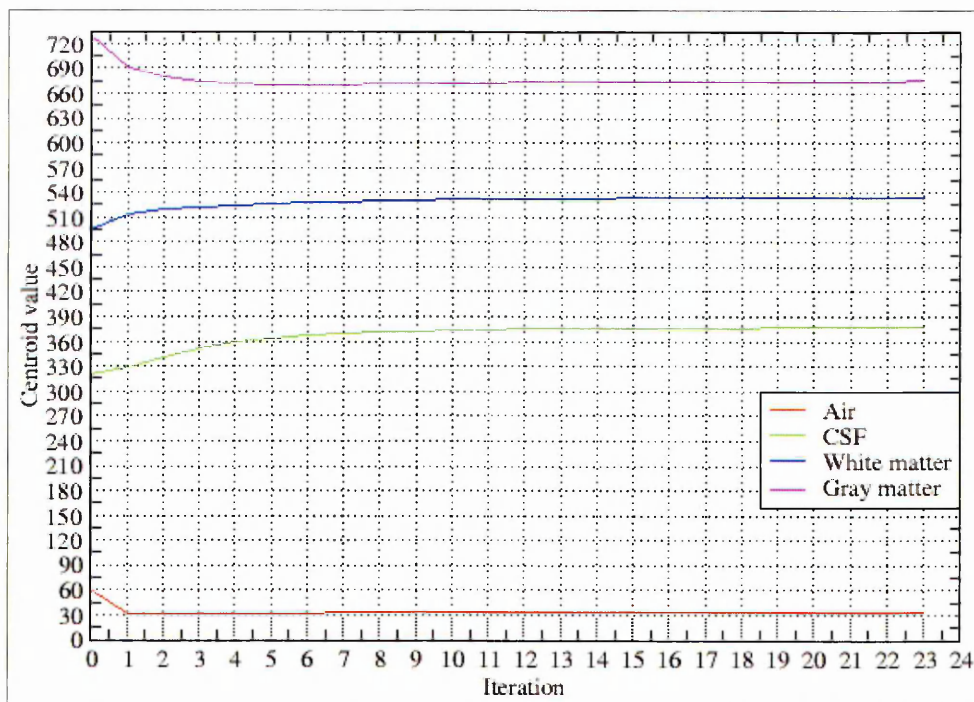
Figure 5.12 - Plot showing the cluster centroid values of the four classes in the PD weighted image slice I0000659, for different iterations.

63
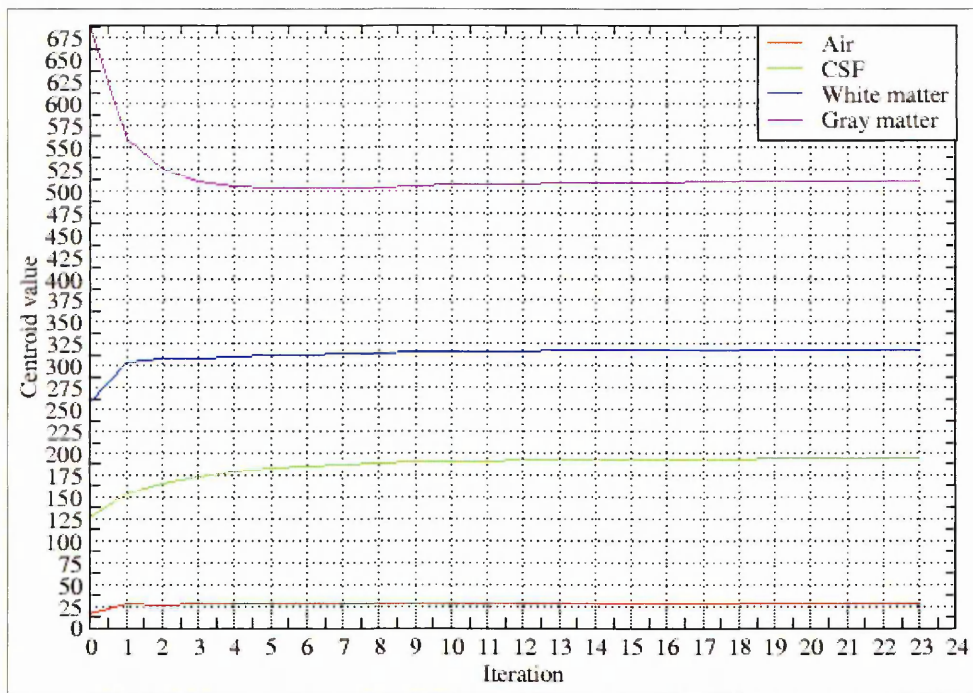
Figure 5.13 - Plot showing the cluster centroid values of the four classes in the T2 weighted image slice I0000660, for different iterations.
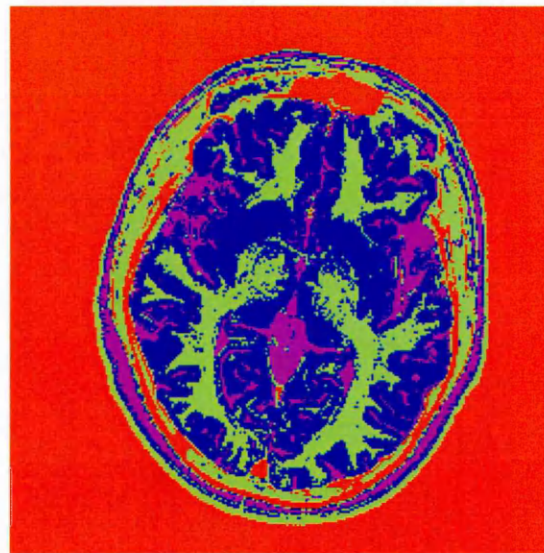
Figure 5.14 - FCM segmentation into four classes viz. Air (Red), CSF (Green), White Matter (Blue), and Grey Matter (Magenta)
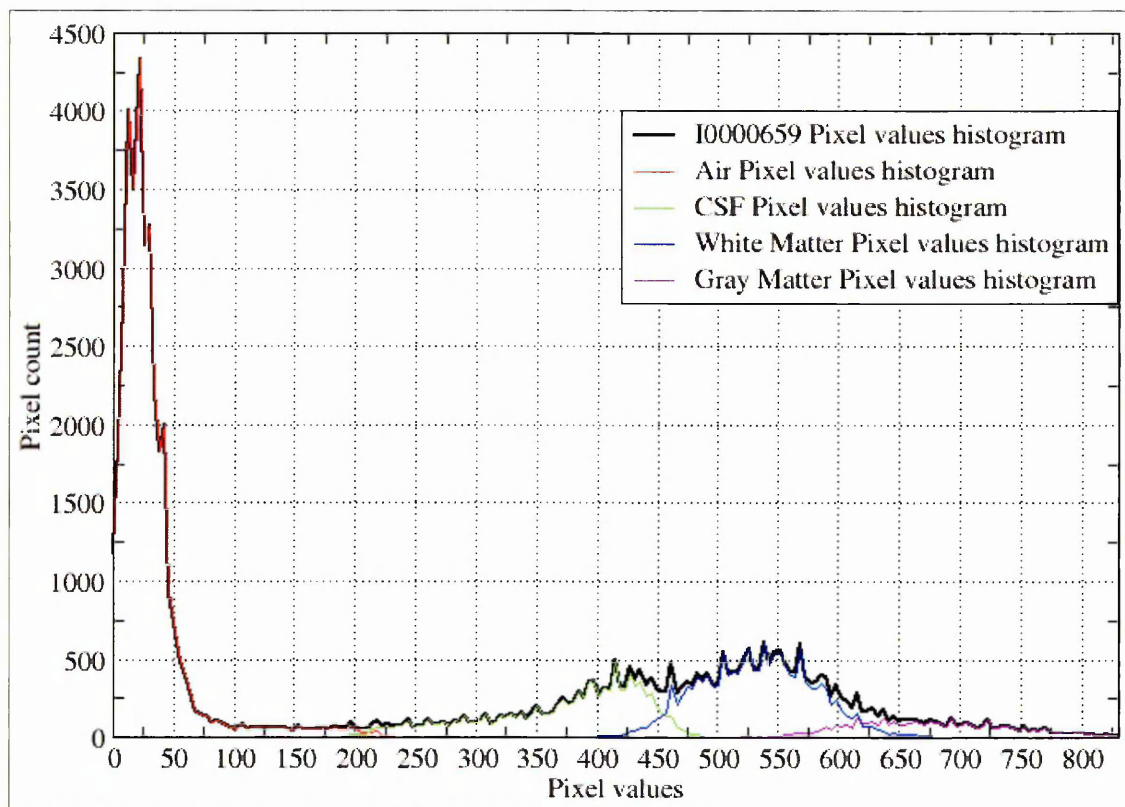
Figure 5.15 - After FCM based segmentation. Distribution of the pixel values of Air (Red), CSF (Green), White matter (Blue) and Grey matter (Magenta) for the PD weighted image slice I0000659.
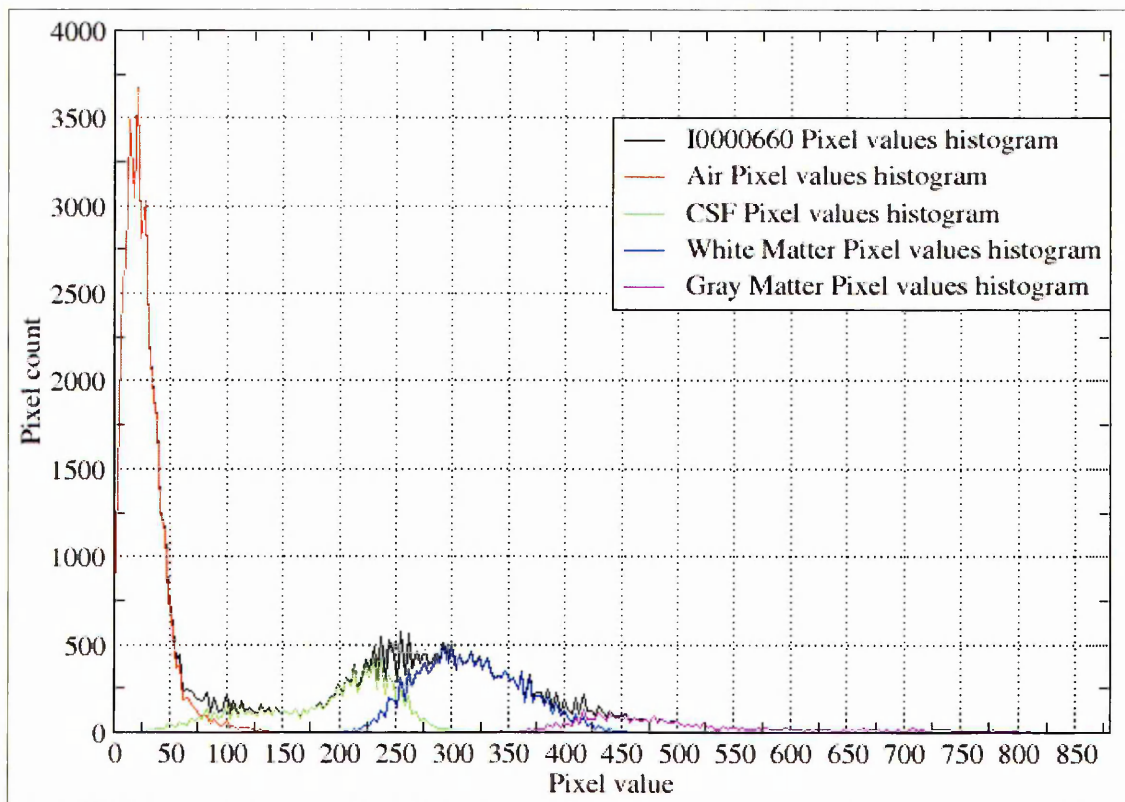
Figure 5.16 - After FCM based segmentation. Distribution of the pixel values of Air (Red), CSF (Green), White Matter (Blue) and Grey Matter (Magenta) for the T2 weighted image slice I0000660.

Figures 5.15 and 5.16 show the distribution of the pixel values within the four different regions *i.e.* Air (Red), CSF (Green), White_Matter (Blue) and Gray_Matter (Magenta), after the FCM based segmentation of the image section I0000659 (PD weighted) and I0000660 (T2 weighted), superimposed on the original values pixel distribution. The overlap seen between the different distributions is due to the fact that information from both the PD and T2 weighted images were used in the FCM based segmentation.

5.2.2.3 Segmentation of MRI Images Using Fuzzy C-Means Based Clustering Class Information

The MRI image section shown in Figure 5.4 (T2 weighted) has an original size of 256×256 pixels. To segment the image using the HCS process requires 65,536 initial clusters. The number of combinations to compare each of the 65,536 clusters with the rest is obtained using expression 5.1 as follows :

$$[65536 \times (65536-1)] \div 2 = 2,147,450,880$$

To reduce the above value, for MRI images, FCM based clustering can be used to identify the pixels belonging to different classes in the image. This class information can be used to achieve an initial classification. The HCS process can be given this prior information about the different tissue types present in the image based on the FCM based clustering.

Table 5.7 lists the pixel distribution values within the four different classes, *i.e.* Air, CSF, White matter and Grey matter, obtained from the FCM based clustering of the MRI image section of Figure 5.4.

Passing the above class information to the HCS process restricts segmentation to within the classes. That is, only intra-class segmentation is performed. The final resulting segmentation, when maximum dissimilarity is allowed between the pixels, will be the same as the the, FCM segmented, class image.

Table 5.7
Distribution of the pixel count for the four classes, *i.e.* Air, CSF, White matter and Grey matter, for the T2 weighted MRI Image slice of Figure 5.4 after FCM based segmentation.

Classes	Number of pixels	Percentage of total volume
Air	35402	54.02
Cerebral Spinal Fluid (CSF)	10647	16.25
White matter	15063	22.98
Grey matter	4424	6.75
Total	65536	100

As the first step of HCS process, initial clustering of the most similar neighbouring pixels was performed for each of the four classes. As detailed in Section 4.3.3 initial clustering was done by comparing the Gray-Tone distribution (GTD) (Section 4.3.1) around each of the pixels within each of the four classes and the most similar neighbouring pixels were clustered together to form the initial set of regions. If the part of the image within a class is homogeneous, with minimal variability, then the GTD around the pixels within the class will be similar and the initial clustering of the most similar neighbouring pixels will result in minimum number of cluster of regions.

The clusters distribution within the four different classes are listed in the Table 5.8. From the values of the number of clusters for the different classes it can be inferred that Air is the most homogeneous class with very little variability and CSF has the highest variability within itself.

Table 5.8
Distribution of the clusters for the four classes, viz. Air, CSF, White matter and Grey matter, for the MRI Image slice of Figure 5.4 after clustering most similar neighbouring pixels.

Classes	Number of Clusters	Percentage of total
Air	97	3.22
Cerebral Spinal Fluid (CSF)	1356	45.08
White matter	800	26.6
Grey matter	755	25.1
Total	3008	100

If the HCS process is restricted to perform the clustering of regions within the tissue type the largest combination of clusters that needs to be evaluated reduces to :

$$[1356 \times (1356-1)] \div 2 = 918,690$$

As detailed in Section 4.3.4 the region merging, of the regions within each of the four classes, was carried out using the agglomerative type of hierarchical clustering process. The dissimilarity between the regions are found based on the dissimilarity between individual pixels of the regions, dissimilarity between the pixels bordering the regions and the dissimilarity between the combined feature property of all the pixels within the regions (Section 4.3.4.1)

A hierarchy of segmentation results was obtained by adopting a dynamic threshold for the allowable dissimilarity measure between merging regions. Figure 5.17 shows the regions present within each of the four classes when the allowable maximum dissimilarity between the regions is 25% of the maximum possible dissimilarity value. Figure 5.18 shows the regions present within each of the four classes when the allowable maximum dissimilarity between the regions is 100% of the maximum possible dissimilarity value.
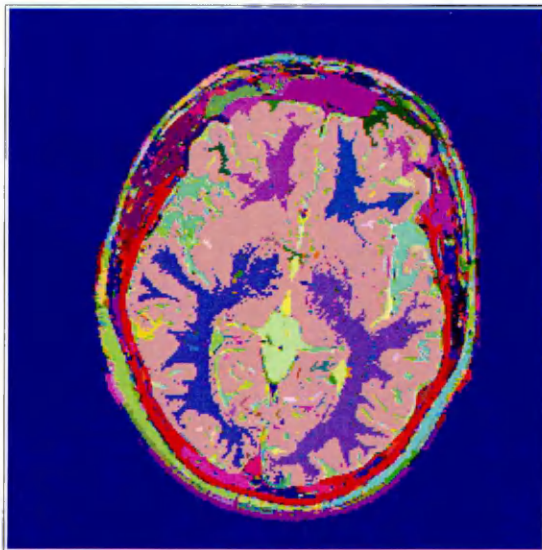
Figure 5.17 - Details of the regions when the dissimilarity between the regions was 25%
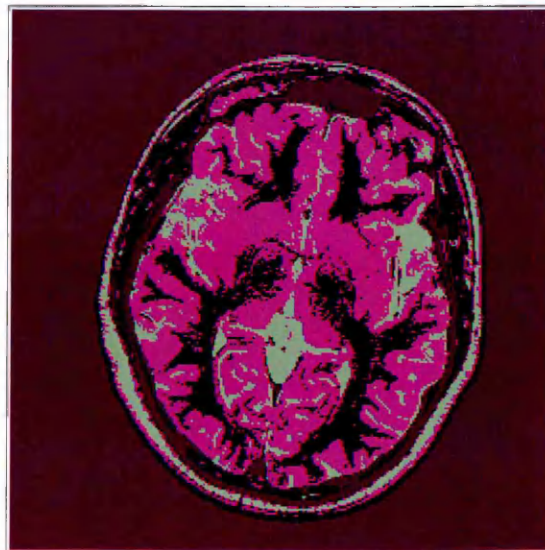
Figure 5.18 - Details of the regions when the dissimilarity between the regions was 100%

When the allowable dissimilarity value between regions is 100% of the maximum possible dissimilarity value all the regions within each of the classes will be combined. Since the HCS process is restricted to perform the clustering of regions only within each of the four classes, the segmentation of the image for 100% dissimilarity (Figure 5.18) could be found to be the same as the initial class image (Figure 5.14) found using FCM clustering.

5.2.2.4 Difficulties in Using FCM Based Clustering Class Information

In using the initial clustering given by the FCM process, the HCS process assumes that within each of the clusters all pixels belong to the same tissue type. FCM's success in clustering the pixels belonging to different tissue types into different clusters depends on the MR signal variability between the different tissue types. But disease affects this variability. For example, previous studies have often found it difficult to distinguish between normal Grey matter and abnormal White matter due to their similar appearance in MRI [Warfield *et al.*, 1999].

To demonstrate the difficulties faced by FCM to segment MR images affected by disease, in this study FCM clustering based segmentation was applied on MR images affected by Parkinson's disease. The PD and T2 weighted MR images are shown in Figures 5.19 and 5.20 respectively.
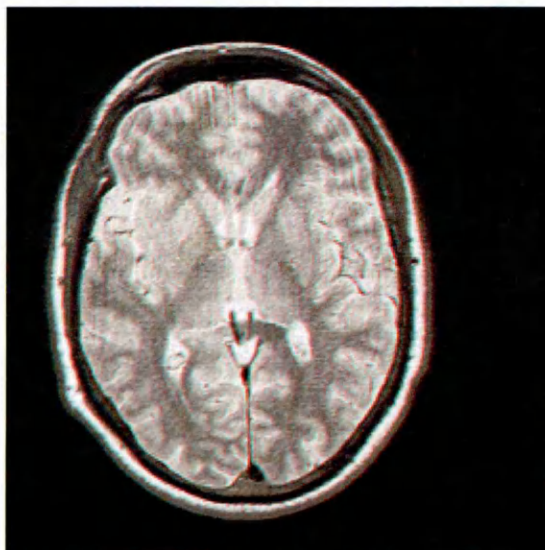
Figure 5.19 - PD weighted Image slice I0000421
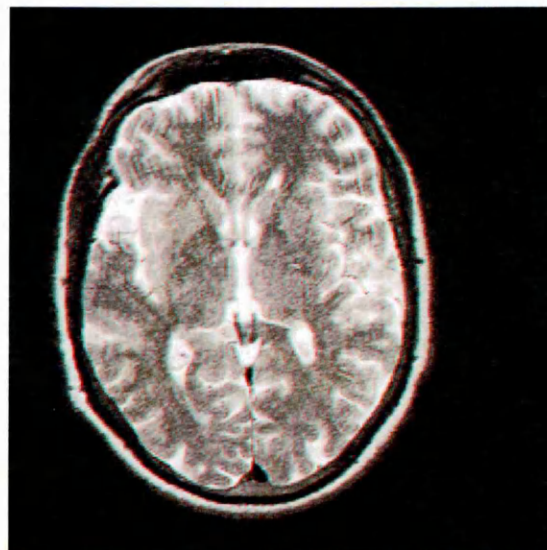
Figure 5.20 - T2 weighted Image slice I0000422

69

The pixel values ranged from 0 to 879 for the PD weighted MR image and 0 to 898 for the T2 weighted MR image. The plots in the Figures 5.21 and 5.22 show the pixel values distributions of the PD (Figure 5.19) and T2 (Figure 5.20) weighted MR images respectively. Comparing the plots, shown in Figures 5.21 and 5.22, with those of the healthy MR image sections, (Figures 5.7 and 5.8), the shapes and the range of the four discernible parts are almost the same. This is also evident by comparing the initial estimate of the distribution of the pixel count for the four classes given in Tables 5.9 and 5.10 with those of the healthy MR image sections given in Tables 5.2 and 5.3.

Table 5.9
Initial estimate of the distribution of the pixel count for the four classes, for the PD weighted MRI image slice of Figure 5.19.

Classes	Pixel value range	Number of pixels	Percentage of total volume
Air	0 to 100	33,706	51.43
CSF	100 to 350	5,733	8.75
White matter	350 to 650	23,491	35.84
Grey matter	650 to 830	2,606	3.98
Total		65,536	100.00

Table 5.10
Initial estimate of the distribution of the pixel count for the four classes, for the T2 weighted MRI image slice of Figure 5.20.

Classes	Pixel value range	Number of pixels	Percentage of total volume
Air	0 to 50	32,526	49.63
CSF	50 to 175	6,704	10.23
White matter	175 to 450	21,844	33.33
Grey matter	450 to 880	4,462	6.81
Total		65,536	100.00
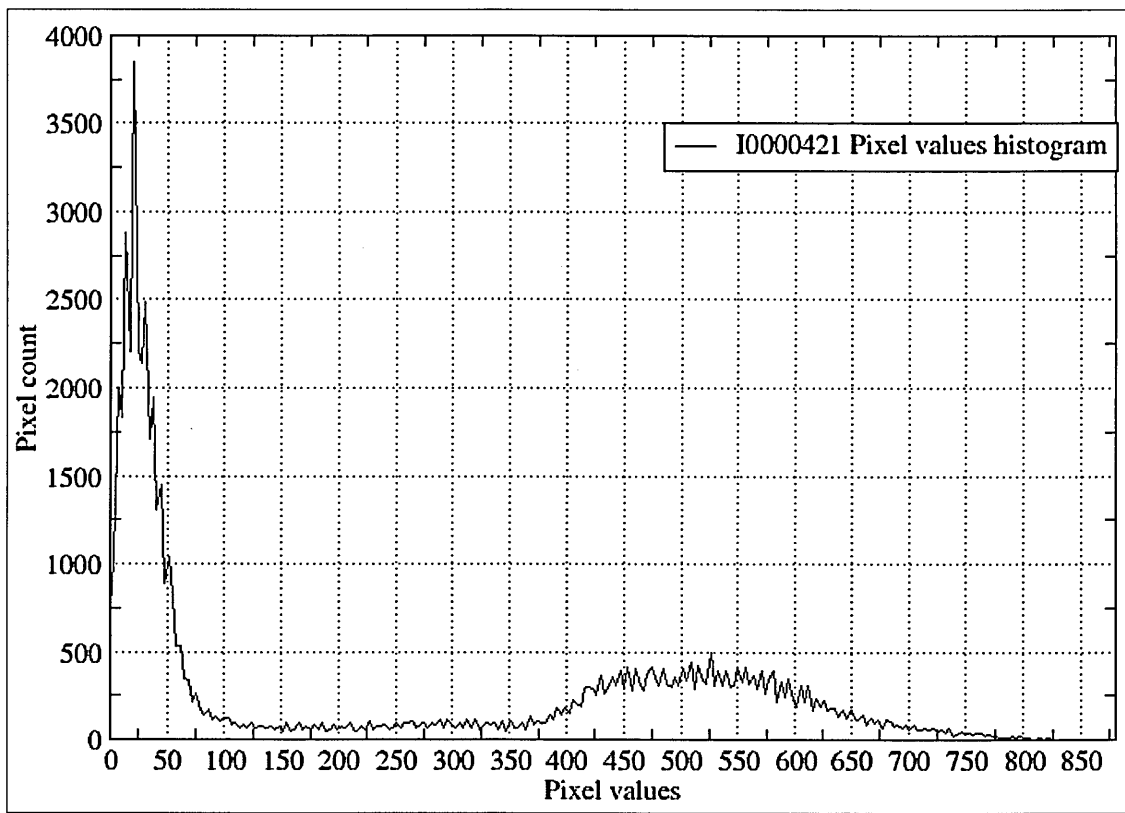
Figure 5.21 - The distribution of the pixel values of the MRI image slice I0000421
(Figure 5.19) (PD weighted)
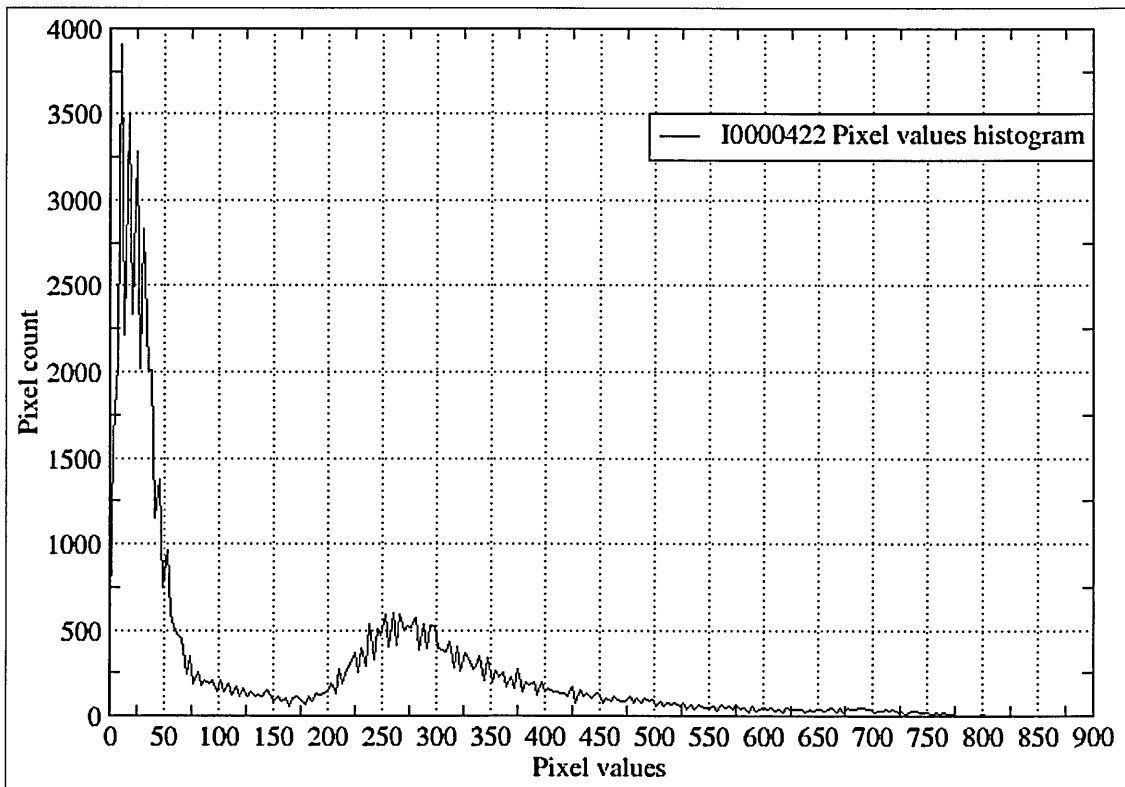
Figure 5.22 - The distribution of the pixel values of the MRI image slice I0000422
(Figure 5.20) (T2 weighted)

Table 5.11

Details of the initial estimate of the four classes' centroids for the PD weighted image slice I0000421 (Figure 5.19)

	Air	CSF	White matter	Grey matter
Pixel Value	15	382	568	674
Pixel Location	23, 25	132, 62	134, 101	110, 138

Table 5.12

Details of the initial estimate of the four classes' centroids for the T2 weighted image slice I0000422 (Figure 5.20)

	Air	CSF	White matter	Grey matter
Pixel Value	45	205	270	682
Pixel Location	23, 25	132, 62	134, 101	110, 138

Tables 5.11 and 5.12 give the details of the initial estimate of the cluster centroid values, for each of the four classes, for the image sections I0000421 (Figure 5.19) and I0000422 (Figure 5.20) respectively.

In Figures 5.23 and 5.24, each of the locations which has the same pixel value as that of the initial cluster centroid pixel value, for the four classes, is marked in colour for the image sections PD weighted (image slice I0000421 Figure 5.19) and T2 weighted (image slice I0000422 Figure 5.20) respectively.

Using the FCM based clustering method, the images were segmented into four different regions (Air, CSF, White matter and Grey matter).

The plot in Figure 5.25 shows the value, for the expression 5.5, for different numbers of iterations. The first iteration value (not shown) was 883.372. It can be seen that it took sixty three iterations for the process to attain a final value of 0.0933016. Comparing this plot with that for the healthy section (Figure 5.11) it can be observed that the latter is smooth and monotonically decreasing but for the former between iterations five and thirty, the value changes very little oscillating between two and three. From iteration thirty one onwards the value starts decreasing again.

Table 5.13 lists the final estimate of the centroid values for the four different classes in the two image slices I0000421 (Figure 5.19) and I0000422 (Figure 5.20).

Figure 5.23 - Start-up class centroid locations marked PD weighted image slice I0000421

Figure 5.24 - Start-up class centroid locations marked T2 weighted image slice I0000422
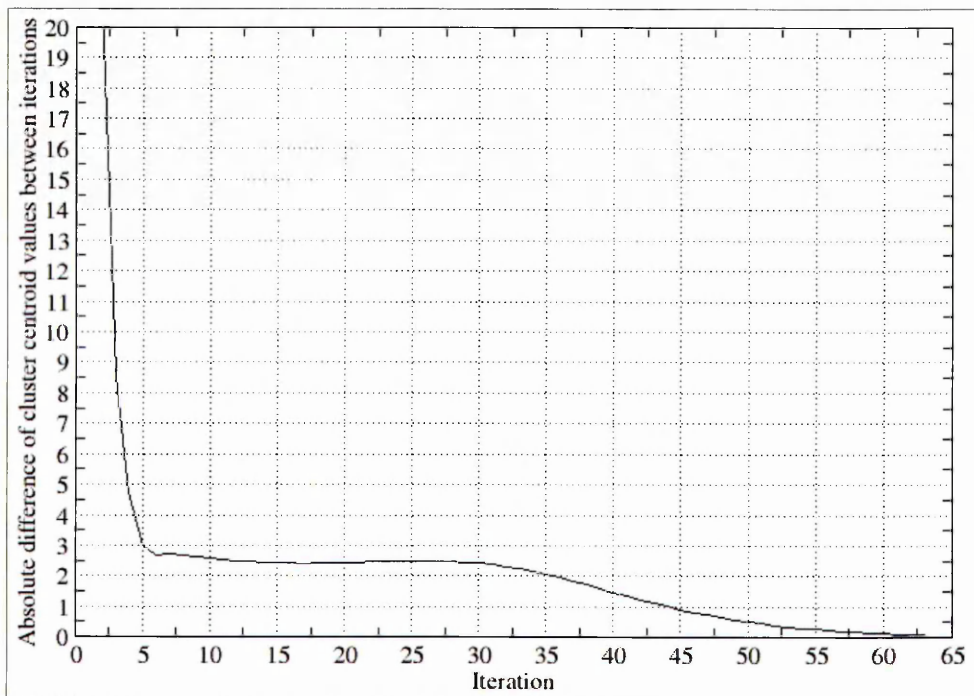
Figure 5.25 - Plot showing the maximum value of the absolute difference (Euclidean distance) between cluster centroid values computed in the previous iteration and those in the current iteration (expression 5.5), for the different iterations.

73

Table 5.13
Details of the final estimate of the four classes' centroids for the image slices I0000421
(Figure 5.19) and I0000422 (Figure 5.20).

	Air	CSF	White matter	Grey matter
I0000421	35.944	306.773	504.712	642.266
I0000422	29.6752	151.157	297.363	524.518

Figures 5.26 and 5.27 show the distribution of the the pixel values within the four different regions, after the FCM based segmentation of the image section I0000421 (Figure 5.19) (PD weighted) and I0000422 (Figure 5.20) (T2 weighted) were superimposed on the original values pixel distribution.
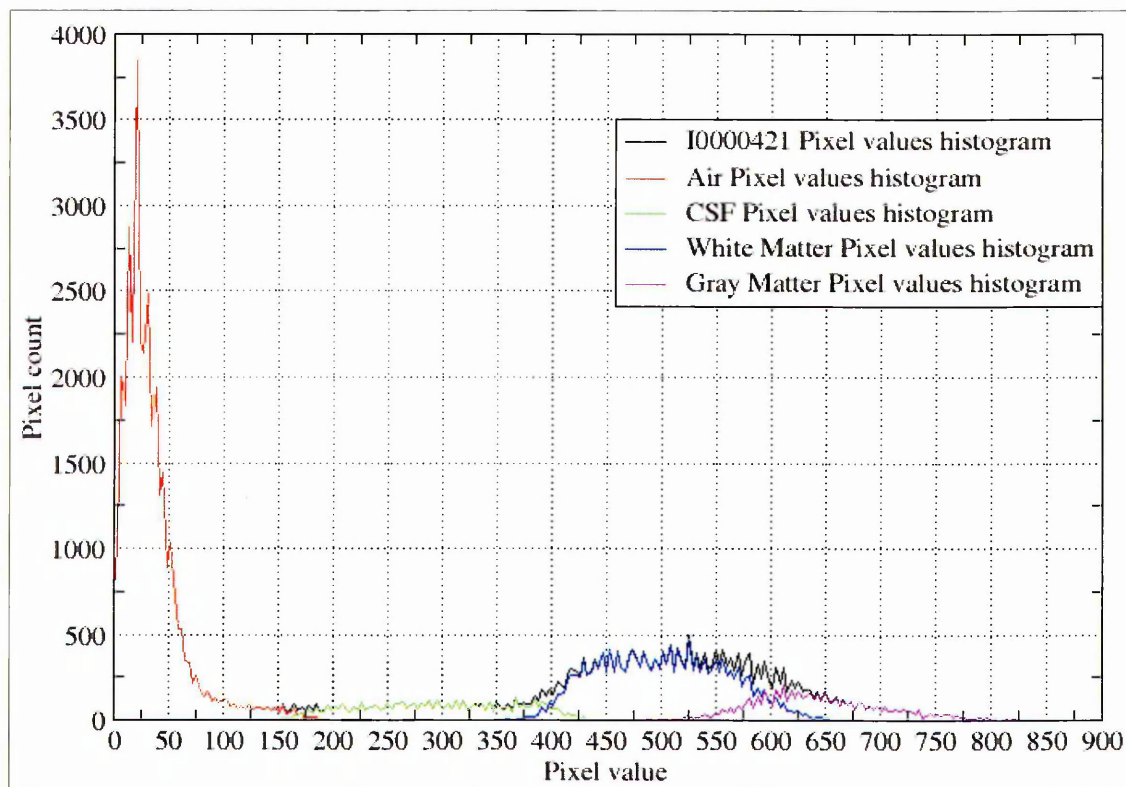
Figure 5.26 - After FCM based segmentation. Distribution of the pixel values of Air (Red), CSF (Green), White matter (Blue) and Grey matter (Magenta) for the PD weighted image slice I0000421 (Figure 5.19).

The FCM clustered four different regions are shown in Figure 5.28. where region types are pseudo coloured. Comparing this segmentation with that obtained for the healthy section (Figure 5.14) it can be seen that CSF (Green) class within the skull is almost non-existent in the segmented diseased section (Figure 5.28).

74
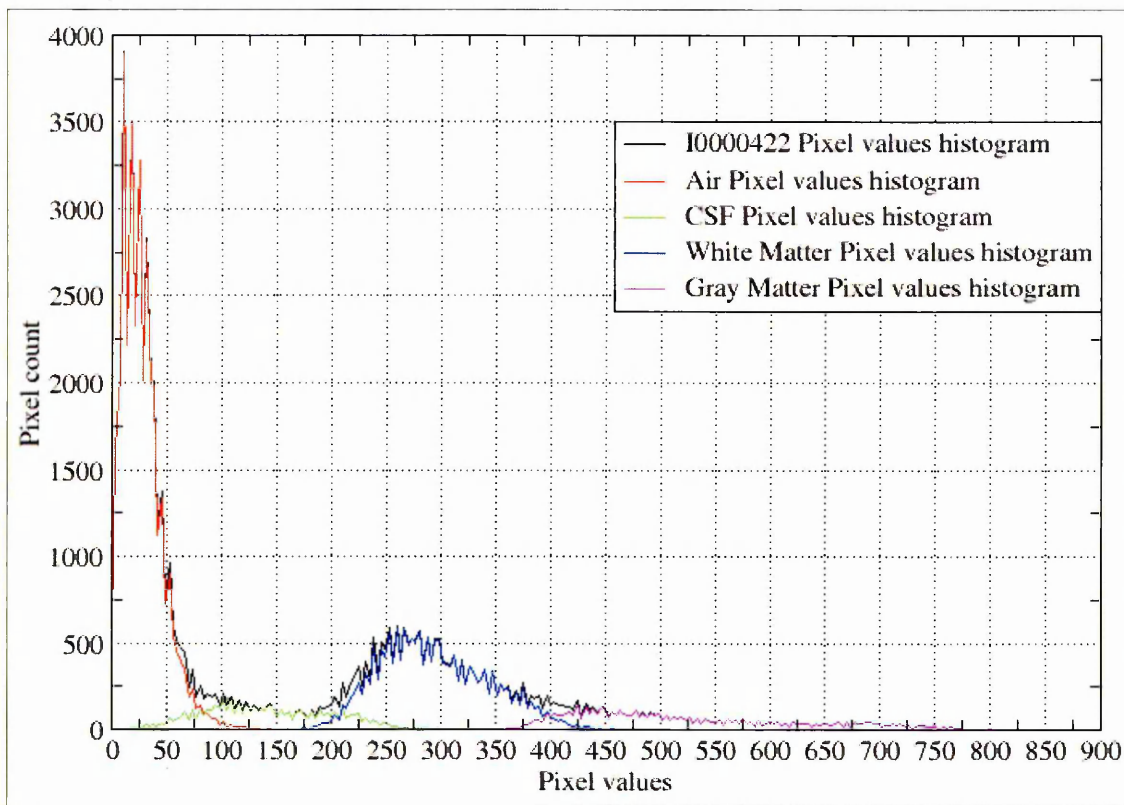
Figure 5.27 - After FCM based segmentation. Distribution of the pixel values of Air (Red), CSF (Green), White Matter (Blue) and Grey matter (Magenta) for the T2 weighted image slice I0000422 (Figure 5.20).
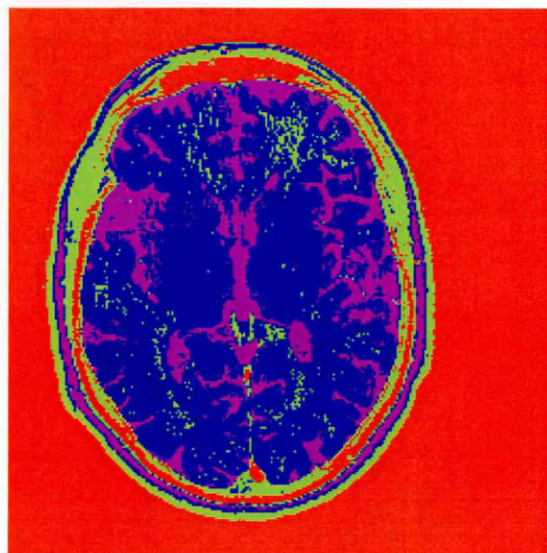

Figure 5.28 - FCM segmentation into four classes viz. Air (Red), CSF (Green), White Matter (Blue), and Grey matter (Magenta)

75

Table 5.14 lists the pixel distribution values within the four different classes, obtained from the FCM based clustering of the MRI image section of Figure 5.20. Comparing these values with that obtained for the healthy image slice, listed in Table 5.5, following observations could be made :

- The volume of the air is almost the same for both the sections.
- CSF volume has almost halved for the diseased section.
- There is a slight increase in the White matter for the diseased section.
- The Grey matter for the diseased section has increased by almost one third.

Table 5.14

Distribution of the pixel count for the four classes, viz Air, CSF, White Matter and Grey matter, for the T2 weighted MRI Image slice of Figure 5.20 after FCM based segmentation.

Classes	Number of pixels	Percentage of total volume
Air	35252	53.7903
Cerebro-Spinal Fluid (CSF)	5700	8.69751
White_Matter	18192	27.7588
Grey matter	6392	9.75342
Total	65536	100

From this segmentation of the diseased MR image, it was found that the FCM clustering process clusters pixels belonging to different classes into the same cluster. This misclassification will affect the performance of the HCS process if intra cluster segmentation was done by the HCS. To avoid this, if it is known which classes have been misclassified by the FCM clustering process, then during the HCS process inter class clustering between those classes can be allowed. This will increase the number of combinations that need to be evaluated but will avoid the error due to misclassification by the FCM segmentation.

Thus it was found that FCM based initial clustering is not always the best solution to solve the combinatorial problem. In this study FCM was not used after this initial investigation. To avoid the combinatorial problem the region of interest based information was used. This is explained in detail in the next section 5.2.3.

5.2.3 Region Of Interest Information

Another way to reduce the combinatorial problem is to restrict the processing of the image to within a region of interest (ROI). The ROI location and size is chosen by an expert based on the information gained from other imaging sources. For example Diffusion weighted MR imaging (DWI) detects alterations in the normal pattern of movement of cellular water due to stroke. DWI is highly sensitive and specific for detecting severely ischemic lesions in the brain [Bihan *et al.*, 2001]. Abnormalities on T2 weighted images do not typically appear until at least 6 hours after symptom onset.[Miller, 2004].

Figure 5.29 shows a Diffusion weighted image where the stroke affected area is clearly visible as white. Figure 5.30 is a T2 weighted image of 512×512 pixels size. To isolate the stroke affected region in the T2 weighted image a ROI is chosen to process only a part of the image. The size and the location of the ROI, in the T2 image, is chosen based on the location of the stroke affected area visible in the Diffusion weighted image.
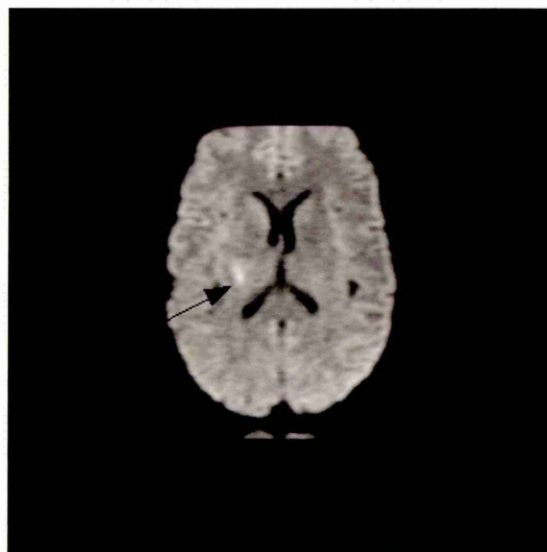
Figure 5.29 - Diffusion weighted image with the stroke affected area visible as white (marked by the arrow head).
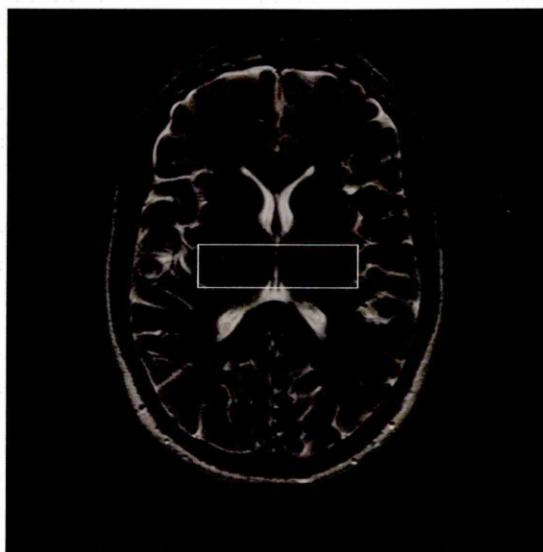
Figure 5.30 - T2 weighted image with the ROI located based on the stroke affected area location in the Diffusion weighted image.

5.2.4 Parallel Calculation

Computer hardware and operating systems have been capable of multitasking for years. Their ability to schedule different tasks (typically called processes) really pays off when separate tasks can actually execute simultaneously on separate CPUs in a multiprocessor system. Although real used applications can be adapted to take advantage of a computer's ability to do more than one thing at once, a lot of operating system code must execute to make it possible. With the advent of threads we've reached an ideal state -- the ability to perform multiple tasks simultaneously with as little operating system overhead as possible [Nichols *et al.*, 1996].

Pthreads is a standardized model for dividing a program into subtasks whose execution can be interleaved or run in parallel. The "P" in Pthreads comes from POSIX (Portable Operating System Interface), the family of IEEE operating system interface standards in which Pthreads is defined. Programmers experience Pthreads as a defined set of C language programming types and calls with a set of implied semantics. Vendors usually supply Pthreads implementation in the form of a header file, which you include in your program, and a library to which you link your program [Nichols *et al.*, 1996].

During the HCS process a major operation is to find the dissimilarity between the existing regions in the image (Section 4.3.4 Region Merging) . Since the estimation of the dissimilarity between different regions is an independent operation, it can be performed in parallel. The part of the program which finds the dissimilarity between the existing regions in the image was parallelised, using Pthreads library, such that the calculation could be done in parallel.

In a dual processor machine, having a pair of Intel™ Pentium-III 500 MHz processors, to process the 64×64 size texture image shown in Figure 6.11, in parallel using two threads, the time taken was 12.25 hours. In the same machine, to process the same image sequentially the corresponding time taken was 16.5 hours. The gain in time, from the sequential operation, when using two threads is only 25 percent. The reason behind this is, only the region merging (Section 4.3.4 Region Merging) part of the HCS process is parallelised. Border pixels reclassification (Section 4.3.5 Border Pixels Reclassification), the other major operation of the HCS process, is not parallelised. Border pixels reclassification is not parallelised because reclassifying border pixels is not an independent operation and hence can be processed only sequentially.

78

5.2.5 Storing Versus Recalculation of Information

The two important pieces of information needed for the HCS process are the similarity between the pixels and the dissimilarity between the different regions. While the similarity between the different pixels is never going to change during the entire operation, the dissimilarity between the different regions will change as the different regions merge. The dissimilarity between the regions that have changed and the remaining regions need to be recalculated.

But, due to the combinatorial nature of the process, the amount of the information that needs to be stored is substantial. For this reason, storing preference is given to information which takes more processing time, like the dissimilarity between regions. Information such as the similarity measurement between pixels is stored only as and when memory becomes available otherwise they are recalculated when required.

The CPU processing time gain between the storing of similarity measurement between pixels versus recalculating the information as and when required was almost 40% for a 3×3 mask size.

For storing, both the similarity measurement between pixels and the dissimilarity between regions, the total memory requirement for a 100×100 ROI during the early stage of the HCS process is around eight gigabytes. In the beginning of the study, the available system memory was limited to only one or two gigabytes of memory. During that period of time the region of interest that could be processed was limited to 100×50 and the similarity between pixel locations were recalculated as and when needed instead of being stored. But later on a system with eight gigabyte of main memory was used which was subsequently upgraded to sixteen gigabyte of memory. This current system could process a ROI of size up to 140×140 with the similarity between the regions as well as between pixel locations being stored.

It should be noted that as and when the regions merge the number of regions in the image is reduced and hence the number of combinations is reduced as well. Moreover there will be no need to store the similarity measurements between pixels which are within the same region, since that information is never going to be needed for the HCS process.

5.2.5.1 Networked Clusters

Cluster is a widely-used term meaning independent computers combined into a unified system through software and networking. At the most fundamental level, when two or more computers are used together to solve a problem, it is considered a cluster. Clusters are typically used for High Availability (HA) for greater reliability or High Performance Computing (HPC) to provide greater computational power than a single computer can provide.

One does not always consider using a cluster to speed-up the computation. One can also use a cluster of computers to enable a job to be done at all. For example when the available system memory was limited to only one or two gigabytes of memory the region of interest that could be processed, using HCS, is limited to 100×50 using a single computer. And if one need to process a larger ROI, since the amount of memory available in a single motherboard is limited, a cluster of machines can be used to augment the total memory.

Latency, which is the delay between the instant a CPU requests a piece of information and the time the information starts to become available, is 40-80 nano second to fetch data from a local memory when opposed to 5-50 micro second across the network [Brown, 2004]. Hence the transfer rate of information between a network of computers is significantly lower than that achieved on a single computer's motherboard. Since larger capacity memory modules are now available, there is no further advantage of using a computer cluster for memory intensive computing. Using a system memory of 16 gigabyte, an ROI of size up to 140x140 was processed successfully.

5.3 Graphical User Interface

The graphical user interface developed as part of this study served two main purposes :
- To optimally display 12-bit medical image data.
- To display the hierarchy of segmentation results produced by the HCS process.

5.3.1 GUI Facility For Displaying Medical Image Data

The availability of digital medical imaging sources like Computed Tomography (CT), Magnetic Resonance Imaging (MRI) and Ultrasound (US) and the use of computers to process the images led the American College of Radiology (ACR) and the National Electrical Manufacturers Association (NEMA) to form a joint committee to create a standard method for storage and transmission of medical image information. The committee created a standard called Digital Imaging and Communications in Medicine (DICOM) to simplify the distribution and viewing of medical images, such as CT scans, MRI images, and ultrasound images. The GUI designed for this study reads in medical image data written in DICOM format. The medical image data generated by CT and MRI is normally 12-bit data stored in two bytes. This produces a gray-scale range of 0 to 4095, but in graphical displays where the primary colours, Red, Green and Blue are represented in 8 bits, only 256 levels of gray-scale can be displayed at any one time. Hence a suitable method needs to be designed to map the 4096 different values to the available 256 levels for displaying purpose.

5.3.1.1 GUI Facility For Displaying CT Medical Image Data

Computed Tomography (CT) imaging is based on X-ray attenuation of various tissues. The digital value assigned to each pixel is called the Hounsfield value (HU) which lies on a scale where pure water has a value 0, air has a value of (-)1000, bone has a value of the order of (+)1000 [Albertyn and Brown, 1996]. Thus a CT image can potentially have up to 2000 different Hounsfield values stored as 16 bit data. But a computer monitor can display only 256 different shades of gray, at any one time. The technique of windowing is an electronic manipulation of the data to enable these 256 shades of gray to be used to represent a limited range, or window, of Hounsfield values.

Traditionally due to the cost involved in producing hard copies (film based), standard window settings were used to map the 2000 possible Hounsfield values to 256 gray values. Previous studies have evaluated the appropriate window setting for producing hard copies pertaining to specific clinical applications [Brink, 1999], [Mayo-Smith *et al.*, 1999].

Until the last half-decade interpreting CT images was based solely on hard copies of the images. With the recent availability of powerful graphical workstations soft copy (electronic) evaluation of the images is replacing the role of hard copy interpretation [Johnson, 2003]. The possibility of directly interacting with the original 16 bit data gives the radiologists the freedom to set the window settings interactively. Studies have assessed the clinical significance of using variable window settings in soft copy interpretation [Lev, 1999].

The graphical user interface (GUI) designed in this study augments the diagnostic value of the CT image data by optimally mapping the range of data values to the available 256 gray level values. In the medical imaging community the windowing parameters are referred to as 'window centre' (C) and the 'window width' (W) of an image. Narrowing the window or compressing the gray scale increases contrast for the purpose of visual perception [Albertyn and Brown, 1996]. Conversely, widening the window will increase the range of Hounsfield numbers displayed in a single shade of gray.

Computed tomography (CT) produces images with a very wide dynamic range. As such, linear intensity window setting techniques must be used to view CT images to provide adequate contrast and detail within specific imaged tissues [Barnes, 1992], [Gomori and Steiner, 1987]. In the case of a CT scan of the chest, CT images are viewed three times, with window settings specific for bone, soft-tissue, and lung detail. The process of selecting window settings and interpreting resultant windowed CT images is time-consuming, even with the advent of digital imaging and display, which allow window settings to be varied rather quickly at an interactive console [Fayad *et al*. 2002].

The images shown in Figures 5.31 and 5.32, illustrate the effect of changing the window settings with linear mapping. Figure 5.31 is a display with a narrow window setting (width 66 HU units, centred at 38 HU unit). This image shows the intracranial tissues quite clearly but the subdural haematoma, shown in white, is indistinguishable from the cranial bone. Figure 5.32 is a display with a wide window setting (width 2126 HU units, centred at 552 HU unit). The image clearly distinguishes the subdural haematoma (marked by the arrow head), but with a complete loss of contrast among intra cranial tissues.

Linear window mapping is useful if one knows what to look for. However to obtain an overall view of the CT image data before choosing a specific range of Hounsfield values, it is necessary to display a wide range of the values optimally using the limited range of available 256 gray scale values.
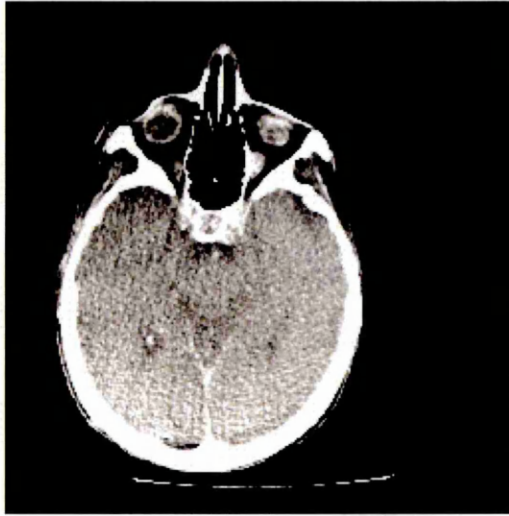
Figure 5.31 - Linear mapping of the Hounsfield values for a window setting width 66 Hu units, centred at 38 Hu unit.

Figure 5.32 - Linear mapping of the Hounsfield values for a window setting width 2126 Hu units, centred at 552 Hu unit.

There has been a previous study to design an appropriate non-linear mapping function to optimally display different tissue types using the same window settings [Jin *et al.,* 2002].

To fit a wide range of Hounsfield values into 256 shades of gray, the GUI designed in this study uses a technique known as equal-probability quantizing [Haralick, 1973]. Equal-probability quantising is an alternative technique that is particularly attractive for distributing the Hounsfield values. The equal-probability quantising technique consists of computing the frequency of occurrence of all allowed Hounsfield values (within a window). If Hounsfield values in a certain range occur frequently, while others occur rarely, the quantisation levels are finely spaced in frequently occurring range and coarsely spaced outside it. In some literature equal-probability quantising method is sometimes referred as tapered quantisation [Gonsalez, 1992].

83

Figure 5.33 illustrates the advantage of using equal-probability quantisation method for mapping the range of Hounsfield values onto the display values. The image is displayed with a wide window setting (width 2126 Hu units, centred at 552 Hu unit). Unlike in the case of linear mapping, Figure 5.32 the image in Figure 5.33 clearly distinguishes the subdural haematoma as well as the intra cranial tissues.

Figure 5.33 - Equal-probability quantizing based mapping of the HU values for a window settings width 2126 HU units, centred at 552 HU unit

The GUI, designed and implemented in this study, provides the facility for the user to interactively choose the window settings. It also provides the facility for linear as well as non-linear mapping of the image data to the chosen window settings.

Most CT machines have a region of interest (ROI) capability allowing the user to define a small area of interest on the screen. The CT machine then displays the average Hounsfield value of all the pixels contained within the ROI box [Albertyn and Brown, 1996]. To provide a similar facility the GUI also provides the user with a region of interest (ROI) facility. Within a given ROI, the GUI calculates the maximum, minimum and average pixel values and displays the information for the user (Figures 5.34 and 5.35). Further details of ROI facility are described in Section 5.3.1.2.

5.3.1.2 Details of the GUI Facility For Displaying Medical Image Data

The image viewing and quantisation GUI facility designed and implemented in this study has the following facilities :

- Side by side image display

  This facility allows the user to have the same image quantised using different window settings displayed side by side for comparison. The user could also display, side by side, images of different modality where in one of the image the diseased area is clearly visible (Figure 5.34).

- Dual interactive cursor

  Dual cursors are useful for comparing relative pixel values of the same image quantised for different window settings.

  Dual cursors are also useful in situations where a diseased area clearly visible in one modality image need to be marked onto another modality image (Figure 5.34). By displaying the images side by side and making use of the dual cursor, one for each image, the user could outline the suspected area on the image where it is not very obvious guided by the location of the suspected area clearly visible on the other image.

- Slider facility to interactively set the image quantising window width and centre. The slider gives a visual control to interactively set the quantising window width and centre parameters and view the original image under varied quantised settings and scrutinise the image for diseased areas which might get accentuated.

- Using region of interest (ROI) marking facility, the user could annotate a part of the image by outlining a ROI enclosing the area (Figure 5.34)

- Image statistics, within the Region of interest (ROI), viewing facility. Using the ROI facility the user could find the image data statistics within a specific area of the image (Figure 5.35). The image data statistics within a ROI might help the user to set the quantising window parameters values to enhance that part of the image within the ROI.

- Image saving facility. The user could save the quantised and/or ROI marked images for future reference.

Figure 5.34 shows a screen shot of the GUI. Two images of different types of MRI images are displayed side by side. The image on the left screen is the Diffusion weighted MRI image and the one on the right is the T2-weighted MRI image. In the

85

Diffusion weighted image (image on the left screen), the stroke affected area is clearly visible in white, (indicated by the black arrow head).
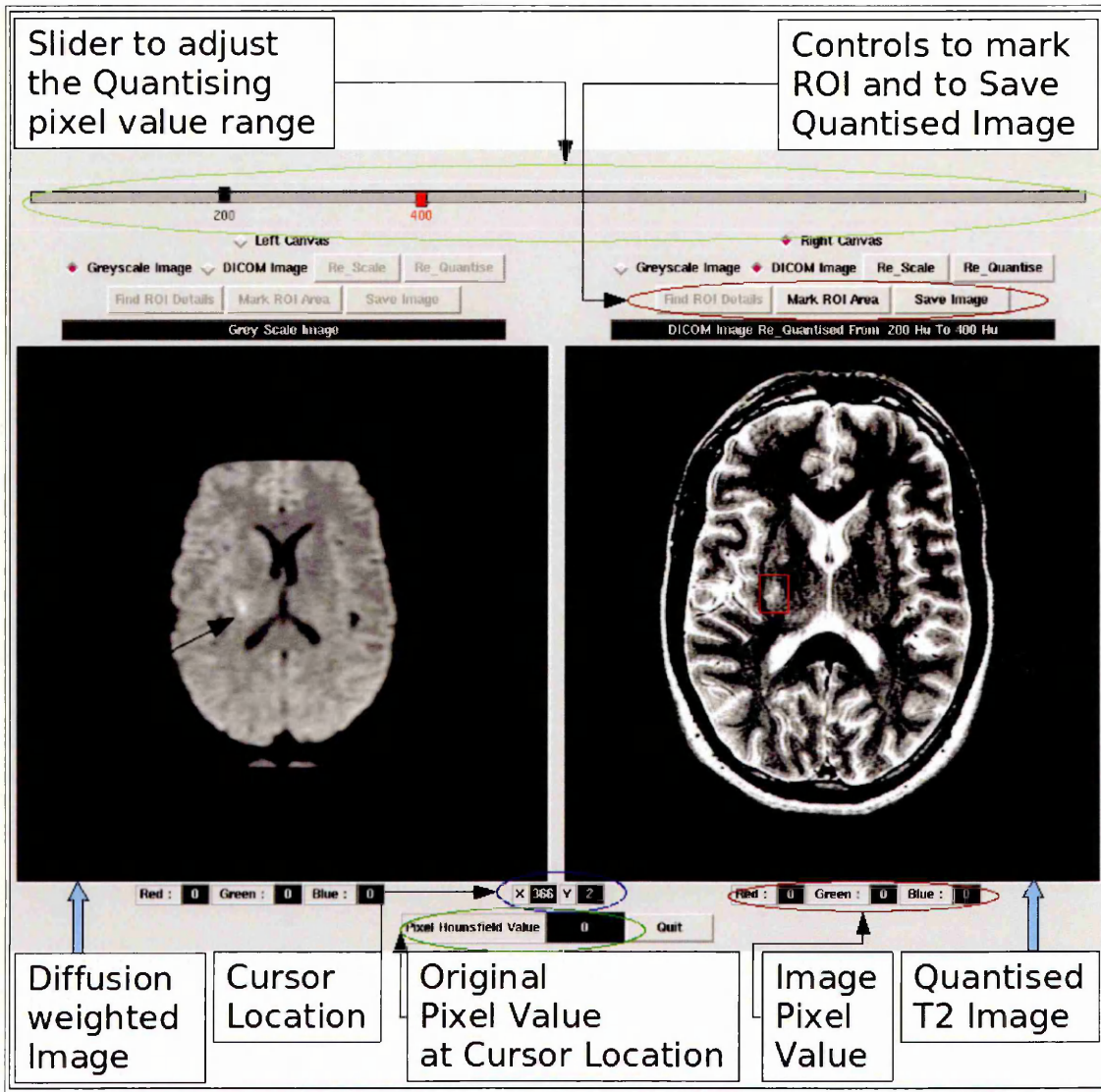
Figure 5.34 - Graphical user interface facility to compare images of different modalities and to accentuate disease affected area using equal-probability quantising method.

Total_No_Pixels	1036	No_Of_Unique_Values	205		
Minm_Value	186	Maxm_Value	430	Avg_Value	280

Figure 5.35 - Statistics of the image data values within the ROI marked by the user.

Making use of the dual cursor facility, the user is able to draw a ROI (outlined in red) around the corresponding area in the T2 weighted image as shown in Figure 5.34. Using the ROI facility the user can find the image data values statistics within the marked ROI as shown in Figure 5.35.

Using the ROI facility to find the image data statistics within a area of the image has an important role in setting the window width and centre parameters for quantising MRI images. This is because for CT images the window parameters could be set using the Hounsfield standard values for different tissue type (see Section 5.3.1.1). However for MRI images no such standard exists and hence the window parameters, for quantising MR images, need to be decided corresponding to each image.

From the statistics of the image data values (Figure 5.35), within the ROI marked the quantising window parameters, of window width 200 centred at 300, were chosen. Using the slider facility (Figure 5.34) to adjust the quantising window parameters the T2 weighted MR image was quantised using equal-probability quantising method.

The area affected by stroke was accentuated in the T2 weighted MR image (outlined in red in Figure 5.34). The locational correspondence of the accentuated area with the stroke affected area visible in white in the diffusion weighted MR image could be confirmed using the dual cursor facility.

Images in Figures 5.36 to 5.38 demonstrate the advantage of using the equal-probability quantisation method and the usage of correct window settings, obtained from the statistics of the image data, to accentuate the diseased area in MR images (Refer Section 6.3.1.1 also).

Figure 5.36 shows the T2 weighted MR image quantised using linear quantisation for a wide window setting of width of 1340 centred at 670. The diseased affected area, indicated by the green arrow head, could hardly be visualised.

Figure 5.37 shows the same T2 weighted MR image, quantised using equal-probability quantisation for the same wide window setting of 1340 centred at 670. The diseased affected area, indicated by the green arrow head, could be visualised better than in Figure 5.36.

Figure 5.38 shows the same T2 weighted MR image, quantised using equal-probability quantisation for a narrower window setting of width 200 centred at 300. The diseased affected area, outlined in red, is well accentuated and could be visualised better than in Figure 5.37 and far better than in Figure 5.36. This is further confirmed in Figure 5.39 where the infarct affected area had been isolated using the HCS process.
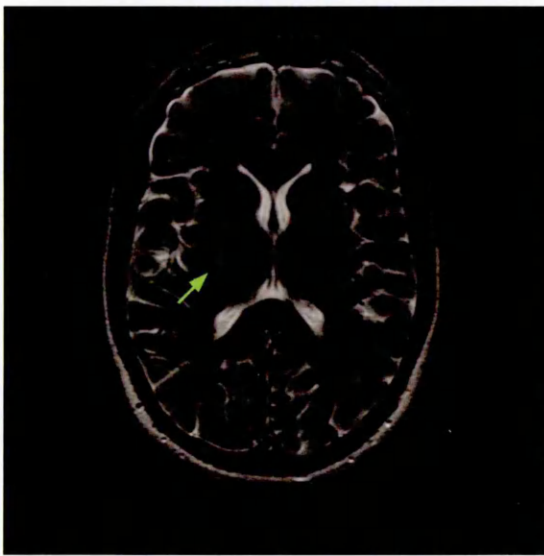
Figure 5.36 - T2 weighted MR image quantised using linear quantisation method for a wide window settings.
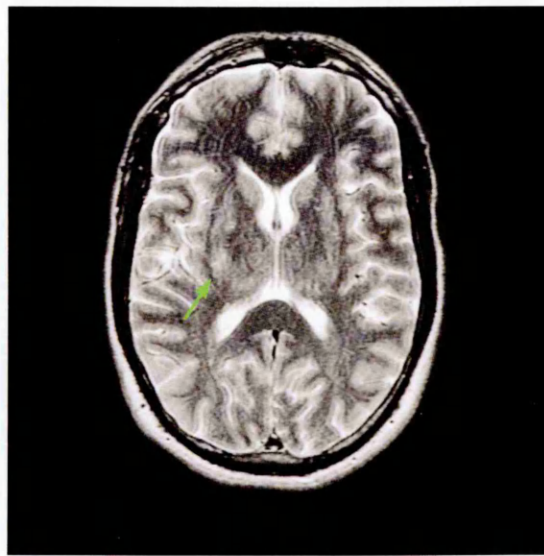
Figure 5.37 - T2 weighted MR image quantised using equal-probability quantisation method for the same wide window settings as in Figure 5.36.

Figure 5.38 - T2 weighted MR image quantised using equal-probability quantisation method for a narrow window setting.

Figure 5.39 - Pixels belonging to the infarct isolated by the HCS process.

This example clearly demonstrates the advantage of the choice of equal-probability method and the importance of choosing the correct windowing parameters for

quantisation. From this discussion it could be inferred that the equal-probability method along with the GUI will facilitate detection of hard to visualise infarct condition. Hence it could be concluded that equal-probability based quantising method along with the GUI, could be used by the neuroradiologists for scrutinising MRI and CT scans.

5.3.2 GUI Facility For Displaying Hierarchy of Segmentation Results

The Hierarchical Clustering based Segmentation (HCS) designed and implemented in this study generates a hierarchy of segmentation results. The hierarchy of segmentation results associated with the dissimilarity values is generated and stored at the end of the HCS processing.

Once the segmentation is performed, the GUI can be used to reproduce the resulting segmentation images associated with a dissimilarity value instantaneously. Making use of the GUI, the user can inspect how the merging process evolves and associates the unique regions at any level with the different types of patterns present in the image. The users can interactively choose the dissimilarity level at which they want to view the segmentation results. When choosing a low value of dissimilarity, the image will show many varied regions similar to the original image. When choosing a high value of dissimilarity the image will only show regions that are significantly different.

The original image may be displayed alongside the processed image showing regions of dissimilarity. A dual cursor facility provided by the GUI allows the user to correlate the segmentation results with the original image data. This enables the clinicians to improve their ability to identify regions that have subtle differences or dissimilarities.

The GUI also helps the user to differentiate dissimilarities in the image down to a single pixel level by providing the clinicians the facility to highlight pixels belonging to the same region which might occur across the image.

The GUI is designed in such a way as to make it easy for the user to view all the different solutions and select the most suitable. This is achieved by the GUI by having the following facilities :

- The different segmentation results can be viewed by using a scroll bar. The divisions in the scroll bar are the percentage of the maximum possible allowable dissimilarity measure between the different regions in the image.

89

- Individual region properties like the number of pixels, the lowest, highest and average pixel value and the distribution of the pixel values within the region can be scrutinised.
- The original image or another segmented image at different level of dissimilarity can be compared with the segmented image by displaying them alongside each other and a dual cursor moves simultaneously on both images.
- In order to allow the users to quickly display segmented image the GUI provides a gallery of the set of segmented images. The user can click on any one of the thumb nail images to have it displayed on the main window. Figure 5.40 shows a gallery of thumb nail images. These images display the different regions found by the HCS process for a set of allowed dissimilarity measure between the regions in the image.
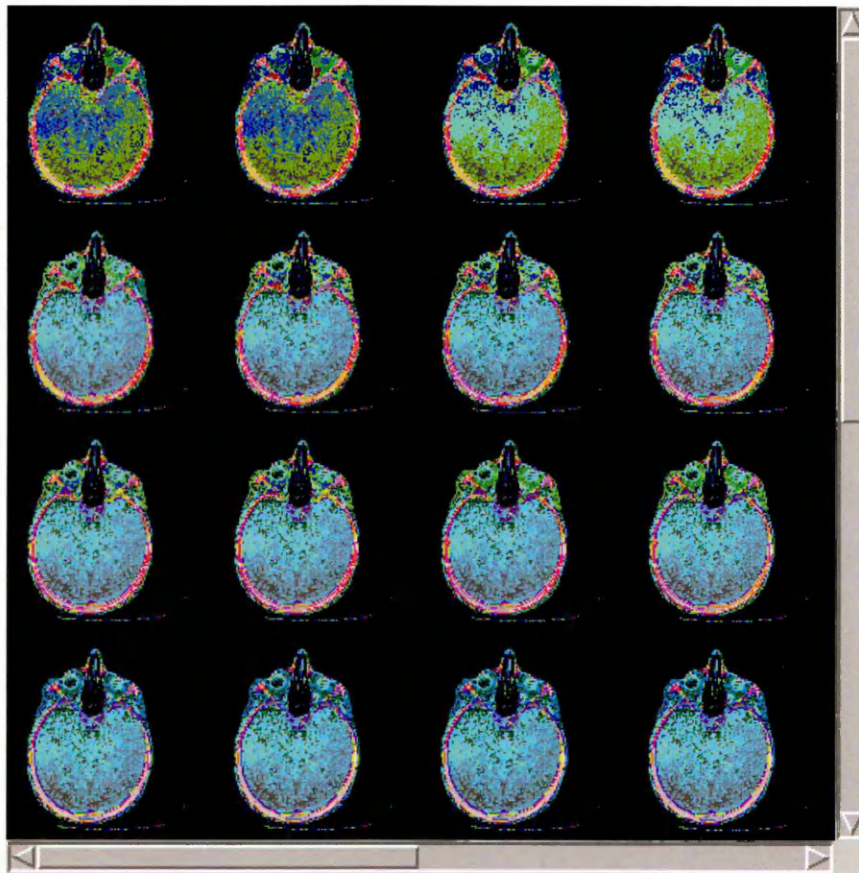
Figure 5.40 - A gallery of thumb nail size segmented images.

Figure 5.40 shows a gallery of segmentation results for a set of allowed dissimilarity measure between the regions in the image. Using the gallery of segmentation results, the user has an overall view of the results available at a glance. Figure 5.41 is a snap shot of the GUI, showing the user controls provided.

90
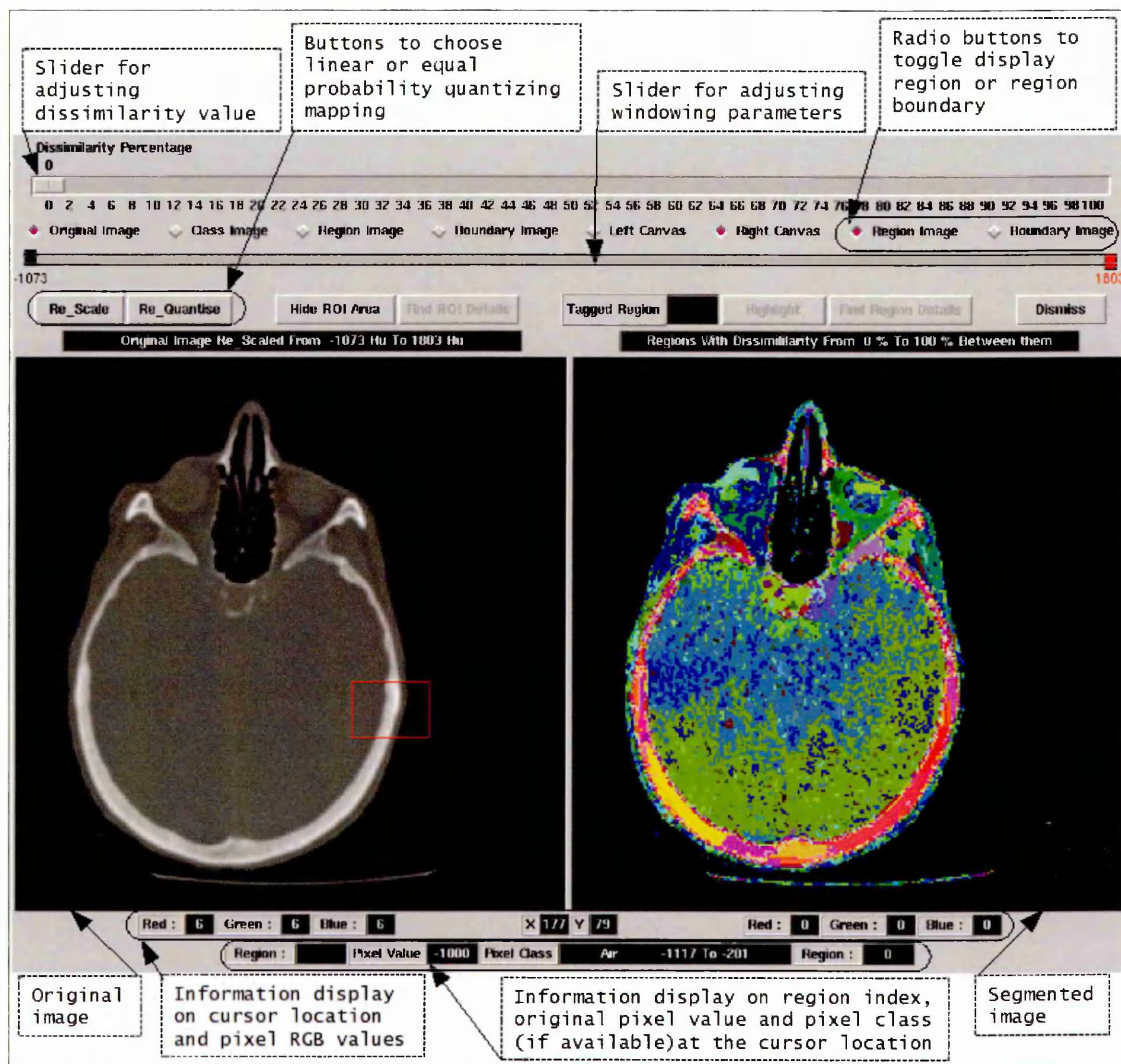
Figure 5.41 - Annotated screen shot of the GUI, to look at the HCS output.

Figure 5.41 shows the different controls of the GUI. It shows an original image along with the segmentation results beside it. The major controls provided by the GUI are :

- The pair of sliders provided for adjusting the windowing parameters can be used to adjust the range of the original pixel values that will be displayed (making use of the 256 display levels).

- To map the original pixel levels to the available 256 display levels, either linear or equal probability quantising method, can be used by pressing the appropriate buttons.

- The slider for adjusting the dissimilarity level can be used to display the segmentation result corresponding to the dissimilarity level at the slider location.

- The segmentation results can be seen as regions or as boundaries of the regions drawn on the original image, by choosing either of the radio button.

- At the bottom of the images, there are display boxes where the actual pixel values of the image and the region index, at the cursor location, are displayed.

91

5.4 Summary

In this chapter following implementation details of the HCS process were discussed :

- Optimisation techniques
- GUI to display quantised medical image data and the HCS process results.

Under the optimisation techniques the following ways of reducing processing time were discussed :

- Performing an initial clustering, making use of the information specific to a class of images for example using the Hounsfield Unit values for the CT images.
- Performing an initial clustering, making use of the segmentation techniques like FCM clustering.
- Identifying a region of interest and have the HCS process applied only within the ROI.
- Parallelising those parts of the process which could be evaluated in concurrent.
- Depending upon the available memory, storing relevant information which is not going to change, instead of recalculating them.

In the current implementation of the HCS process, all the above optimization techniques were implemented and tested for their performance. It was found that FCM clustering was suboptimal in segmenting MR images affected by physlogical conditions like Parkinson's disease.

The functionalities provided by the developed GUI for quantising medical image data and to view the HCS process segmentation results were discussed in detail.

Chapter 6

Performance Analysis of Hierarchical Clustering Based Segmentation

6.1 Introduction

The Hierarchical Clustering Based Segmentation (HCS) process, developed in this study, is a modular process consisting of the following major operations (for details refer Section 4.3) :

- Feature measurement
- Pixel pair similarity measurement
- Initial clustering of the most similar neighbouring pixels
- Regions merging
- Border pixels reclassification

The modular framework, of the HCS process, makes it possible to make use of the most appropriate implementation of the different modules to suit the problem that needs to be solved. In this chapter, with the help of suitable test cases, the performance of the different implementation of the modules, in achieving the objectives of the study, will be evaluated.

6.2 Feature Measurement Performance

The success of any subsequent clustering or merging process is affected by the method by which the property of the individual pixels is found. The feature measure, which quantifies the property of the individual pixels, should yield regions such that the dissimilarity among the pixels within the regions is low and the dissimilarity among the pixels between the regions is high.

In the following section it will be shown that the performance of the Gray Tone Distribution (GTD) feature measure, which is one of the novel aspect of this study, is well suited for segmentation of tonal and micro-texture images.

93

6.2.1 Gray Tone Distribution (GTD) Feature Performance

In this section, making use of sample test images, the following capabilities, of the GTD feature will be demonstrated :

- Capability to precisely identify the boundary between the different regions in an image.
- Capability to highlight the constituent regions within a textured area.
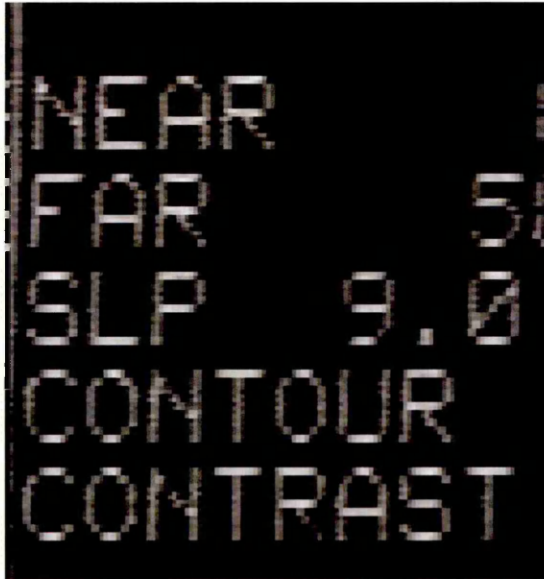
Figure 6.1 - A tonal image
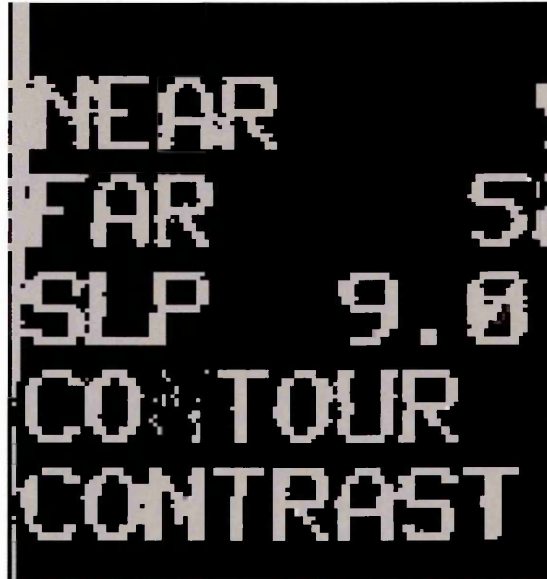
Figure 6.2 - Segmentation output of the tonal image

Table 6.1
Statistics of pixel values for the tonal image of Figure 6.1

Minimum	Maximum	Average	Standard deviation
0	255	125	72.26

6.2.1.1 Tonal Image Segmentation

Figure 6.1 shows a predominantly tonal image of size 127×142 pixels. As shown in Table 6.1 and Figure 6.3, within the image there is quite a wide variation of the tonal values. But since there is no repetitive pattern in the image, it is tonal rather than textured.

94
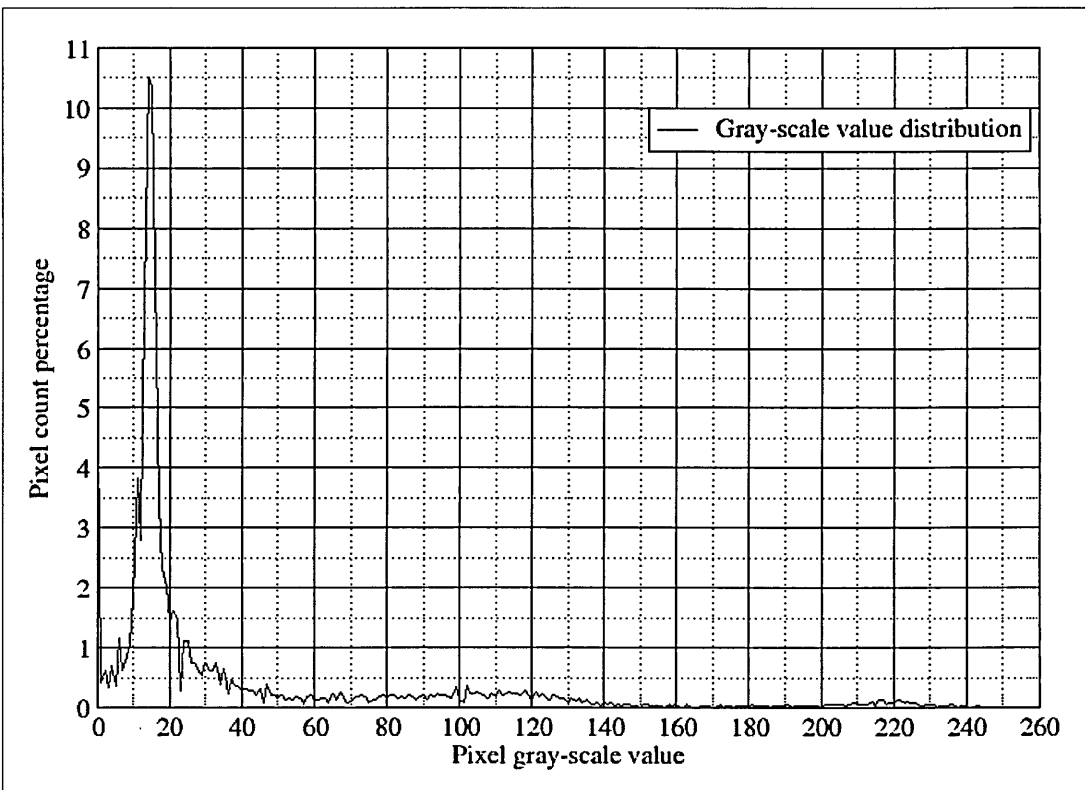
Figure 6.3 - The pixel values distribution for the tonal image of Figure 6.1.

The segmentation results of Figure 6.2 demonstrates the following capabilities of the Gray Tone Distribution (GTD) feature :

- Accurate delineation of regions which are of size just few pixels.
- Highlighting subtle difference in tonal distribution.

The GTD feature is an important attribute because it allows border pixels to be accurately delineated from the different regions in an image. This is clearly demonstrated in the process of segmenting the tonal image shown in Figure 6.1. From the segmentation result shown in Figure 6.2, it can be seen that all the characters are merged as belonging to the same region (pseudo coloured as white).

From the above results it is confirmed that the GTD feature is well suited to accurately delineate regions which are hardly a couple of pixels wide. For this reason the GTD feature was used by the current study in the segmentation of medical images. Where accurate border pixel delineation is very crucial in segmenting images where the regions may be a few pixels wide. The effectiveness of the feature will be again demonstrated by delineating regions in the CT image of the brain (Refer Section 6.4.1).

95

In segmenting the image in Figure 6.1, the result shown in Figure 6.2 may not be what a human observer prefers. The image contains five lines of words in lighter shade against a black background. A human observer would segment the lightly shaded words belonging to the same region and the dark background as a separate region. From the segmentation result shown in Figure 6.2, it can be seen that the HCS process had segmented almost all of the characters as belonging to one region, and pseudo coloured as white. But the letter **N** in the word **CONTOUR** had been partly segmented as background. This might seem as a discrepancy but it might be the case that, that part of the image differs subtly from the rest of the lightly shaded characters and HCS might be highlighting this subtle difference. Hence this demonstrates another capability of the GTD feature, *i.e.* to highlight the subtle difference in tonal distribution.

The subtle difference in gray tone distribution, referred to above is not observable by the human eye. This property of the GTD feature is very useful in picking up small regions of in-homogeneity in an otherwise homogeneous regions of medical images. Thus regions of abnormality otherwise missed by the human observer could be picked up by the feature and highlighted. This is further demonstrated in delineating brain area affected by stroke in the MRI image of the brain (refer Section 7.3.2). Also by delineating the diseased area in a medical ultrasound image, the HCS process could highlight the subtle difference within the diseased area to give an indication the probable location of the core of the the disease (refer Section 7.6).

6.2.1.2 Brodatz Texture Image Segmentation

Figure 6.4 shows an image, of size 64×64 pixels made up of two Brodatz [Brodatz, 1999] texture patches named D68 (lighter shade) and D93 (darker shade) in the Brodatz texture album. The repetitive pattern, which demonstrates that the image is a textured image rather than a tonal image, can be seen. Table 6.2 gives the gray scale values statistics of the two texture patches. Since both patches are textured images, the high values of standard deviations show that there is a quite a variation of the gray scale values within the textured patches.

Figure 6.5 shows the histogram plot of the gray scale distribution of the two textured patches. There is an overlap, albeit minimal, of the gray scale values of the two textured patches. Hence pure gray scale value based segmentation will not be suitable. The

image was segmented using GTD feature. Figures 6.6-6.8 illustrate the initial, intermediate and the final segmentation results respectively of the HCS process.
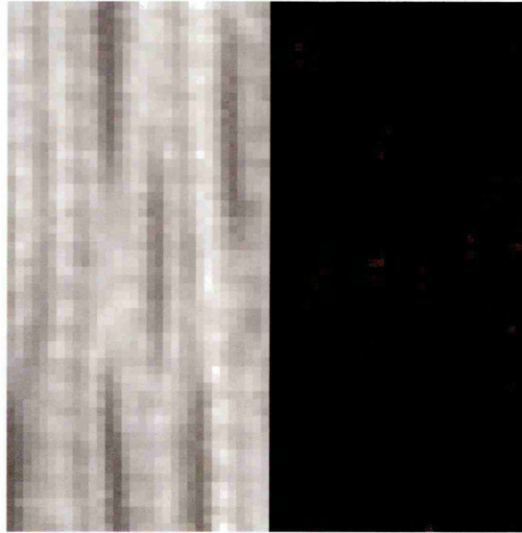
Figure 6.4 - A textured image made up of
D68, D93 Brodatz texture patches

Table 6.2
Statistics of the Gray scale values within the two textured patches in the image shown in
Figure 6.4

Brodatz texture patch	Minimum	Maximum	Average	Standard Deviation
D68	94	255	175	48
D93	10	129	54	28

The HCS process designed for this study did not have a stopping criteria while merging the regions (Refer section 4.2). As the allowable dissimilarity between the regions is increased more and more regions merge together (Refer section 4.2). Consequently at the final stage even the two regions (Figure 6.8), which represent the two discernible texture patches (Figure 6.4) will be merged as a single region. This is in line with how a human observer discerns the different components of the image. At the coarsest resolution one considers the whole image as one entity. But at finer resolutions one is able to visualise the dissimilarity within the individual patches of the texture. The success of the HCS process will be evaluated for its ability to duplicate the above described human visualising process.

The intermediate segmentation result (Figure 6.7) demonstrates the following capability of the GTD feature. The two texture patch image shown in Figure 6.4 was segmented using the GTD feature. Figure 6.6 shows the different regions at the start of the merging process. Figure 6.7 shows the different regions at an intermediate stage of merging. The regions at the intermediate stage of merging correlates with the repetitive textured patterns visually visible. Figure 6.7 illustrates how the GTD feature could accurately delineate the borders of the repetitive patterns occurring across the image and tag them as similar regions within the textured patches.
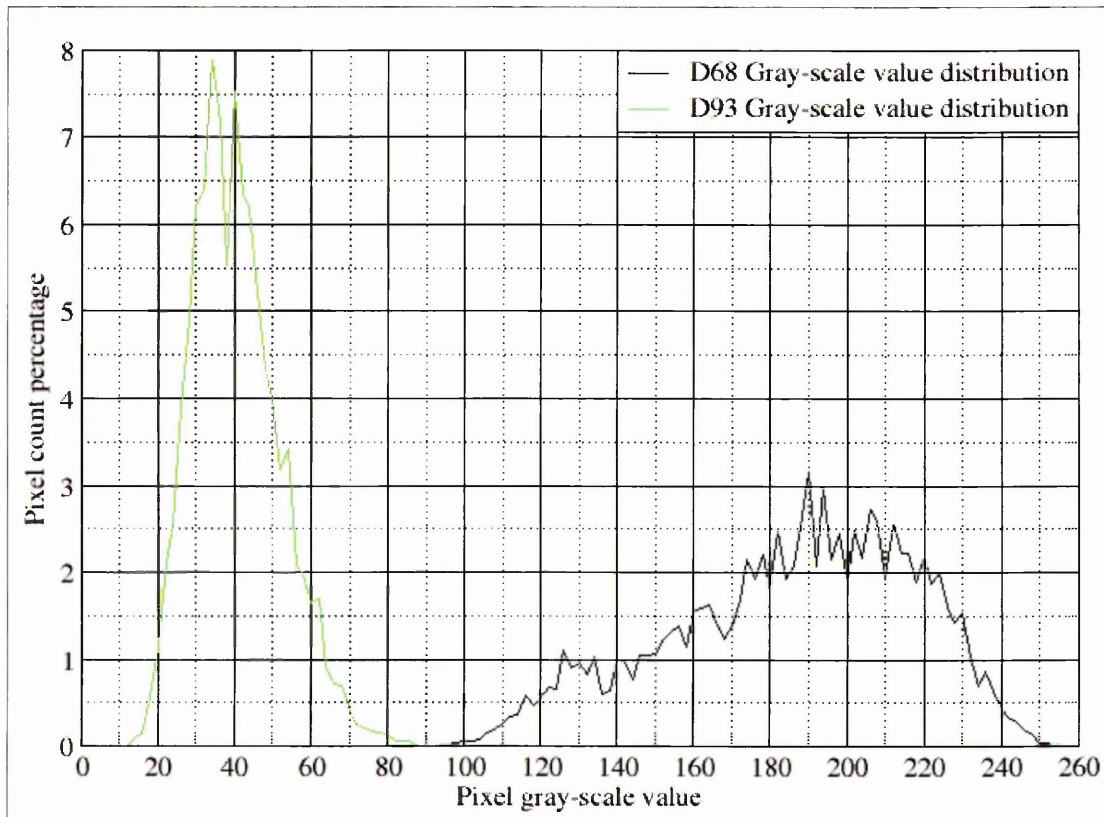
Figure 6.5 - Gray scale values distribution within the texture patches of Figure 6.4
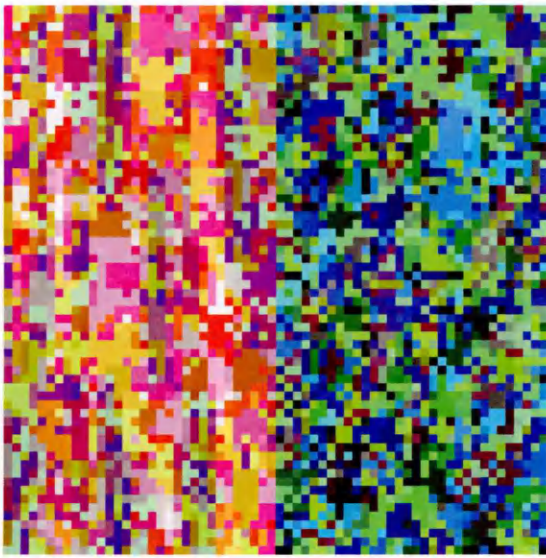
Figure 6.6 - Initial segmentation of Image in Figure 6.4
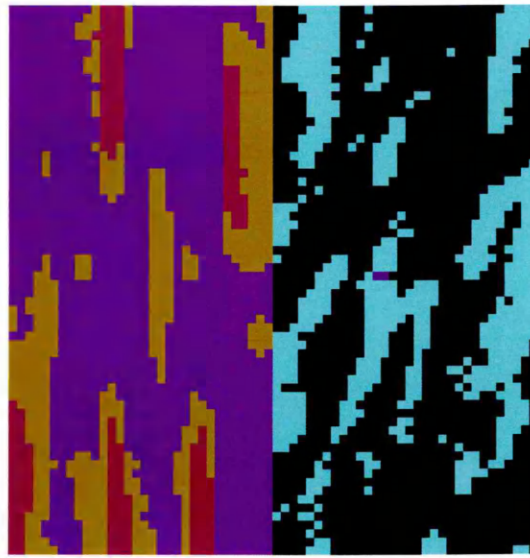
Figure 6.7 - Intermediate segmentation of Figure 6.4
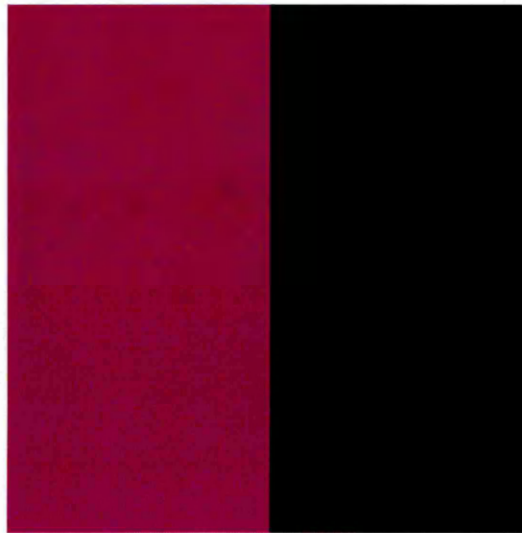
Figure 6.8 - Final segmentation of the two texture patches of the image in Figure 6.4

As the merging is iterated, with higher levels of allowable dissimilarity between the regions, the original image is finally segmented into its two constituent regions as shown in Figure 6.8. Figure 6.8 illustrates how the GTD feature could accurately delineate the border of the two different texture patches in the image.

The usefulness of the GTD feature, to accurately delineate regions of dissimilarity within an otherwise homogeneous region, will be further demonstrated by delineating part of an ultrasound medical image affected by disease within a healthy tissue (Refer Section 7.6).

6.3 Region Merging Performance

As detailed in section 4.3.4 in the HCS process region merging was performed by the agglomerative type of hierarchical clustering process, also known as bottom-up method. In order to find the similarity between two regions, the following factors were taken into account :

- similarity between individual pixels of the two regions.
- similarity between the pixels bordering the two regions.
- similarity between the combined feature property of all the pixels in the two regions.

Intuitively the above factors are appropriate considering the fact that a human observer considers all three measures while visualising the different regions in an image. In this section the above hypothesis will be experimentally demonstrated by showing how the accuracy of the segmentation improves by taking into account the above factors. The demonstration will be achieved by using HCS to segment an image made up of two texture patches. The image made up of texture patches was used for the following reasons :

- the ground truth is precisely known since the patched image is created.
- to demonstrate that feature measure plays a crucial role in segmentation.
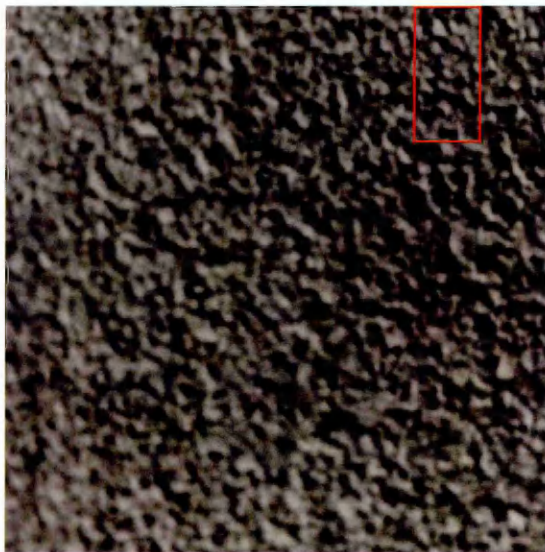
Figure 6.9 - Brodatz texture Cork of size 256×256. The 32× 64 patch is outlined in red.
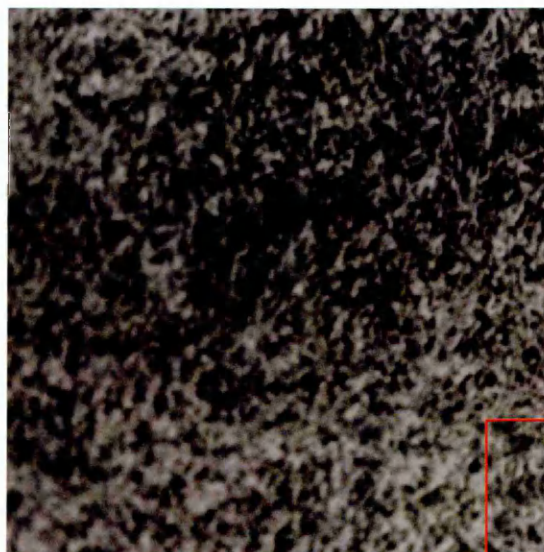
Figure 6.10 - Brodatz texture Grass. of size 256×256 The 32×64 patch is outlined in red.

Figures 6.9 and 6.10 show two Brodatz [Brodatz, 1999] textures *i.e.* Cork and Grass respectively. Figure 6.11 shows a 64×64 size image made up of the two Brodatz patches Cork (left patch of size 32×64) and Grass (right patch of size 32×64). The patches are barely distinguishable to even a human observer. Table 6.3 gives the grey scale values statistics of the two texture patches. Figure 6.12 shows the plot of the grey scale distribution of the two texture patches. From the plot shown in Figure 6.12, it could be seen that the gray level distribution of the two textures are almost the same. This is a very typical case, of textured images, where the images are differentiated by the arrangement of the gray levels, i.e. their spatial distribution, rather than its frequency distribution. Since there is very little difference between the gray level distributions of the two textured patches, GTD features will not be able to successfully differentiate between the two textured regions.
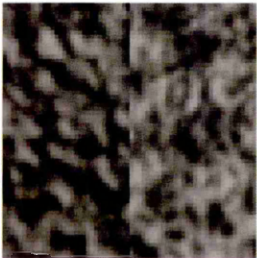
Figure 6.11 - A 64×64 size texture image
made up of 32×64 Cork and 32×64 Grass
Brodatz texture patches

Table 6.3
Statistics for the Gray scale values within the two texture patches in the image shown
in Figure 6.11

Brodatz texture	Minimum	Maximum	Average	Standard deviation
Cork	24	196	110	48
Grass	20	188	104	28
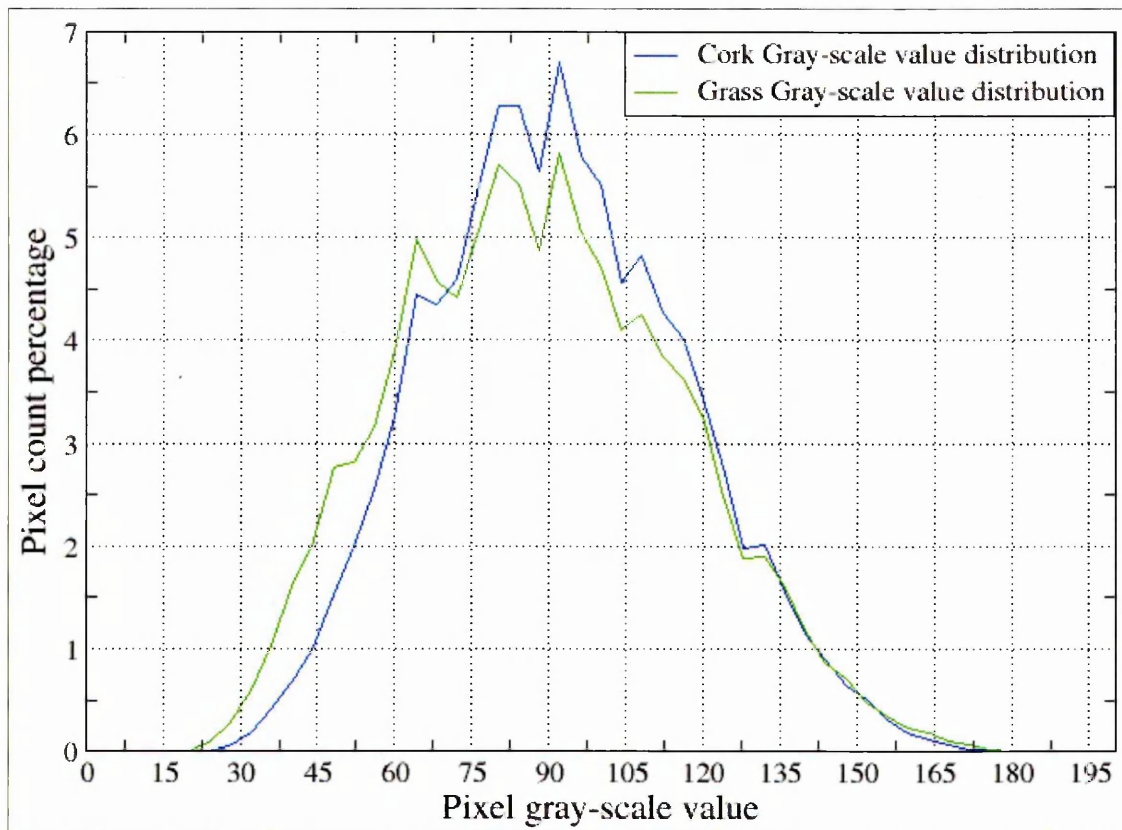
Figure 6.12 - Gray scale values distribution within the Cork and Grass Brodatz
texture patches in the texture image of Figure 6.11

GTD feature's inability to properly segment the texture image patches, of Figure 6.11, could be seen in the misclassified image shown in Figure 6.13. The image in Figure 6.13 shows the segmentation output when there are two regions (pseudo coloured as black and blue). The misclassification could be seen since the two different regions in the image found by the HCS process, using GTD feature, are not the same as the two different textured patches in the actual image in Figure 6.11. Figure 6.14 shows the borders of the two regions outlined on the original image. From Figure 6.14 it can be seen that the GTD feature has segmented the image into regions based on tonal characteristics, the darker part of the image segmented as one region and the lighter part of the image segmented as the other region.

Since HCS is a modular process, the feature measurement part of the process alone could be changed, depending on the type of image, keeping the rest of the processing steps the same. The HCS process used Local-Binary-Pattern and Contrast (LBP-C) feature (See Appendix 2) to segment the texture patches shown in Figure 6.11. LBP-C performed better than GTD to segment such subtle texture patches. The LBP-C feature final segmentation result is shown in the Figure 6.17.

102
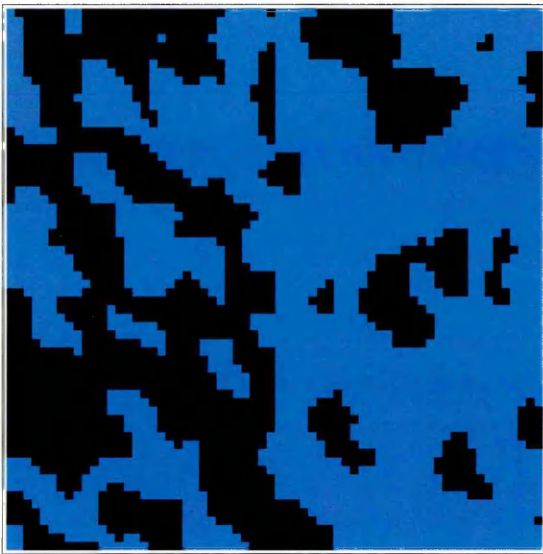
Figure 6.13 - Segmentation of the Cork, Grass Brodatz texture patches, of Figure 6.11, by the HCS process using GTD feature.
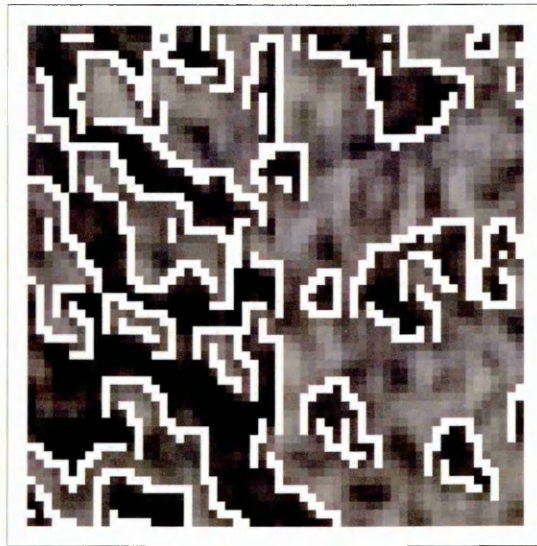
Figure 6.14 - Border of the two regions found by the HCS process, using GTD feature.
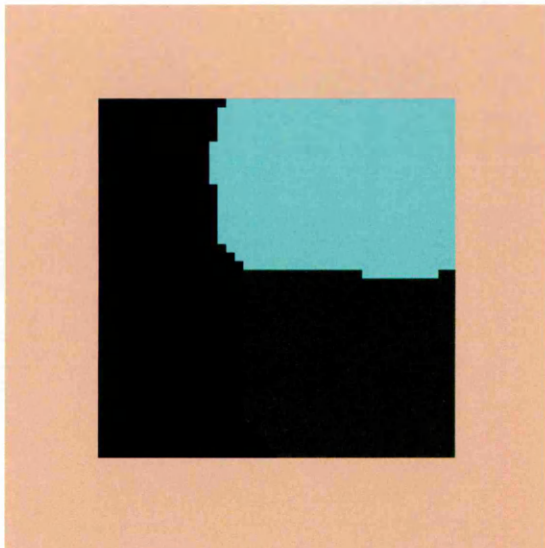
Figure 6.15 - Intermediate segmentation of the Cork, Grass Brodatz texture patches, of Figure 6.11, by the HCS process using LBP-C feature.
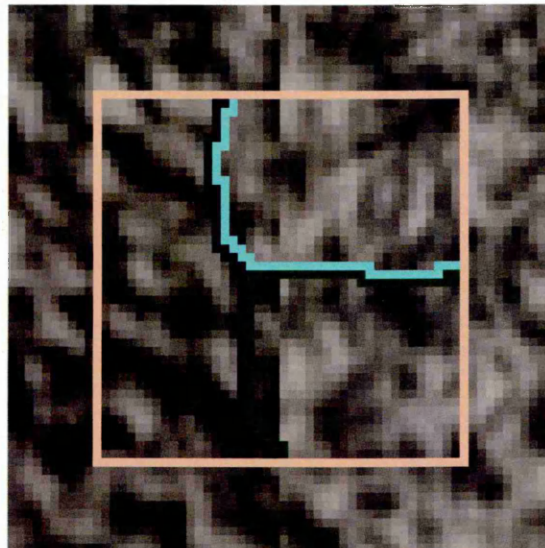
Figure 6.16 - Border of the three regions found by the HCS process, using LBP-C feature, outlined on the original Cork, Grass Brodatz texture patches image of Figure 6.11.

103
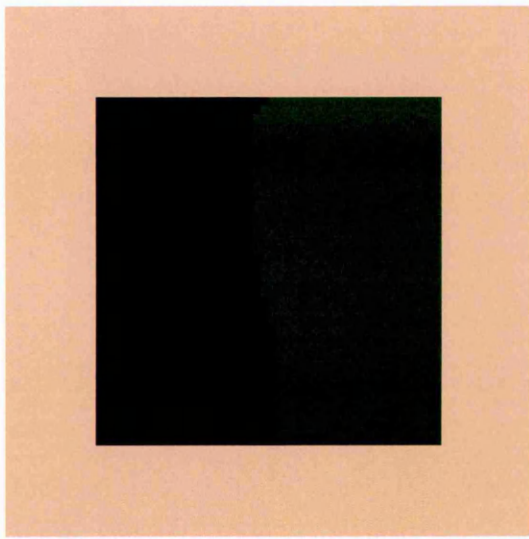
Figure 6.17 - Final segmentation of the Cork, Grass Brodatz texture patches, of Figure 6.11, by the HCS process using LBP-C feature.
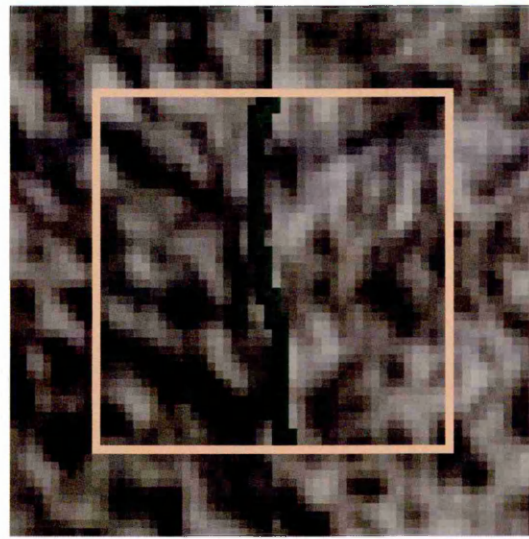
Figure 6.18 - Border of the two regions found by the HCS process, using LBP-C feature, outlined on the original Cork, Grass Brodatz texture patches image of Figure 6.11.

6.3.1 Unsuitability Of LBP-C Feature For Medical Image Segmentation

Even though the LBP-C feature is well suited for segmenting texture patches like the one shown in Figure 6.11; the major disadvantage of the LBP-C feature is that unlike the GTD feature, it could not localise the border pixels of the constituent regions. This could be seen in the intermediate segmentation result, where there were three regions, as shown in Figure 6.15. The three regions' border are outlined in Figure 6.16, it could be seen that the segmented regions borders do not overlap the texture patches border.

The reason for LBP-C feature not being able to localise the border is because the feature is calculated within a 21×21 pixel size mask centred at the pixel under consideration (See Appendix 2). For the pixels bordering the two textured patches the feature value is calculated using information from both the textures and hence cannot be specific for any one of the textures. In the case of GTD, this situation is avoided by positioning the mask at different orientations with the pixel under consideration at different locations within the mask (See Sections 3.5.2 and 4.3.2 for details). This ensures that the property of a pixel at the border is found using only the information from the texture to which it actually belongs. Therefore the reason for using GTD is that one can delineate regions with precise border localisation. Precise border pixel localisation is very crucial in medical image segmentation (See Section 8.2.2.2). Hence LBP-C feature is not suitable

104

for segmenting medical images where the constituent regions are barely a few pixels wide.

6.3.2 Effect Of Region Merging Factors In Segmentation Performance

Even if an ideal feature measure is chosen, which is suitable for the type of image being processed, how it is used affects the success of the segmentation process. In this section it will be discussed how the different region merging factors of HCS process (See Section 4.3.4.1 for details) affect the performance of the LBP-C feature.

The LBP-C feature distribution was calculated by moving a 3×3 window within a 21×21 size mask. Rejecting the pixels on the border of width 11 all around the 64×64 size image (Figure 6.11), the total number of pixels that were classified in the image were 1764 (42×42). *i.e.* 882 pixels in each of the texture patch viz. Cork and Grass.

The HCS performance shown in the graph in Figure 6.19 is achieved by the HCS process when all the three factors, *i.e.* similarity between individual pixels, similarity between pixels bordering the regions and the similarity between the combined feature property of all the pixels in the regions, (Section 4.3.4.1 for details) were considered for the region merging. The percentage of misclassification when the merge was complete, *i.e.* there were only two regions yet to be merged, is as follows :

- The misclassification for the Cork texture was 4.54% (*i.e.* 40 of 882).
- The misclassification for the Grass texture was 1.81% (*i.e.* 16 of 882).
- The overall misclassification considering both Cork and Grass was 3.175% (*i.e.* 56 of 1764).

Normally to find the similarity between regions, only the similarity between the combined feature property of all the pixels within the regions are considered [Ojala and Pietikäinen, 1999]. Using the same LBP-C feature distribution, the textured patches in the image in Figure 6.11 was segmented using only the similarity between the combined feature property of all the pixels within the regions. The resulting segmentation performance is shown in Figure 6.20. From the graph it could be seen that when the merge is fully complete, the overall misclassification considering both Cork texture and Grass texture together was 49.2% (*i.e.* 868 of 1764).

105
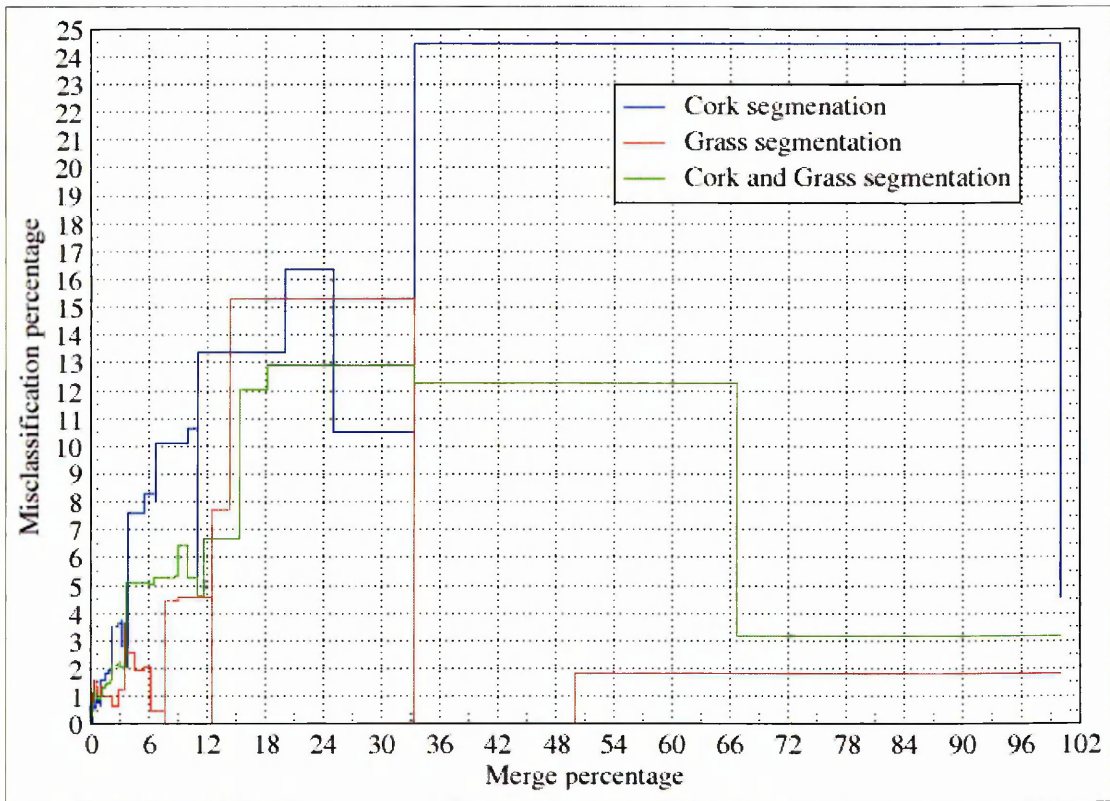
Figure 6.19 - Misclassification versus merge percentage for the segmentation of the Cork, Grass Brodatz texture patches, of Figure 6.9, by the HCS process using LBP-C feature, when all the factors were taken into account and when all the regions in the image were compared for merging.
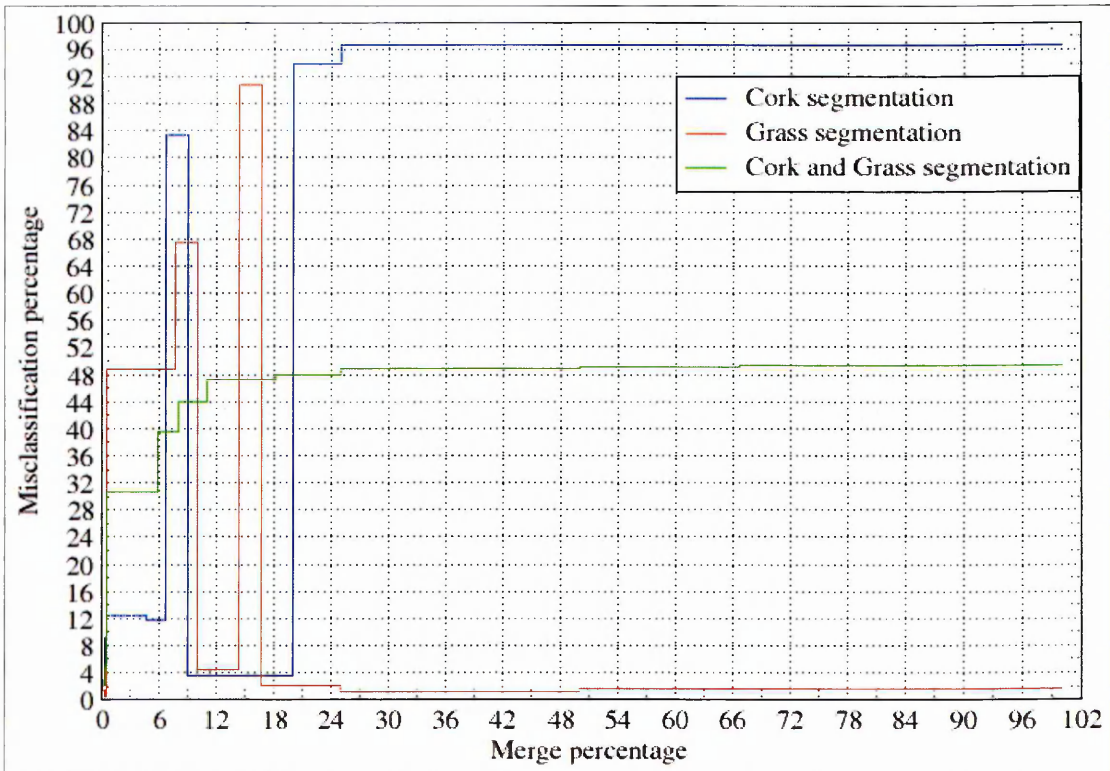
Figure 6.20 - Misclassification versus merge percentage for the segmentation of the Cork, Grass Brodatz texture patches, of Figure 6.9, by the HCS process using LBP-C feature, when only combined feature measure was used to measure the similarity between regions.

106

The other factors which play an important role in obtaining the best segmentation performance (shown in Figures 6.17-6.18) are :

- Comparing all the regions in the image to find the most similar regions.
- Reclassifying border pixels after every merge of similar regions.

Comparing all the regions in an image to merge the most similar regions is a practical necessity in medical image segmentation where similar regions might occur across the image and may not be spatially adjacent to one another. In segmenting textured images, comparing all the regions in an image to merge the most similar regions improves the segmentation results. The reason for this is that the repetitive pattern which forms the texture may not be spatially adjacent to one another. The performance of the LBP-C feature based segmentation using the HCS process when only spatially adjacent regions are merged is shown in the graph of Figure 6.21. From the graph shown in Figure 6.21 it can be seen that when the merge is fully complete, the overall misclassification considering both Cork and Grass was 31.3% (*i.e.* 552 of 1764).
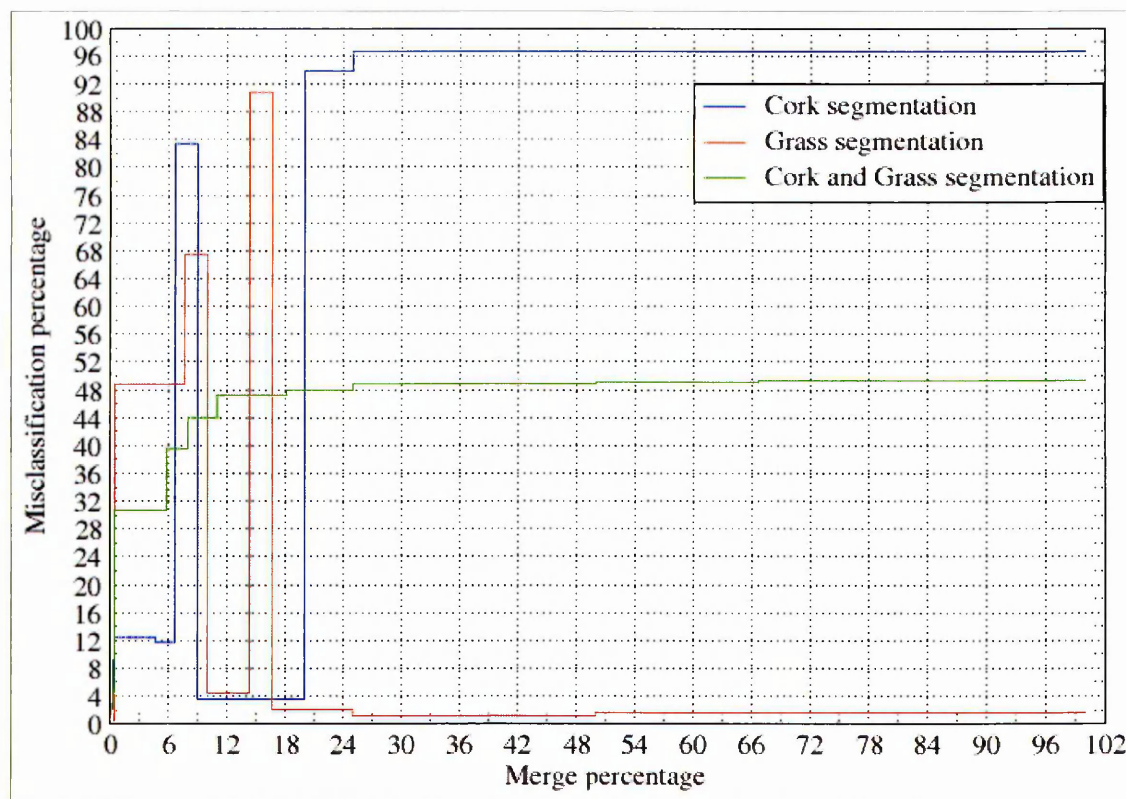
Figure 6.21 - Misclassification versus merge percentage for the segmentation of the Cork, Grass Brodatz texture patches, of Figure 6.9, by the HCS process using LBP-C feature. when only spatially adjacent regions are compared for merging.

107

As explained in section 4.3.5 (Methodology chapter), after every merge of similar regions, the pixels on the borders were evaluated to find out whether they actually belonged to the regions they were currently in or whether they needed to be reclassified to any other regions to which they might be more similar. Border pixel reclassification does improve performance. When all the factors for merging of regions are taken account and all the regions in the image were compared to find the most similar regions, but the border pixels were not reclassified then merging performance degrades as shown in in the graph of Figure 6.22. This shows that when the merge is fully complete, the overall misclassification considering both the Cork texture and Grass texture was 12.02% (*i.e.* 212 of 1764).
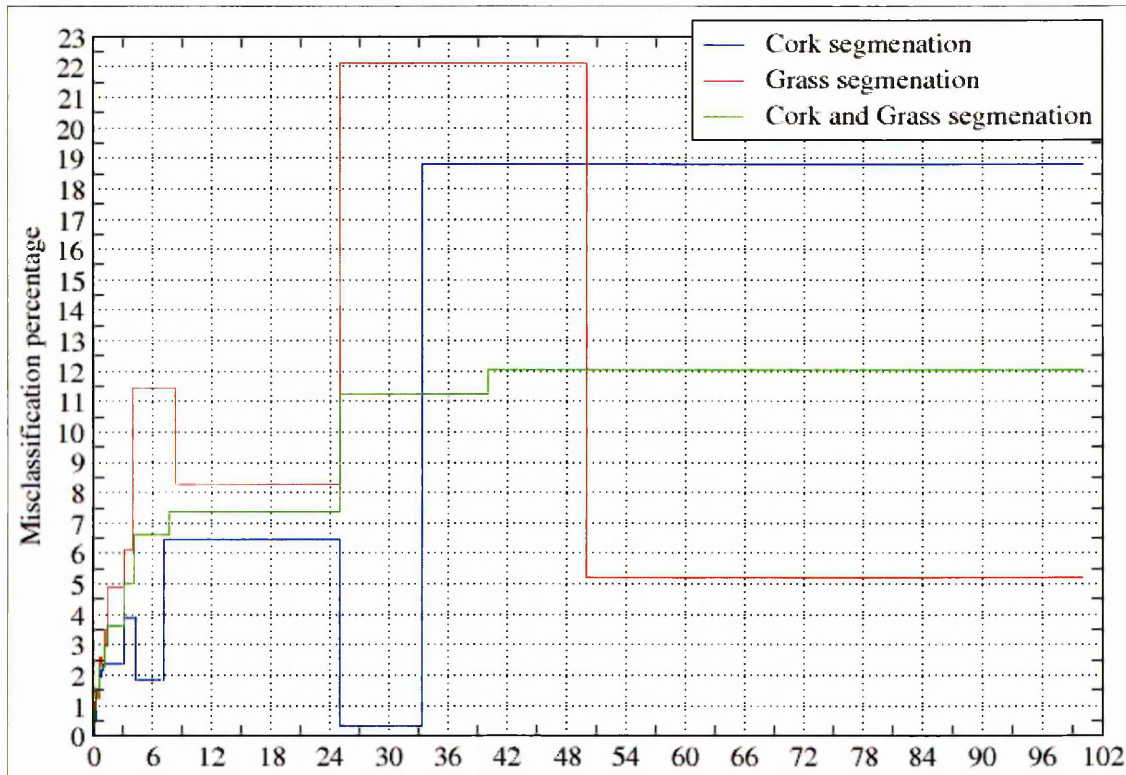
Figure 6.22 - Misclassification versus merge percentage for the segmentation of the Cork, Grass Brodatz texture patches, of Figure 6.9, by the HCS process using LBP-C feature, when border pixels are not reclassified after every region merging.

From the above discussion it can be concluded that all the factors, *i.e.* similarity between individual pixels, similarity between pixels bordering the regions and the similarity between the combined feature property of all the pixels in the regions, need to be used to get the best possible results (shown in Figures 6.17-6.18). Also factors like merging regions which are spatially disjoint and reclassifying pixels bordering the

merged regions after every merge further improve performance. The above conclusions were further validated by using the HCS process on some real world medical images (See Sections 6.4.2 and 6.4.3).

6.4 Medical Image Segmentation Example

Medical images have the following typical features:

- Regions having similar properties may not be adjacent.
- Regions may be as small as few pixels.
- Regions which are anatomically and/or clinically very different may have very subtle difference in image properties.

To successfully segment medical images, the segmentation process should be able to handle the unique features of the medical images. In this section the performance of the HCS process, in this context, will be discussed.

The major features which make HCS unique are :

- Comparison of feature distribution for all possible mask orientations (see Sections 3.5.2 and 4.3.2).
- Evaluating all the possible combinations of the regions, currently in the image, to find and merge the most similar regions (see Sections 4.3.4 and 4.4.1).
- Reclassifying the pixels bordering the regions which have merged (see Section 4.3.5).

These unique features play an important role in addressing the issues typical to medical images of finding the possible regions and highlighting dissimilar parts. This will be demonstrated in Section 6.4.1 by an example where HCS was successfully used to highlight the diseased area in a CT image.

6.4.1 Precise Border Pixels Delineation

Figure 6.23 shows the CT image of a section of the brain. Figure 6.24 shows the suspected area in the brain outlined in white by a neuroradiologist. A Region of Interest (ROI) (shown by a rectangle) was selected enclosing the suspected area and the processing was carried out within the ROI. The processing was done within the ROI to significantly reduce the amount of processing time. Processing within the ROI is one of the optimisation techniques adopted in this study (See Section 5.2 for details).
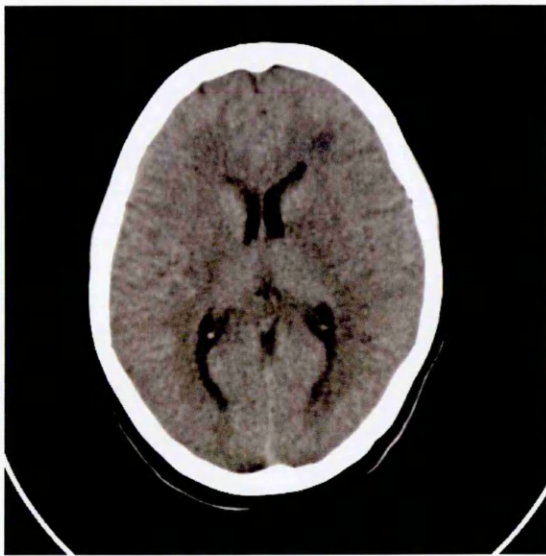
Figure 6.23 - A CT image section
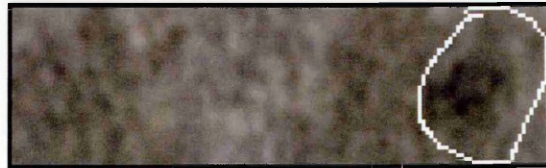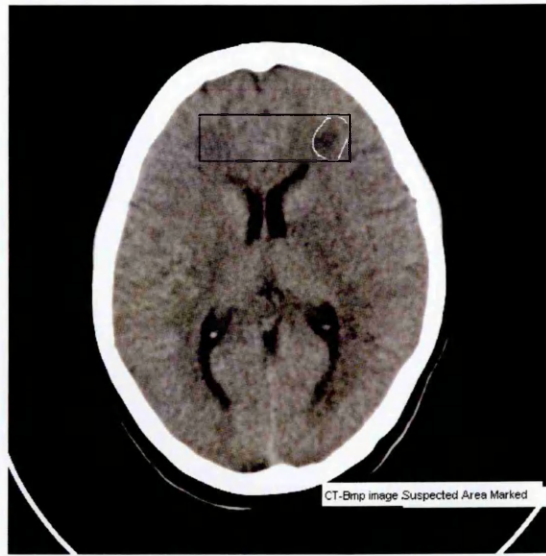
Figure 6.24 - Image showing the suspected area, outlined in white and the ROI rectangle drawn in black.
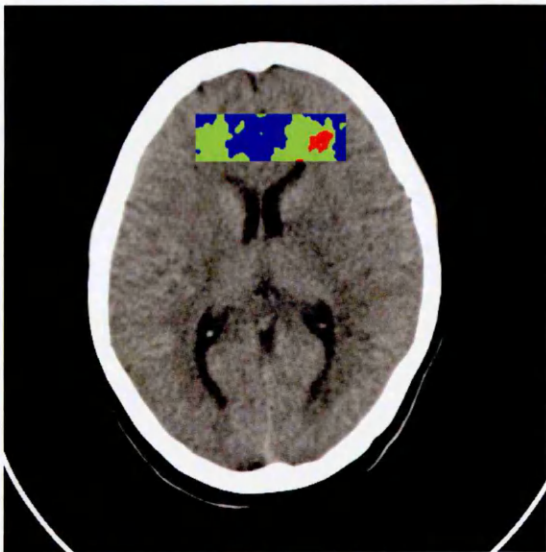
Figure 6.25 - Intermediate segmentation regions, within the ROI., when all the regions within the ROI, are compared and merged.
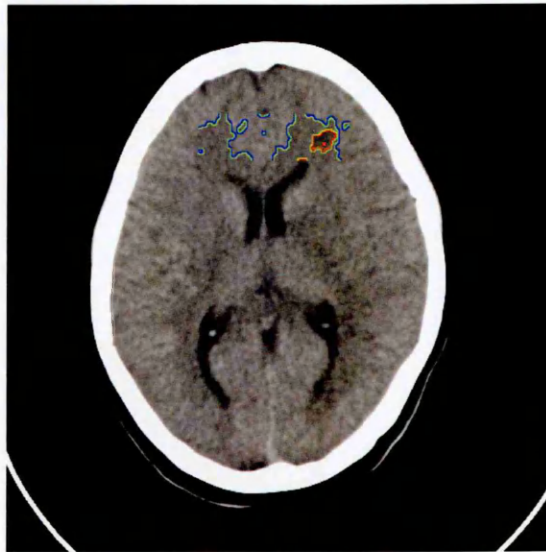
Figure 6.26 - Intermediate segmentation regions' boundary outlined.

110

The result of segmenting the regions within the ROI, when there were four regions, is shown in Figure 6.25. Figure 6.26 shows the boundaries of the four intermediate regions. From Figures 6.25 and 6.26 it could be seen that the major classes in the original image, viz. White Matter (Green), Gray Matter (Blue) and infarct (Red), had been segmented. The fourth region is a single pixel size region (Yellow) within the infarct. Figure 6.26 shows how the region boundaries, separating the Grey matter, White matter and the Infarct, are very precise. This illustrates how the unique way the major operations, like the pixel feature comparison (Sections 3.5.2 and 4.3.2), similar regions merging (Sections 4.3.4 and 4.4.1) and reclassifying border pixels (Section 4.3.5), of the HCS process were implemented have contributed towards an acceptable segmentation result.
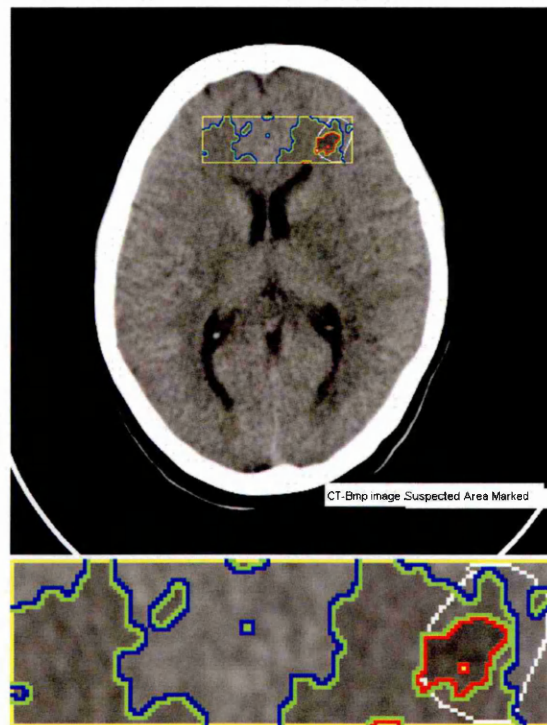
Figure 6.27 - HCS process delineated
border superimposed on top of the expert's
outline of the diseased area.

Precise border delineation plays a crucial role in medical image segmentation especially in disease management. For example to evaluate the drug response one might want to measure the area of the image affected by the disease over a period of time to establish whether the disease is under remission or not. For this purpose computer aided image segmentation like HCS process will be able to give a consistent and precise border delineation. This is evident from Figure 6.27 where the border of the diseased area is superimposed on the expert marked area of the disease. The HCS process made use of

the expert's initial estimation of the diseased area location to place the ROI and processed only within that ROI. This will be the case in a disease management scenario where the initial location is available either from prior observation or through subsequent evaluation. But the precise delineation is what is crucial, say to evaluate a drug response.

In Figure 6.27, it could be seen that while the expert's outline of the diseased area is only very approximate, which includes substantial part of the healthy part of the image, the HCS process delineation is much more precise. This precise delineation ability of the HCS process, is a major contribution of this study.

The precise border pixel delineation could be achieved by HCS only through the unique way the following major operations, of the HCS process, were implemented :

- Similar regions merging (Sections 4.3.4 and 4.4.1).
- Reclassifying border pixels (Section 4.3.5).

This will be further validated by giving counter examples (See Sections 6.4.2 and 6.4.3) how the results degrade substantially if the above operations were implemented differently.

6.4.2 Necessity For Comparing Spatially Disjoint Regions

A unique feature of the HCS process is the evaluation of all the possible combinations of the regions, currently in the image, to find and merge the most similar regions (Sections 4.3.4 and 4.4.1). This operation of the HCS process is highly computer processing intensive due to the combinatorial nature of the operation. But the method of evaluating spatially disjoint regions is essential in the case of the medical image segmentation. The contention above is validated by giving a counter example where when spatially disjoint regions are not compared the segmentation result shown in Figure 6.28 is unacceptable.

Figures 6.28 and 6.29 show the intermediate segmentation results of the HCS process, when only spatially adjacent regions were compared and merged. In Figure 6.28 there are 101 clusters and in Figure 6.29 there are 40 clusters. The larger clusters belonging to the major classes are coloured as Yellow and Green (White Matter), Blue (Gray Matter) and Red (infarct). Other smaller clusters are coloured with other distinct colours.

Comparing the segmentation result shown in Figure 6.28 with that of Figure 6.25, in Figure 6.28 similar regions (White matter) are tagged as separate clusters (Yellow and Green coloured clusters) because they are spatially disjoint. And on subsequent merging the White matter and Grey matter regions are merged together (Figure 6.29 Green coloured cluster) instead of the White matter merging with the White matter on the other part of the image (Yellow coloured cluster in Figure 6.29). This misclassification occurred because spatially adjacent regions were only considered for merging. This example demonstrates that in medical image segmentation it is necessary to compare all the regions to find the best possible combination of regions for merging.
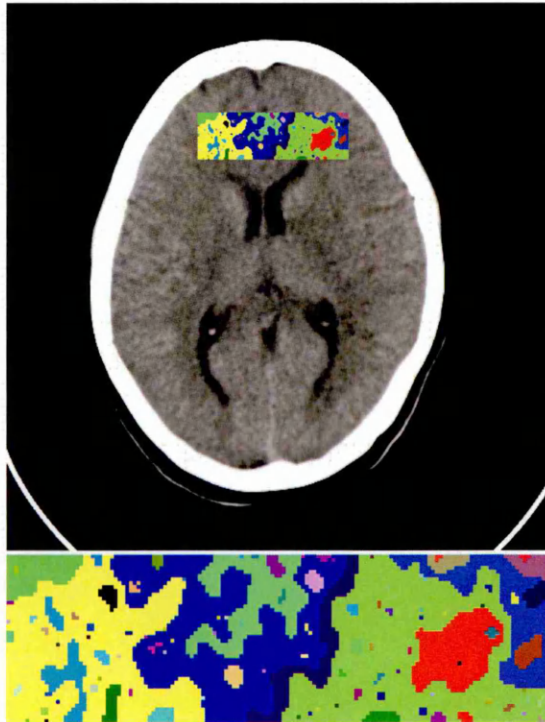
Figure 6.28 - Intermediate segmentation when only spatially adjacent clusters are compared.
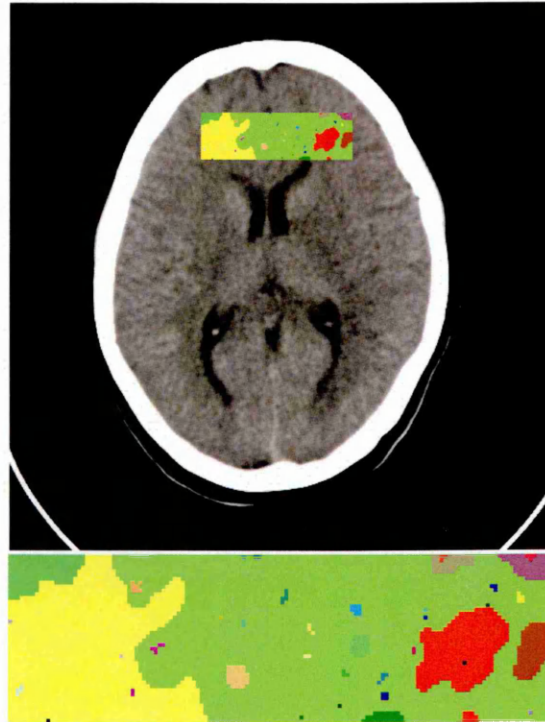
Figure 6.29 - Intermediate segmentation where spatially adjacent Grey matter and White Matter regions were merged.

6.4.3 Necessity For Border Pixels Reclassification

Border pixels reclassification is carried out immediately after each merging of similar regions. During the border pixels reclassification, the pixels bordering the regions that had merged (with other similar regions) and their bordering regions, were further evaluated to determine the most suitable region they (the bordering pixels) belong to (see Section 4.3.5 for details). Border pixel reclassification is one of the most time consuming operation during the HCS process. But without it the segmentation results were found to be suboptimal.

113

During the early stages of the HCS process, the dissimilarity allowed between regions for merging is small. This will result in the HCS process collating pixels into regions which capture the local inhomogeneity within an otherwise homogeneous regions. As the merging is advanced more and more pixels will join to form regions which capture the overall homogeneity of the regions with pixels having minor inhomogeneity accommodated within the region. During the process of merging, the pixels which have been merged with other regions were allowed to merge back to the regions to which they actually belong, through border pixels reclassification.
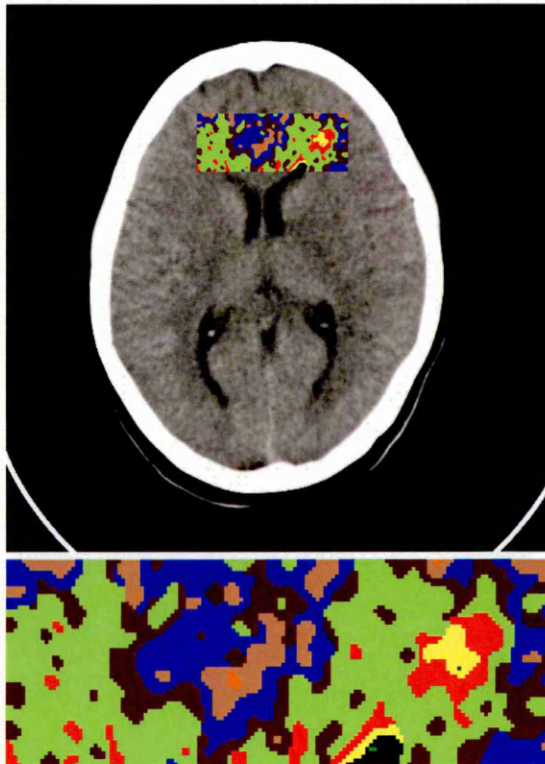
Figure 6.30 - Intermediate segmentation, with border pixels reclassification, where misclassification had occurred.
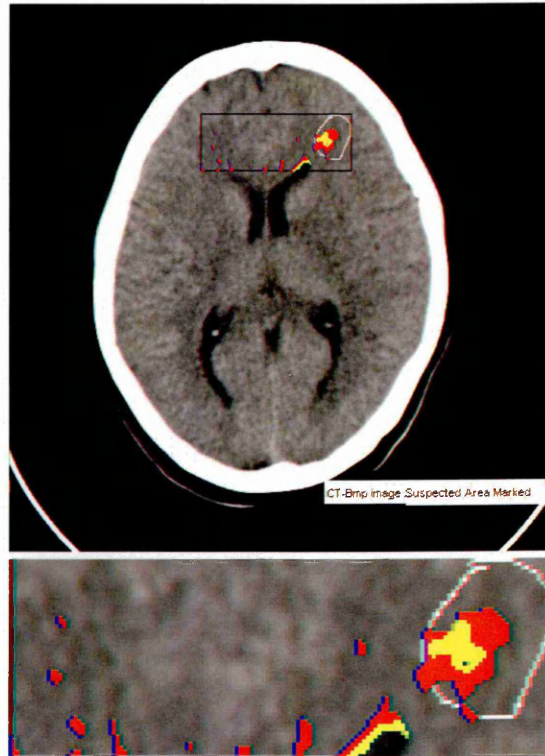
Figure 6.31 - Image highlighting the pixels belonging to the misclassified cluster.

If border pixels reclassification is not carried out those pixels which do not belong to the regions to which they merged during the early stage of merging, will not have a chance to merge back to the regions they actually belong. This will distort the segmentation and result in errors. This is illustrated in this section by segmenting the CT image shown in Figure 6.24.

Figure 6.30 shows the intermediate segmentation results of the HCS process, done with border pixels reclassification. In Figure 6.30 there are 10 clusters. The larger clusters belonging to the major classes are coloured as Red and Yellow (infarct), Green (White Matter) and Blue (Gray Matter). Other smaller clusters are coloured with other distinct colours. Figure 6.31 shows only the pixels of the larger cluster belonging to the major class infarct (coloured as Red and Yellow). From Figures 6.30 and 6.31 it could be seen that the cluster belonging to the major class infarct has misclassified pixels on the other part of the image.

Figure 6.32 shows the clusters in the segmented image on subsequent merging where most of the pixels which were misclassified as belonging to the diseased region had been reclassified correctly through border pixel reclassification. Figure 7.33 shows the rectified segmentation showing the pixels belonging to the diseased region alone. The minor misclassification, seen in Figure 6.33, may be due to the diseased area in the white matter having the same signal signature as the pixels belonging to the Ventricle.
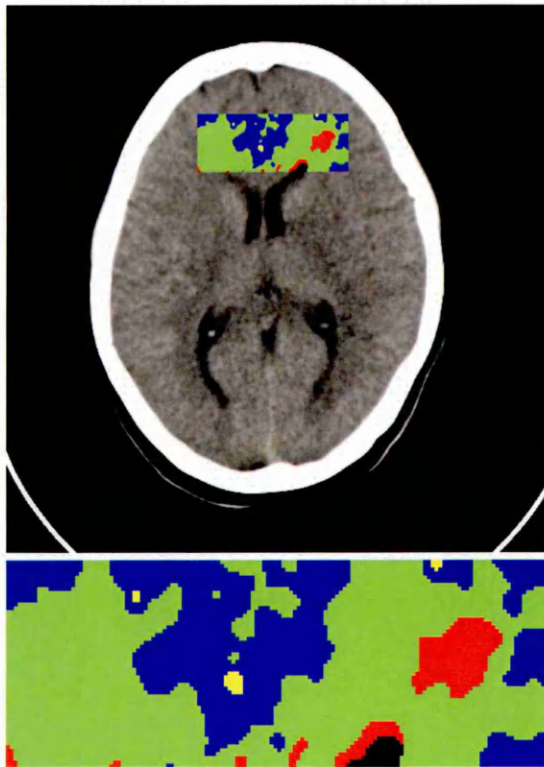
Figure 6.32 - Clusters in the image after subsequent merging where part of the misclassification had been rectified.
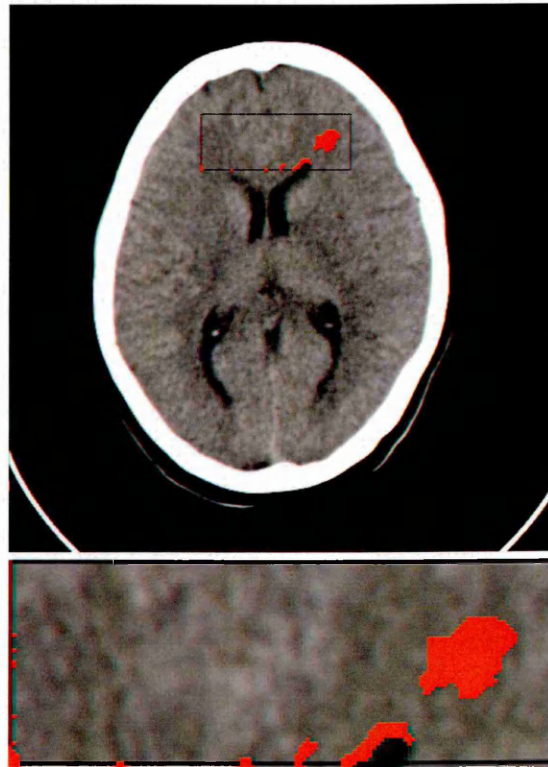
Figure 6.33 - Image showing the rectified cluster pixels alone.

Figure 6.34 shows the intermediate segmentation results of the HCS process, performed without border pixels reclassification. In Figure 6.34 the pixels belonging to the larger clusters of the major classes White Matter and the infarct are coloured as Green and Red. Pixels clustered as belonging to the Grey matter class are not coloured. From Figure 6.34 it could be seen that the cluster belonging to the major class infarct has misclassified pixels on the other part of the image. The misclassification seen in Figure 6.34 is very similar to misclassification shown in Figure 6.30.

Figure 6.35 shows the clusters in the segmented image on subsequent merging where the misclassification had worsened. Figure 6.35 illustrates how the earlier misclassified pixels, not able to disassociate with their wrongly classified region (since no border pixel reclassification is done), influences subsequent merging to wrongly merge the diseased area with the rest of the white matter.
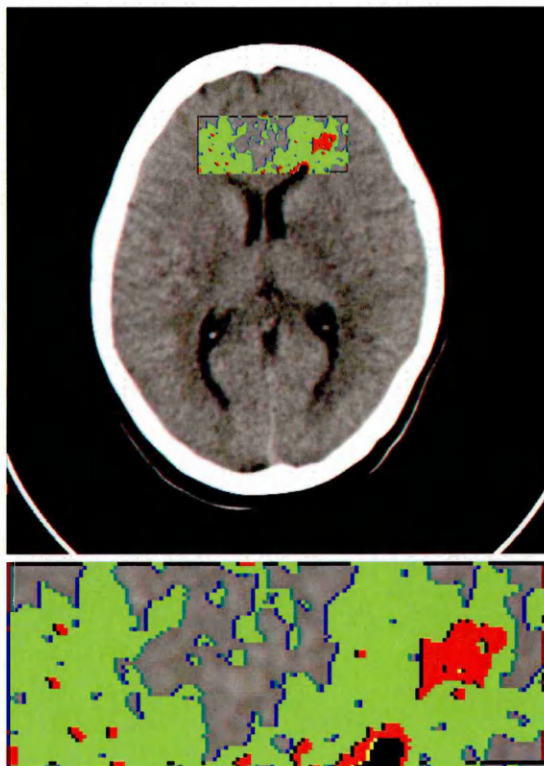
Figure 6.34 - Intermediate segmentation, without border pixels reclassification, where misclassification had occurred.

Figure 6.35 - Clusters in the image after subsequent merging where misclassification had worsened.

116

6.5 Comparison of HCS with NASA's HSEG

A comparative study of the developed HCS system with Hierarchical image segmentation (HSEG) developed by NASA [Tilton NASA Case No. GSC 14,328] [Tilton, 2003] has been carried out in this study.

HCS was compared with HSEG for the following reasons :
- HSEG (See Section 3.3.3) is one of the segmentation methods which is similar to HCS (Section 3.4.1).
- An application domain of HSEG is to segment medical images and it has been licensed to Barton Medical Imaging to be used in its medical image analysis software product MED-SEG™ [Barton Medical Imaging].

6.5.1 HSEG Performance

An evaluation version 1.0 of the HSEG software was requested and received from NASA. The version 1.0 was not able to segment the diseased area in the CT image data shown in Figure 6.24. The developer of the software was contacted and on his request the segmentation results attained through HCS process (Figure 6.25) was sent. The developer acknowledged that version 1.0 of HSEG software was not able to segment the diseased area. As a result HSEG software was debugged, updated and version 1.1 was released, by the developer (See Appendix 3).

Version 1.1 of the HSEG software was used to segment the CT image of Figure 6.23 within the ROI shown in Figure 6.24. The results of the HSEG segmentation process are shown in Figures 6.36-6.38.

6.5.2 Comparison of HSEG Performance with HCS

The result of HSEG within the ROI, when there were three clusters, is shown in Figure 6.36. Figure 6.37 shows the boundaries of the three intermediate clusters. From Figures 6.36 and 6.37 it could be seen that the major classes in the original image, viz. White Matter (Green), Gray Matter (Blue) and infarct (Red), had been segmented into separate clusters. But there is some misclassification where the pixels belonging to the White Matter on the other part of the image had been clustered as belonging to the infarct.
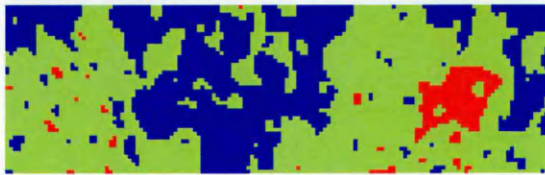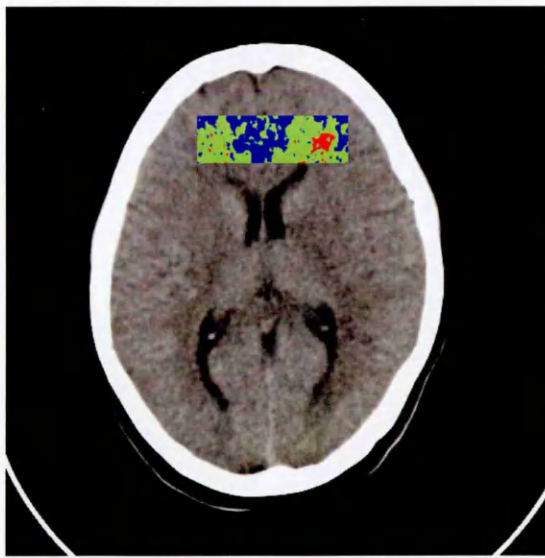
Figure 6.36 - HSEG intermediate segmentation output where the suspected area has been segmented with some misclassified pixels.
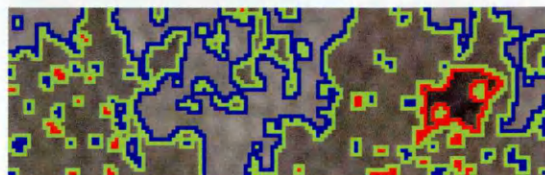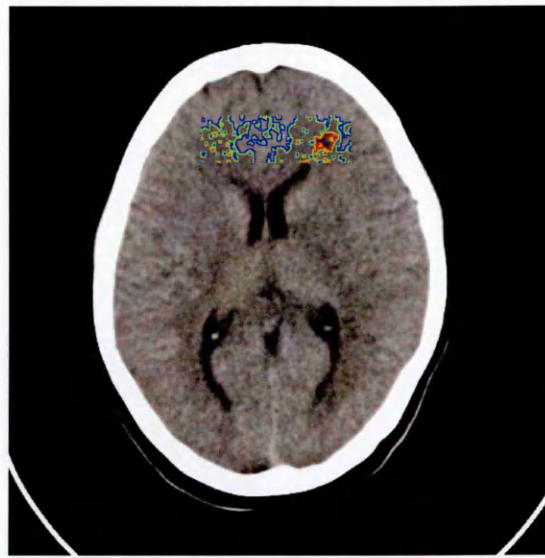
Figure 6.37 - Borders of the segmented clusters during the intermediate segmentation using HSEG.
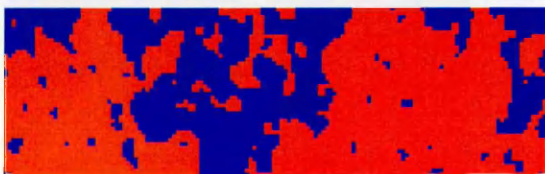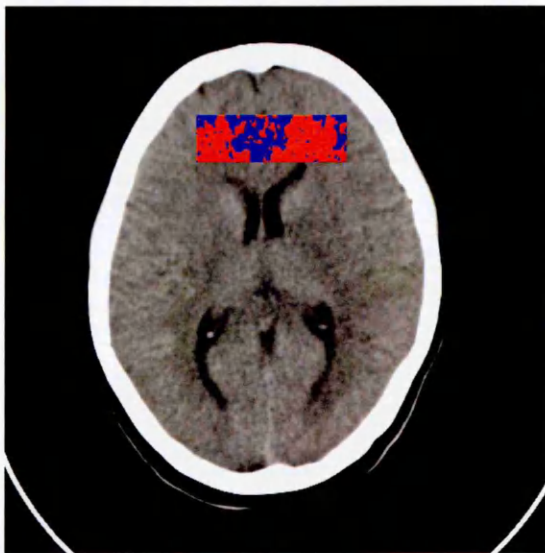
Figure 6.38 - HSEG subsequent clustering output, where the region highlighting the suspected area in the earlier stage has combined with the white matter.
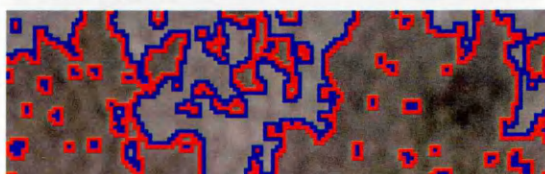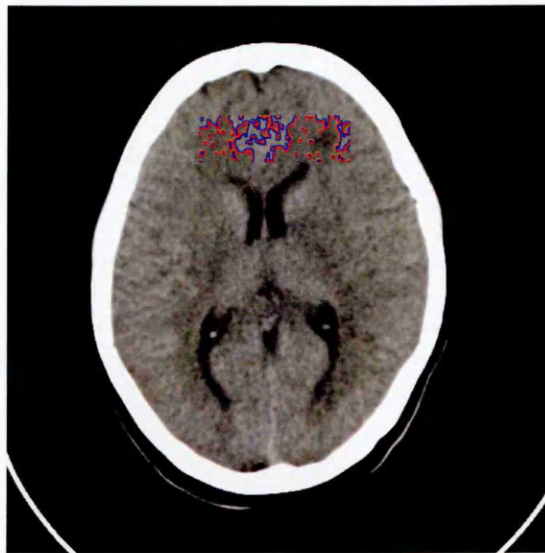
Figure 6.39 - Borders of the regions on subsequent clustering, by HSEG, showing the boundaries of the misclassified clusters.

118

Figures 6.38 and 6.39 show the result of subsequent merging. From Figures 6.38 and 6.39 it could be seen that the White Matter and the infarct had merged together to form one single cluster (Red).

Comparing the results of the HSEG (Figures 6.36 and 6.38) with that of the results obtained by HCS without border pixel reclassification (Figures 6.34 and 6.35), it can be seen that the results are almost the same. This confirms that HCS border pixel reclassification is the main differing step with that of the HSEG. It is also demonstrated that HCS process with its border pixel reclassification step gives a far better segmentation result (Figures 6.25 and 6.26) as compared with HSEG. Therefore this comparison illustrates that border pixel reclassification has an obvious advantage over HSEG which does not have such a similar step.

These results illustrate the fact that HSEG does merging of regions that are not spatially adjacent like what HCS does. But HSEG does not do border pixel reclassification (which HCS does).

The major advantage of HSEG over HCS is the time it takes to process. In a similar configured machine, while HSEG takes only a few minutes HCS with its border pixel reclassification takes couple of days to converge. However with rapidly increasing computer processing power, this processing time would be reduced.

Figure 6.40 - Linear mapping of the Hounsfield values for a window setting width 66 Hu units, centred at 38 Hu unit.
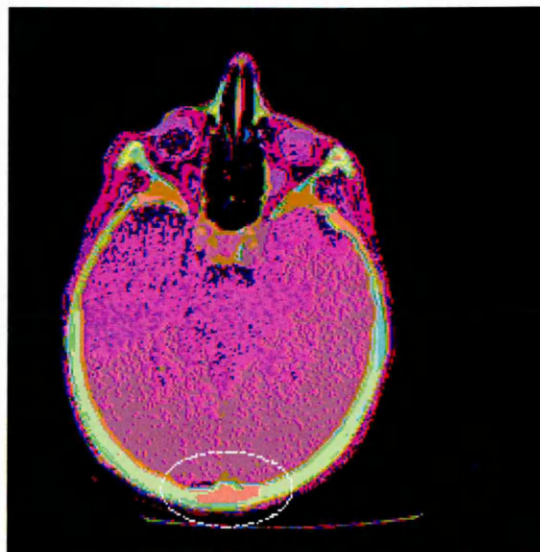
Figure 6.41 - Segmented CT image highlighting dissimilarity within the cranial bone (outlined in white)

119

6.6 Usefulness of the GUI for Highlighting Abnormalities

While viewing the CT image data critical CT scan findings could be obscured by inappropriate window settings (Figure 6.40). With an infinite possibility of display choices an unsuitable compromise for a particular clinical situation may be selected [Jin *et al.,* 2002]. This limitation of display of CT image data using the windowing technique is alleviated using the GUI dissimilarity highlighting facility. The segmented image in Figure 6.41 clearly highlights the dissimilarity within the cranial bone region. This dissimilarity display may prompt the physician to set the correct window to scrutinise the region highlighted by the dissimilarity within an otherwise homogeneous region (in this case the lower cranial bone region) shown in Figure 6.41.

The dissimilarity-highlighting feature was also successfully used for highlighting infarct in MRI T2-weighted images that are hard to visualise. Figures 6.42 and 6.43 are the Diffusion weighted and T2 weighted MR images of a stroke patient, respectively. The Diffusion-weighted image clearly shows the area in the brain, affected by the stroke, in white (pointed by black arrow).
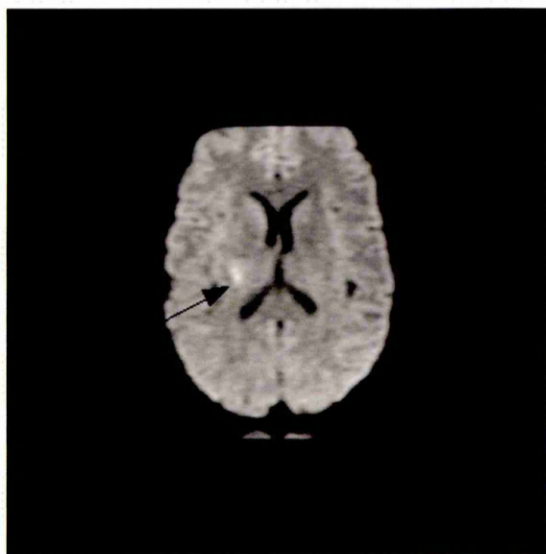
Figure 6.42 - Diffusion weighted MRI   Figure 6.43 - T2 weighted MRI
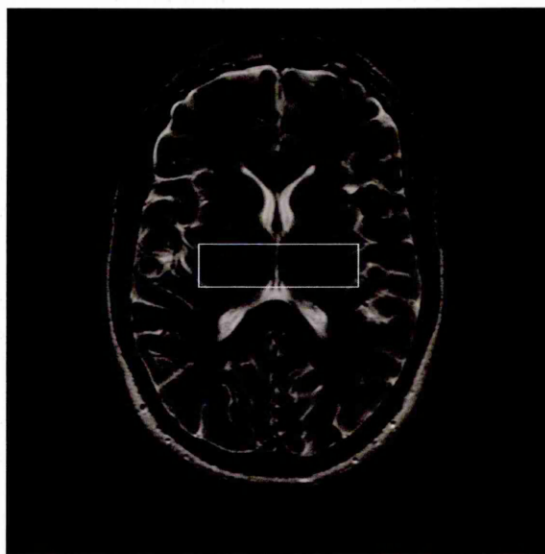
The GUI was evaluated to find whether it could highlight the diseased area in the T2-weighted image. Figure 6.44 displays the different dissimilar regions in the T2 weighted image, for a specific dissimilarity level. The GUI has got a facility, named region tagging, using which the user could highlight the pixels belonging to a specific region.

Figure 6.45 shows a region, that was dissimilar from the rest of the image, which was isolated and highlighted using the GUI region tagging facility. The isolated dissimilar region corresponds to the stroke affected area that is clearly visible in the diffusion-weighted MRI image (Shown in Figure 6.42).

The radiologist's assessment was that the GUI was able to highlight the abnormal area correctly on the T2 weighted scan (confirmed by the Diffusion weighted scans). He also observed that most physicians and possibility neuroradiologists could miss the signal changes on the T2 weighted scan (See Appendix 4 for the neuroradiologists assessment). For this reason the GUI will be useful in highlighting and visualising subtle changes in medical images.
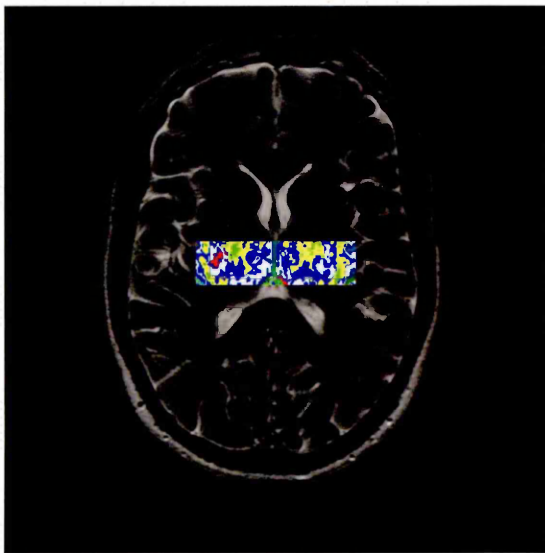
Figure 6.44 - Different dissimilar regions for a specific dissimilarity level.

Figure 6.45 - One of the dissimilar regions for a specific dissimilarity level.

6.7 Summary

In this chapter the performance of the HCS process was analysed. The suitability of the Gray-Tone distribution (GTD) feature, developed for this study, to segment tonal and micro-textural images was demonstrated. The micro-textural nature of the medical images was confirmed by comparing the performance of the GTD feature based versus Gray-Tone based, segmentation of simulated MRI images.

To find the similarity between the regions in a image the necessity of the following three factors was demonstrated :

- Similarity between individual pixels of the two regions.
- Similarity between the pixels bordering the two regions.
- Similarity between the combined feature property of all the pixels in the two regions.

The suitability of the HCS process to segment medical images was demonstrated by evaluating the following capabilities of the HCS process :

- Precise border pixels delineation.
- Comparing and merging spatially disjoint regions.
- Border pixels reclassification.

The HCS process developed was compared with NASA's HSEG process. It was confirmed that HCS border pixel reclassification was the main differing step with that of the HSEG. It was also demonstrated that HCS process with its border pixel reclassification step gave improved segmentation result than HSEG.

Finally the GUI ability to isolate and highlight areas of dissimilarity in medical images, based on the HCS output was evaluated by a neuroradiologist.

Chapter 7

Highlighting Dissimilarity in Medical Images Using HCS

7.1 Introduction

Tissue abnormalities in medical images are indicated by part of the image being dissimilar from other homogeneous areas representing healthy parts. The dissimilarity may be subtle or strong depending on the medical modality and the type of tissue abnormality. For example in CT images, which are based on X-ray attenuation pathological lesions will be detected when there is alteration of water content of the lesion and surrounding tissues together with presence of calcification, haemorrhage *etc.* [Culebras, 1997]. The pathological lesion will be either hypo, or iso or hyperdense to normal tissues – that is either low or similar or high attenuation to normal tissues. Gray scale imaging is excellent for detection of gross alteration in attenuation in pathological lesion, but subtle alteration in lesions with almost similar attenuation to normal tissue may be missed.

Dissimilarity may not always be due to tissue abnormality. It might be due to image noise or due to variability within the same tissue type. Hence any dissimilarity highlighting process would benefit from high level human interaction with a segmentation hierarchy to select the appropriate image segmentation for a particular application. This is because one of the capabilities of the human vision process is the ability to visualise them at different levels of details.

The HCS process designed and implemented in this study automatically generates a hierarchy of segmented images. The hierarchy represents the continuous merging of similar, spatially adjacent or disjoint regions, as the threshold of dissimilarity between regions is gradually increased. The usefulness of the HCS process in highlighting the dissimilarity in medical images will be demonstrated in this chapter.

7.2 Processing of the Medical Images of Different Modalities

One of the main objectives of the current study is to design a segmentation process which will be unsupervised and be completely data driven. This objective ensures that the segmentation process can be applied to any medical image modality, with equal success, without any prior information about the image data and without any need to train the segmentation process with the relevant image data (See Section 1.3). To ensure that this objective is achieved, images of the different modalities (viz. MRI, CT and US) were processed with the same set of parameters and with the same set of procedural steps listed below.

The Hierarchical Clustering Based Segmentation (HCS) process, designed and implemented in this study, is a modular process consisting of the following major operations (for details refer Section 4.3) :

- Feature measurement.
- Pixel pair similarity measurement.
- Initial clustering of the most similar neighbouring pixels.
- Regions merging.
- Border pixels reclassification.

The implementation of the above to process the different images is as detailed in Sections 7.2.1 to 7.2.5.

7.2.1 Feature Measurement

The feature extraction method used to process the images of different modalities (*viz.* MRI, CT and Ultrasound) was based on gray-tone distribution (GTD) (See Section 4.3.1). The GTD feature was chosen for following reasons (See Section 6.2.1)

- Accurate delineation of regions just a couple of pixels in size.
- Highlighting subtle differences in tonal distribution.

7.2.2 Pixel Pair Similarity Measurement

To find the similarity between a pair of pixels, of the images of different modalities (viz. MRI, CT and Ultrasound) the gray-tone distribution around each pixel was compared. To ensure precise border delineation, the mask was placed at different orientations

around the target pixel. All possible combinations of feature distributions between the two pixels were compared to find the best possible similarity value (See Section 4.3.2).

7.2.3 Initial Clustering of the Most Similar Neighbouring Pixels

Initial clustering of the most similar neighbouring pixels (See Section 4.3.3) was not performed on any of the images. At the initial starting of the region merge loop (See Flow chart Figure 4.4) each pixel in the image was tagged as a unique region.

7.2.4 Regions Merging

To generate a hierarchy of segmented images, the region merging was carried out using the agglomerative type of hierarchical clustering process, also known as bottom-up method (See Section 4.3.4). To find the similarity between regions, found in the images of different modalities, the following factors were taken into account :(See Section 4.3.4)

- Similarity between individual pixels of the two regions.
- Similarity between the pixels bordering the two regions.
- Similarity between the combined feature property of all pixels in the two regions.

In order to ensure that the merging result arrived upon did not depend upon the merging regions, all possible combinations of the regions, currently in the image were evaluated (See Sections 4.3.4 and 4.4.1)

7.2.5 Border Pixels Reclassification

After the merging of similar regions, the border pixels of the regions that had merged with other similar regions and their bordering regions were further evaluated to allocate them to the most suitable region (See Section 4.3.5).

7.3 Highlighting Dissimilarity in MRI Images

Cerebral ischemic stroke is one of the most fatal diseases despite current advances in medical science. Patients presenting with suspected stroke require rapid diagnosis and treatment.

125

Nearly 60% of CT scans performed within the first few hours after cerebral infarction are normal [Laughlin, 1998]. This is because CT may be adequate to detect intracranial hemorrhage, but in the case of nonhemorrhagic stroke, the CT scan may be negative for the first 24 to 36 hours [Parizel *et al.,* 2001].

Conventional (spin-echo) MRI (T1 and T2 weighted) depends on an increase in tissue water content within the ischemic brain parenchyma to visualize the infarct. Since oedema takes time to develop, images obtained with spin-echo sequences can be normal in the first 6 to 8 hours after an acute stroke [Laughlin, 1998].

7.3.1 Diffusion Weighted Magnetic Resonance Imaging

Diffusion-weighted MRI (DW-MRI), is a technique used for relating image intensities to the relative mobility of endogenous tissue water molecules. Two equal and opposite large magnetic field gradients are applied before the data is acquired. In the absence of any motion of the water molecules, the magnetic spins will be de-phased by the first gradient, and then completely re-phased by the second gradient. However, because the actual motion of the water molecules is that of a random walk, the second gradient will not completely re-phase the spins. The signal intensity will therefore be exponentially attenuated proportional to the mean diffusion length. Areas with relatively high mean diffusion length will appear dark on the DW-MRI images relative to areas with low mean diffusion length.

Potential clinical applications of water diffusion MRI were suggested very early [Le Bihan *et al.,* 1986] The most successful application of diffusion MRI since the early 1990s has been brain ischemia [Warach *et al.,* 1992], following the discovery in cat brain by Moseley *et al.* [1990] that water diffusion drops at a very early stage of the ischemic event.

Newer diffusion-weighted pulse sequences depend on free movement of water molecules for contrast. With cerebral ischemia, diffusion is impeded within minutes, although the exact mechanisms responsible for this are not yet completely understood. Thus, diffusion-weighted imaging sequences can detect areas of acute ischemia earlier, when conventional MRI and CT may be normal [Sorensen *et al.,* 1996] [Warach *et al.,* 1995] [Laughlin, 1998].

126

Conventional CT and MR imaging are not sufficiently sensitive to evaluate stroke in the hyper acute stage. Conventional MR scans can detect acute stroke by 6 to 12 hours. The ultimate goal for imaging is to define the area of brain infarction and perfusion deficit, and to identify any ischemic tissue that can be salvaged by medical or surgical therapy [Makkart *et al.,* 2003]. Diffusion MRI provides some patients with the opportunity to receive suitable treatment at a stage when brain tissue might still be salvageable [Le Bihan *et al.,* 2001].

Diffusion weighted image in Figure 7.1 shows the stroke affected area in white marked by a black arrow head.
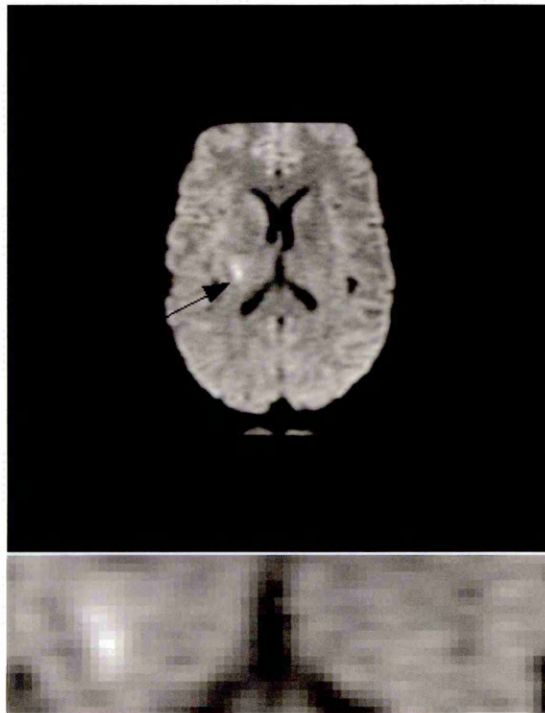
Figure 7.1 - Diffusion weighted MR image with stroke affected area visible as white.
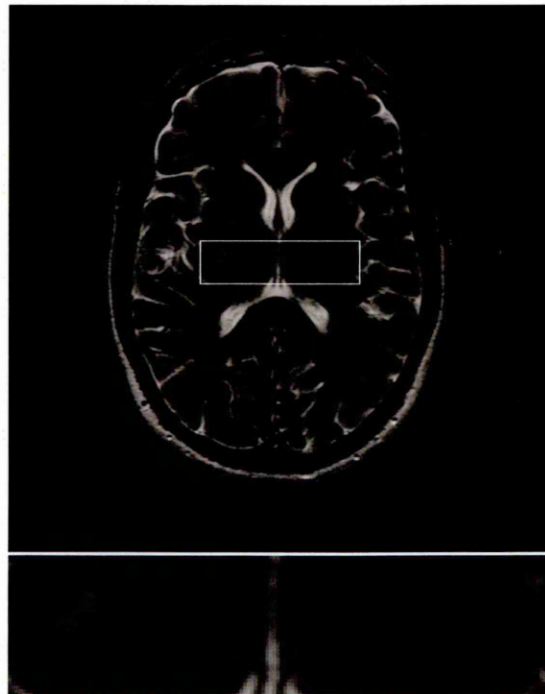
Figure 7.2 - ROI marked T2 weighted MR image

Although over the last 20 years diffusion MRI has become an established technique with a great impact on health care and neurosciences, like any other MRI technique it remains subject to artifacts and pitfalls. In addition to common MRI artifacts, there are specific problems that one may encounter when using MRI scanner gradient hardware for diffusion MRI, especially in terms of eddy currents and sensitivity to motion [Le Bihan *et al.,* 2006].

The most important difficulty was motion sensitivity, which can cause severe ghosting artifacts or complete signal loss. As molecular displacement must be observed on the order of micrometers, it is no surprise that any motion-even unavoidable involuntary head motion or physiological, blood pressure-related pulsations of the brain tissue-would interfere with these measurements. The problem is even more serious when scans must be obtained in disoriented and confused stroke victims, whose head movements are excessive.

The development of faster sequences that are more robust to bulk motion was largely inspired by the need to cope with motion sensitivity. The simplest method of avoiding motion artefacts is to use a motion insensitive method such as echo planar imaging (EPI) [Turner *et al.*, 1990]. The sequence most frequently used for DWI (diffusion weighted imaging) is single shot EPI. It has attained a pre-eminent position in this field, due to its speed, insensitivity to motion and high sensitivity. The disadvantages of single-shot EPI are a limited spatial resolution and the distortions caused by susceptibility gradients.

The poor spatial resolution of the DWI, shown in Figure 7.1, could be seen when compared to the T2 weighted image, shown in Figure 7.2, of the same part of the brain of the same patient.

7.3.2 Identifying Stroke Affected Area in T2 Weighted Magnetic Resonance Imaging

Since the T2 weighted image has better spatial resolution, giving better anatomical details of the area of the brain affected by stroke, it is desirable to identify the stroke affected area in the T2 weighted image at the very early stage of the stroke. So it was decided to find out whether the HCS process could discern the subtle signal changes, that could have been caused at the early stage of the stroke, in the T2 weighted image.

There have been many reports on studies highlighting the advantage of DWI in the early detection of the stoke affected area. All of them state that abnormalities on T2 weighted images do not typically appear until at least 6 hours after symptom onset [Miller, 2004].

But it should be noted that although conventional MRI sequences most often do not

show evidence of stroke in the acute phase, conventional MRI may show signs of intravascular thrombus such as absence of flow void on T2-WI. Also a few hours after stroke onset, a loss of arterial void signal is sometimes observed (30-40% of patients); it is best observed on T2-WI.

Taking into account the above possibilities that there may be some signal change in the T2-WI, albeit very slight, during the hyperacute stage (less than 24hrs) the objective of the current study was to find out whether HCS could highlight the subtle changes correlating with the DWI image highlighted area.
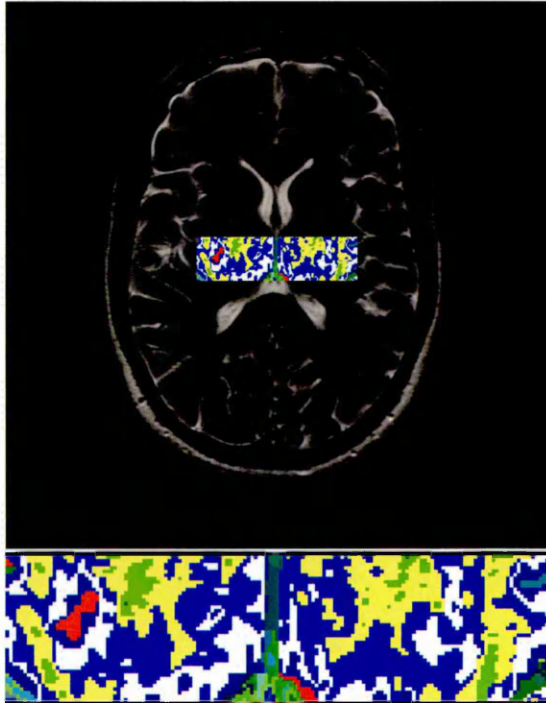
Figure 7.3 - Dissimilar regions highlighted by HCS at an intermediate stage.
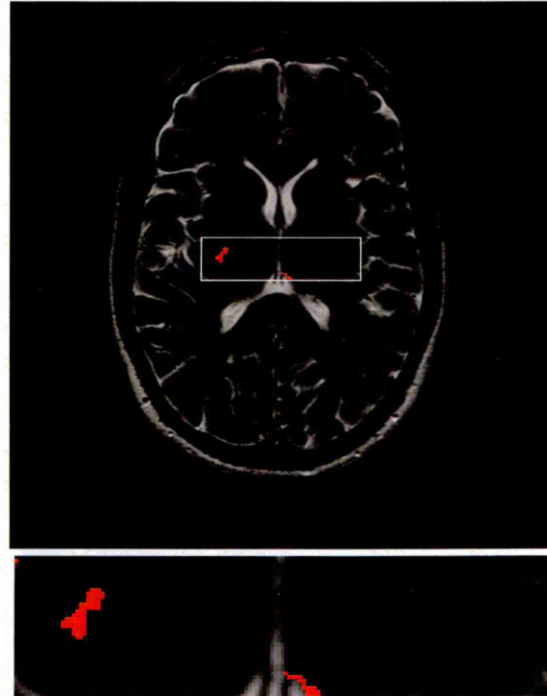
Figure 7.4 - Pixels belonging to one of the dissimilar regions highlighted by HCS

The current study is the only study, to the author's knowledge, that has attempted to evaluate the possibility of identifying the stroke affected area in a T2 weighted image during the hyperacute stage (less than 24hrs) which is correlated with a DWI result.

Figure 7.3 shows forty two different clusters segmented in the image by HCS during an intermediate stage of the segmentation. In Figure 7.3 the larger size clusters are shown coloured in Blue, Yellow, Green and White. Other smaller size clusters are given other unique colours. The cluster which has got pixels around the probable location of the

infarct (as seen in the diffusion weighted image shown in Figure 7.1), is coloured in Red. Using the cluster tagging facility of the GUI the cluster of pixels around the probable location of the infarct was isolated. Figure 7.4 shows the pixels belonging to the isolated regions segmented during an intermediate stage of the segmentation. Comparing the isolated region in Figure 7.4 with the DWI in Figure 7.1 it can be seen that the pixels belonging to the isolated region correlates with the stroke affected area visible as white in the DWI image.

The results shown in Figures 7.3 and 7.4 were presented to a neuroradiologist for evaluation. His written opinion (see also Appendix 4) regarding the usefulness of the developed method is reproduced below :

"I have been going through all the processed images. My preliminary assessment is that the programme is able to pick up the abnormal area correctly on the T2 weighted scan (confirmed by the diffusion weighted scans). I would also like to mention that the signal changes seen on the T2 weighted scan, would be missed by most physicians and possibly neuroradiologists.

My concerns at this stage are

> *(i) Is the programme consistent. To answer this you could analyse the same area again*

> *(ii) Is the programme picking up noise and by chance is it in the same location as the lesion. This could be checked by running the programme on other examples of similar lesions and by increasing the size of the area evaluated."*

The first concern, regarding the program consistency, is answered by the fact that the program is designed to always give the same segmentation results. The program has been amply tested as described in Section 4.4.1 of the Methodology chapter. Hence running the program any number of times would always result in the same segmentation. The second concern has been addressed by processing a cross-sectional image adjacent to this.

Figure 7.6 - Adjacent slice ROI marked
T2 weighted MR image

Figure 7.5 - Adjacent slice DW MR image
with stroke affected area visible as white.

The MRI image slices in Figures 7.5 and 7.6 are of the same stroke patient but of the adjacent cross-section. The modalities are DWI, shown in Figure 7.5, and T2-Weighted shown in Figure 7.6, of the adjacent cross-section. The DWI image, shown in Figure 7.5, shows the area in the brain which is affected by the stroke in white, marked by an arrow.

Figure 7.7 shows forty different regions segmented in the image by HCS during an intermediate stage of the segmentation. In Figure 7.7 the larger size clusters are shown coloured in Blue, Yellow and Green. Other smaller size clusters are given other unique colours. The cluster which has got pixels around the probable location of the infarct (as seen in the diffusion weighted image shown in Figure 7.5), is coloured in Red and White. Using the cluster tagging facility of the GUI the two clusters of pixels around the probable location of the infarct were isolated. Figure 7.8 shows the pixels belonging to the isolated regions segmented during an intermediate stage of the segmentation.

Comparing these regions with the DWI shown in Figure 7.5, it can be seen that the pixels belonging to the isolated regions correlate reasonably well with the stroke affected area visible as white in the DWI image.

131
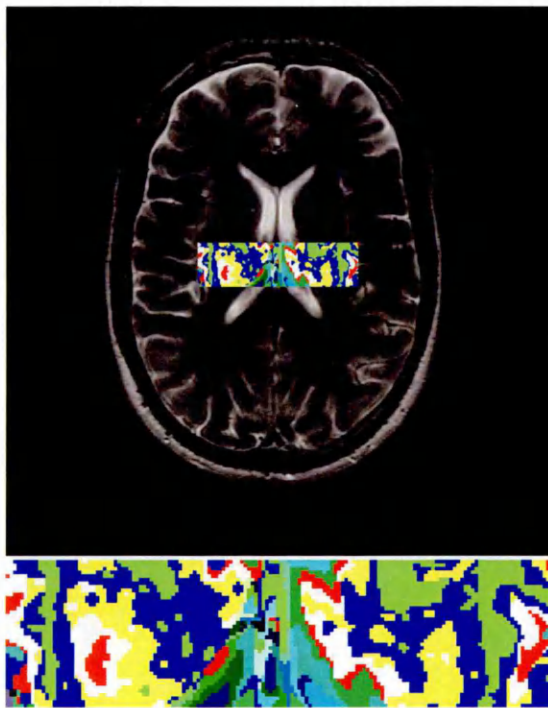
Figure 7.7 - Dissimilar regions highlighted by HCS at an intermediate stage.
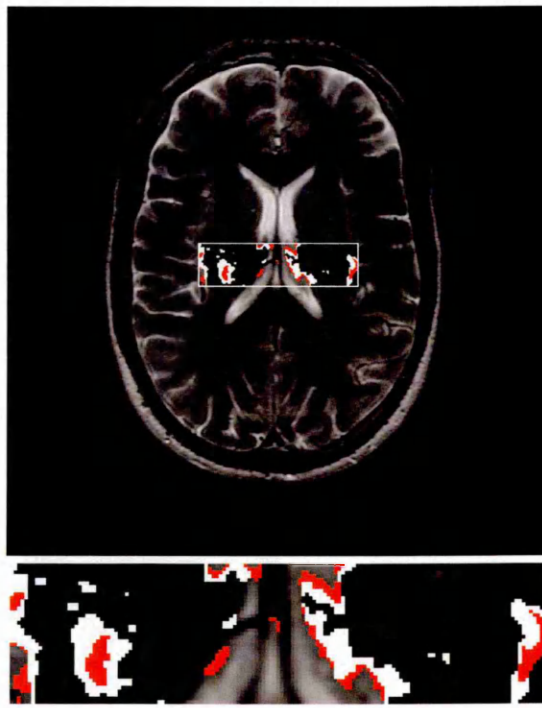
Figure 7.8 - Pixels belonging to two of the dissimilar regions highlighted by HCS at an intermediate stage.

7.4 Identifying Stroke Affected Area in CT Images During Hyperacute Stage

Given the results obtained by processing the MRI images, the neuroradiologist was encouraged to try HCS program on CT images generated during hyperacute stage. His observation and suggestions are reproduced below :

"CT is the primary imaging modality for the imaging of hyperacute stroke. CT scans in the hyperacute stage (less than three hours) are mostly normal or show very subtle changes. The treatment for strokes needs to be started in the hyperacute stage and therefore any process that can help identify a lesion would be very useful.

Going by the results so far on the T2, I would suggest running the programme on an example of CT scan of a hyperacute stroke. The examples I have sent show no detectable abnormality."

Since HCS produce a hierarchy of results it was presumed that HCS would most likely pick up the subtle changes in the signal during hyperacutes stage. Hence it was decided to apply HCS on CT images attained during hyperacute stage.

132

7.4.1 CT Perfusion Study

While MRIs are considered the reference standard for post stroke analysis, they are rarely performed and generally impractical because they take around 30 minutes to perform, they require a stroke patient to be still to capture clean images (the patient may be moving or thrashing), they require doctors to check for metallic objects in the patients body (which may be impossible if no family members are present) and the MRI units themselves are often not adequately staffed or not located near the emergency room.

CT perfusion offers distinct advantages because most hospital emergency rooms use them frequently for other purposes, they take one to two minutes to scan (versus 30 minutes for MRI), and provide clear images even if a patient cannot lie perfectly still. Most hospitals need only to buy software (at a relatively inexpensive cost) to upgrade their systems and institute training programs.

Under the National Instituted of Health (NIH) stroke guidelines, hospitals typically administer Recombinant Tissue Plasminogen Activator (rtPA) (a clot-busting drug) to patients within a three-hour window of stroke onset. After six hours, it's generally considered too risky to administer even interarterial clot busting medicines, due to the risk of a potentially deadly haemorrhage.

CT perfusion allows radiologists to determine which portions of a stroke patient's brain are dead, and which portions are dying but capable of being salvaged. Once a ratio of dead to dying brain is calculated, doctors can determine the best course of treatment. Only those patients whose brains are damaged but still alive will benefit from that treatment of acute revascularization of a blocked blood vessel [Kaste, 2004].

7.4.2 Image Data

The images were CT Perfusion images. The images were considered to be noisy. The images were of four cross-sectional slices having stroke lesion or infarct. For each of the four cross-sectional slices 43 images were taken, at regular time interval (maybe 5 Seconds interval) after a contrast had been injected. So in total there were 4x43 = 172 images. In each of the 4 sets of 43 Images the first few images (say 1 to 6 of the 43)

133

would not have any contrast effect the last set of images (say 37 to 43 of the 43) would have maximum contrast effect. The effect of the stroke would be highlighted in those images where the contrast would have taken effect.

Figure 7.9 shows one of the first few images, before the contrast had taken effect, of one of the four cross-sectional image. Figure 7.10 shows one of the last few images, after the contrast had taken effect, of the same cross-sectional slice. In Figure 7.10 the arrow head points at the suspected area. Figure 7.11 shows the colour coded image after the contrast had taken effect.
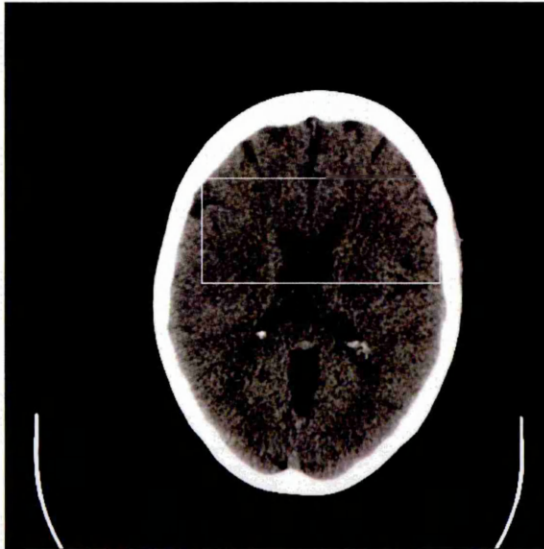
Figure 7.9 - One of the cross-sectional slices before contrast

Figure 7.10 - Same cross-sectional slice after contrast

7.4.3 Objective

The objective of the study was for each of the 4 sets of the 43 images decide the size and location of the ROI by looking at the last images (say 37 to 43 of the 43) where the infarct is clearly visible. Then process the first few images (say 1 to 6 of the 43) within the ROI and find out whether HCS is able to highlight the infarct correlating with the location of infarct seen on the images where contrast had taken effect.

Referring to the images shown in Figures 7.9-7.10 the image shown in Figure 7.9 should be processed within the ROI to find out whether the HCS could highlight the suspected area correlating with the location of the suspected area in Figure 7.10 (pointed by the arrow head).
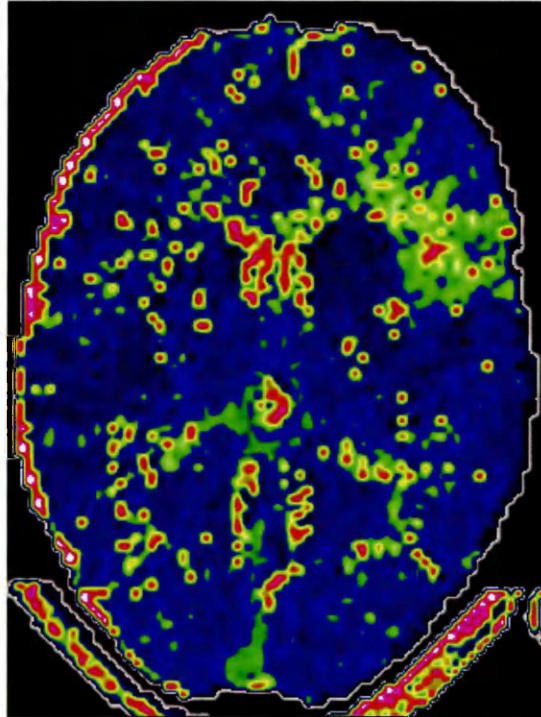
Figure 7.11 - Colour coded Perfusion Image

7.4.4 Highlighting Stroke Affected Area in CT Images During Hyperacute Stage

All image data, before being processed by the time consuming HCS process, was inspected using equal-probability quantizing [Haralick, 1973] (see Section 5.3.1.1 for details) process to find out whether there was enough discernible information for HCS to work. There had been an earlier study where the authors had shown that in nonenhanced CT of the head, detection of ischemic brain parenchyma is facilitated by soft-copy review with variable window width and centre level settings to accentuate the contrast between normal and oedematous tissue [Lev, 1999].

The visual inspection of the image data using equal-probability quantizing was done using a custom built GUI. The GUI, shown in Figure 5.34, was developed to quantise

and view images for different window settings (see Section 5.3.1.2 for details). For example Figure 5.36 shows the T2 weighted MRI image data seen normally and Figure 5.37 shows the same image displayed after being quantised using equal-probability quantizing process. In Figure 5.37 one can visualise the suspected area (pointed by green arrow head) much more clearly when compared to Figure 5.36. Thus on inspecting Figure 5.37 one can come to the conclusion that there is enough discerning information for HCS to highlight the suspected area. This came true at the end of HCS processing since it successfully highlighted the suspected area as shown in Figure 5.39.

By analysing the image shown in Figure 7.9, using equal-probability quantising process GUI it was found that there was not enough discerning information for HCS to highlight the suspected area.

The reason for the standard CT image not being able to show any change in the hyperacute stage could be explained as follows. Conventional CT and MRI (T1 and T2 weighted) images are focussed on capturing the structural changes in the brain. For example conventional (spin-echo) MRI (T1 and T2 weighted) depends on an increase in tissue water content within the ischemic brain parenchyma to visualize the infarct while MRI diffusion and CT perfusion studies evaluate the physiological change to tissues related to metabolism. Using CT perfusion study one can obtain information about tissue level parenchymal brain perfusion. Since physiological changes occur at relatively long time before structural changes take into effect, conventional CT images may not show any difference during hyperaccute stage.

The appeal of MRI methods over CT is due to the following reason. Standard CT examination of acute ischemic stroke will typically appear normal in the first hours after stroke onset. The methods of magnetic resonance angiography, perfusion weighted imaging (PWI), and diffusion weighted imaging (DWI) provide information on arterial patency, tissue blood flow, and parenchymal injury from the earliest times after onset of ischemic symptoms in a brief, non-invasive examination. DWI detects tissue injury within minutes of ischemia, has high sensitivity and specificity for the diagnosis of ischemic stroke, and permits measurement of lesion volumes that correlate with clinical severity and prognosis. If untreated, the lesion seen with DWI typically enlarges over hours to days and will progress to infarction. PWI depicts focal cerebral ischemia. The volume of ischemic tissue seen with PWI, in the majority of cases, is greater than the

region of parenchymal injury evident on DWI, and this diffusion-perfusion mismatch is considered to be a marker of the ischemic penumbra, the tissue at greatest risk for infarct progression [Warach, 2001]. This discussion confirms that CT images, before contrast taking into effect, at hyperacute stage do not have any signal change.

HCS can highlight the dissimilarity precisely even if it is subtle. But in the absence of any change in the signal there will be no basis for HCS to differentiate the diseased area from the healthy part of the brain. Therefore the study has concluded that HCS cannot be used to highlight stroke affected area in a CT image, captured during hyperacute stage.
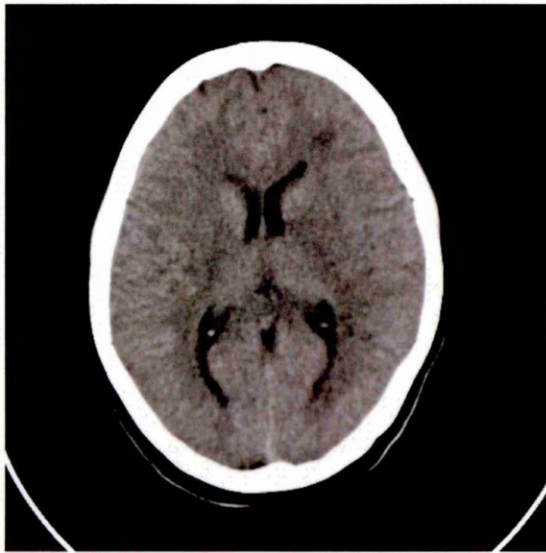
Figure 7.12 - A CT image section

CT-Bmp image Suspected Area Marked
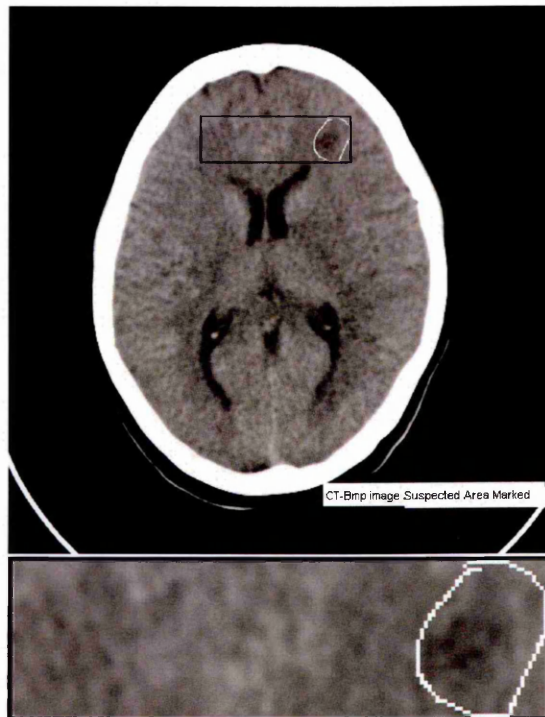
Figure 7.13 - Image showing the suspected area, outlined in white and the ROI rectangle drawn in black.

7.5 Highlighting Infarcts in CT Images

Figure 7.12 shows the CT image data of a patient affected by stroke. Figure 7.13 shows the suspected area in the image outlined by the expert in white. A ROI was chosen to enclose the suspected area as shown in Figure 7.13. The image was processed by the HCS process within the ROI.
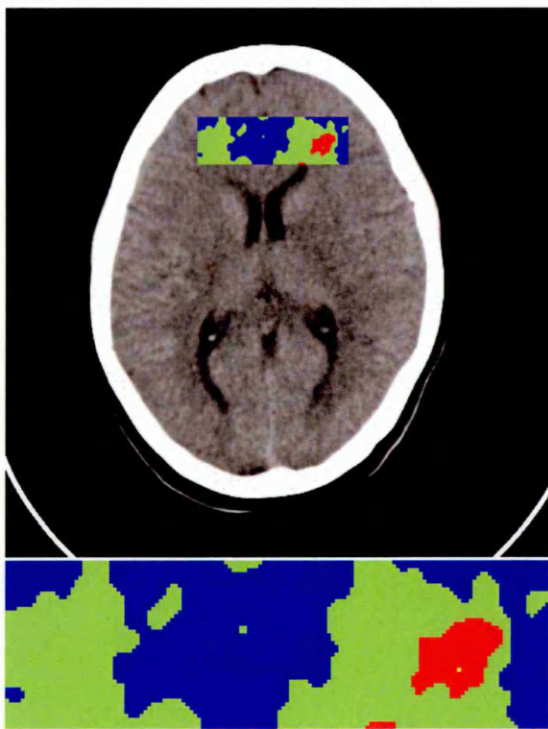
Figure 7.14 - Intermediate segmentation regions, within the ROI during HCS process.
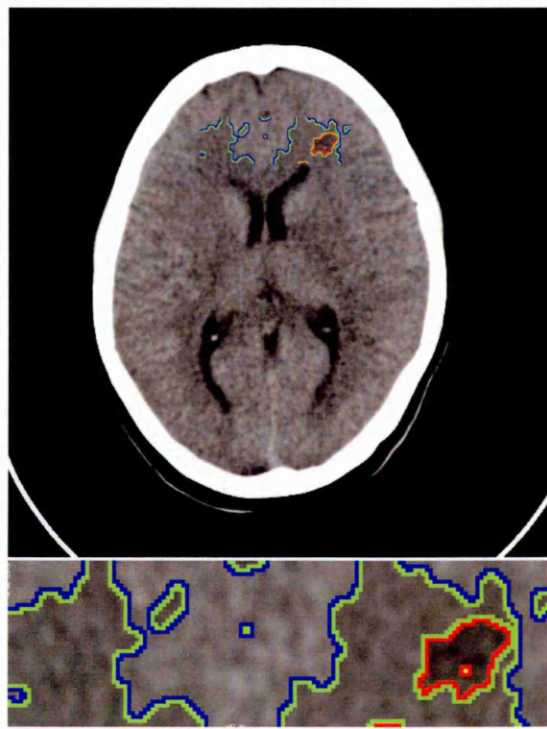
Figure 7.15 - Intermediate segmentation regions' boundary outlined.

Figure 7.14 shows the regions found by the HCS process during the intermediate stage. Figure 7.15 shows the boundaries between the regions found during the intermediate stage. From Figures 7.14 and 7.15 it could be seen that the major classes in the original image, viz. White Matter (Green), Gray Matter (Blue) and infarct (Red), had been segmented. The area affected by the disease had been clearly demarcated from the rest of the healthy tissue, by the HCS process.

7.5.1 Expert Opinion

When the expert was presented with the results shown in Figures 7.14 and 7.15, he marked the part of the image which had been misclassified as infarct by the HCS process. Figures 7.16 and 7.17 show the misclassification (top of the left ventricle horn) circled in white by the expert.

Although the misclassification was quantitatively minor and had occurred at an area which is anatomically quite different from the part affected by the disease, it was decided to find out whether the misclassification could be rectified.

138
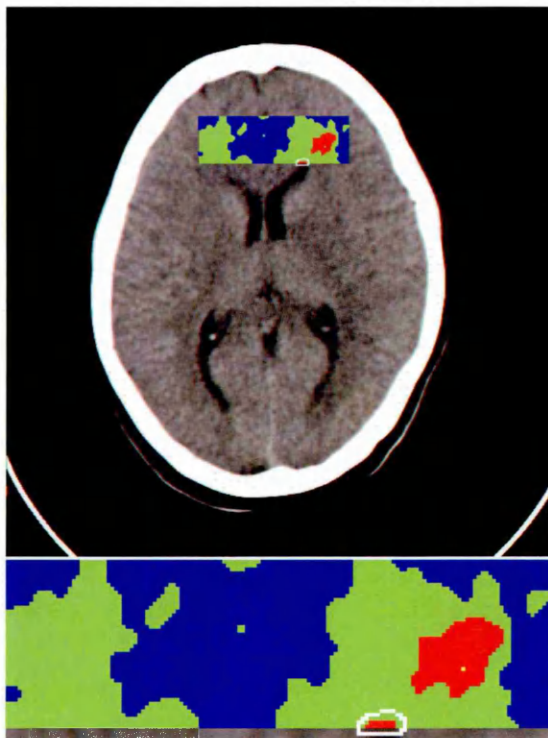
Figure 7.16 - Intermediate segmentation regions, with the misclassified part outlined in white by the expert.
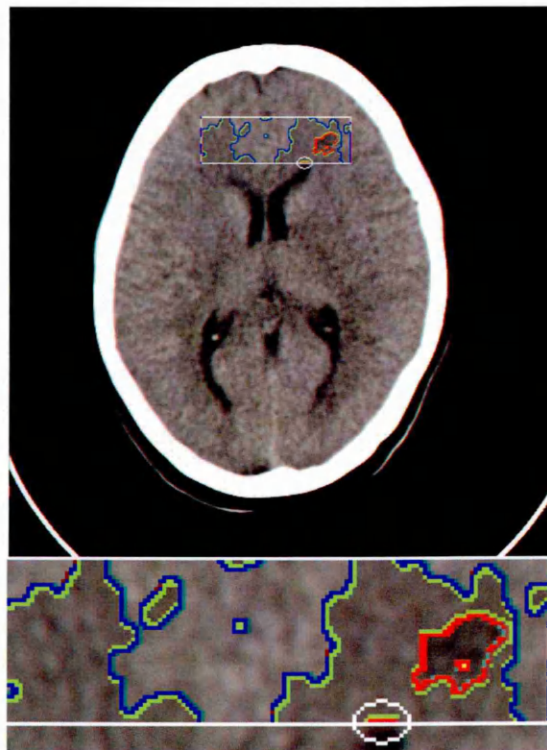
Figure 7.17 - Intermediate segmentation regions' boundary, with the misclassified part circled in white by the expert.

7.5.2 Subsequent Processing

It was hypothesised that if more of the ventricle part was included within the ROI, HCS might be able to rectify the misclassification. Hence the CT image shown in Figure 7.12 was processed with a slightly bigger ROI which included larger part of the top tip of the left ventricle horn as shown in Figure 7.18.

The HCS result is shown in Figures 7.19 and 7.20. Figure 7.19 shows the regions found by the HCS process during the intermediate stage. Figure 7.20 shows the boundaries between the regions found during the intermediate stage. From Figures 7.19 and 7.20 it could be seen that the major classes in the original image had been segmented.

These figures also shows that the HCS process had classified part of the Ventricle as part of the infarct (coloured in Red). When presented with such a result, it is left for the human expert to reject those pixels that are not consistent with his expert knowledge.
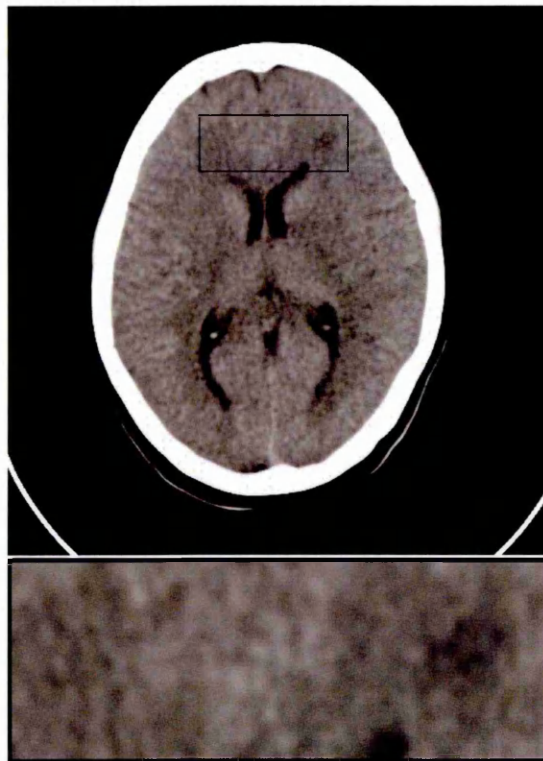
Figure 7.18 - The CT image section with
a slightly larger ROI marked on it.
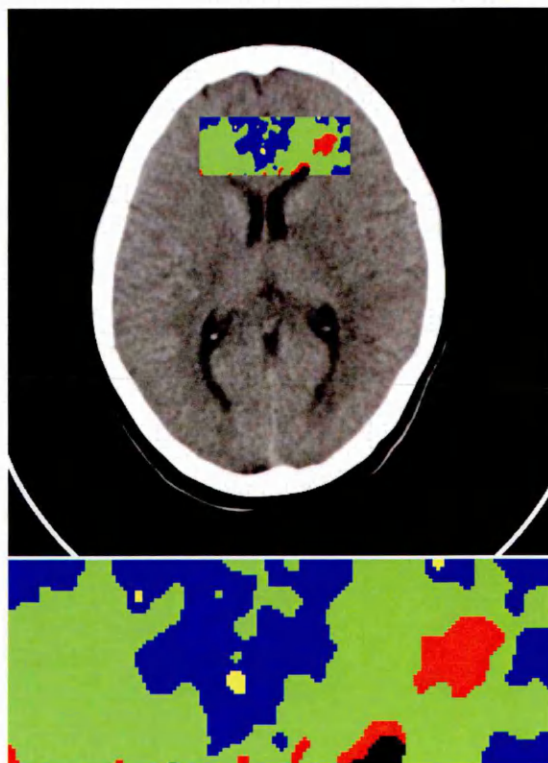
Figure 7.19 - Intermediate segmentation
regions, for a slightly bigger ROI
including a bit of the top of the Ventricle.
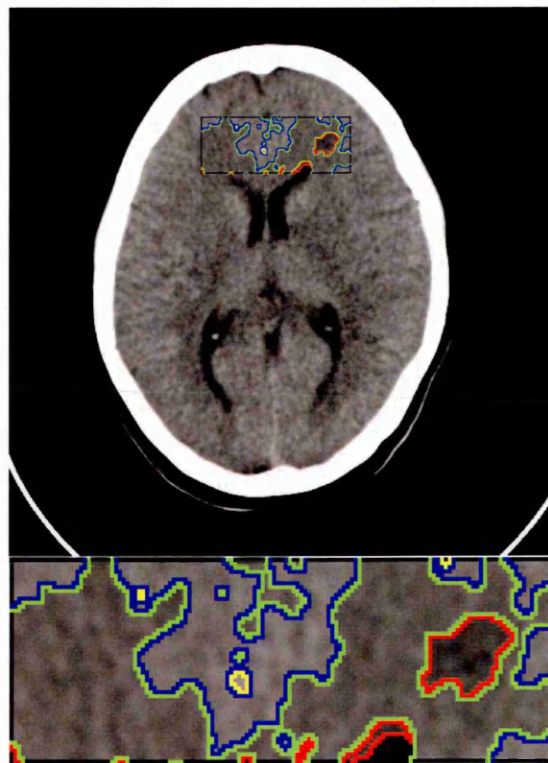
Figure 7.20 - Intermediate segmentation
regions' boundary, for a slightly bigger
ROI including a bit of the top of the
Ventricle.

7.5.3 Further CT Image Processing

Three more CT image sections of the brain of three different patients were processed. The ROI, within which the processing was performed, was chosen based on the markings by the expert. In the following sections 7.5.3.1 - 7.5.3.3, the results obtained in processing the three different CT sections are discussed.

Figure 7.21 - CT image of a section of the brain showing the infarct affected area marked in white by the expert.
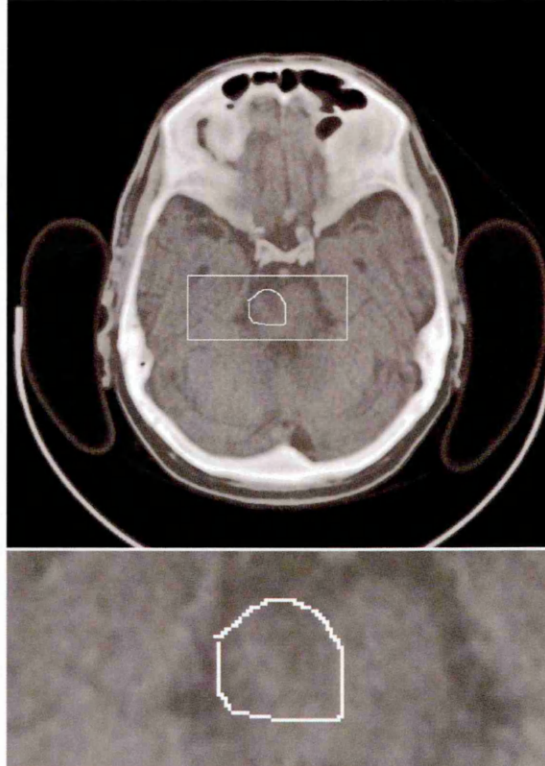
Figure 7.22 - The location and the size of the ROI enclosing the infarct affected area.

7.5.3.1 Infarcts in the Right Side of the Pons

Figure 7.21 shows the infarct affected area of the brain outlined in white by the expert. The image was processed within a ROI which enclosed the part of the image affected by the stroke. Figure 7.22 shows the location and size of the ROI chosen.

Figure 7.23 shows the four major clusters segmented within the ROI by the HCS process during an intermediate stage. Figure 7.24 shows the borders of the clusters. The cluster which includes the pixels from the area outlined by the expert is coloured red and the rest of the clusters are given other unique colours.

141

It can be seen from Figures 7.23 and 7.24 the red coloured cluster includes other pixels which were not within the expert outlined area. From the boundary outlined image shown in Figure 7.24 it could be seen that the area of the image within the red boundary has got visually very similar pixels.
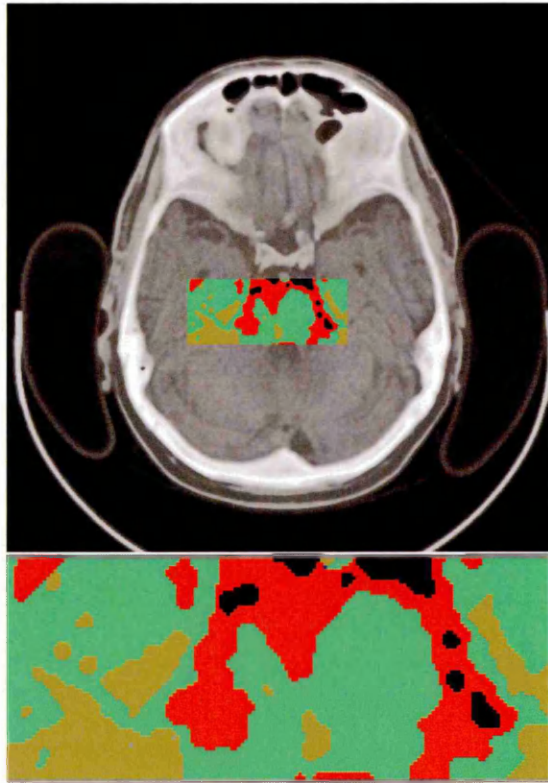
Figure 7.23 - The regions during an intermediate stage of the HCS process.
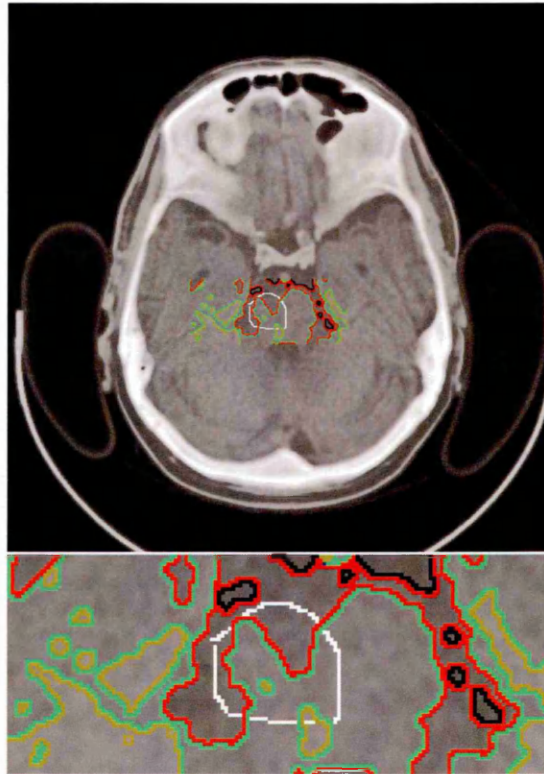
Figure 7.24 - Borders of the regions during an intermediate stage of the HCS process.

7.5.3.1.1 Expert Opinion and Discussion

When the segmentation, shown in the Figures 7.23 and 7.24, was given to the expert for their evaluation. He responded that the segmentation had misclassified areas not belonging to infarct as belonging to infarct. This is indicated in Figure 7.25 where the expert has marked the true area of the infarct. Figure 7.26 shows the boundaries of the regions segmented by the HCS process superimposed on the image subsequently marked by the expert. The boundary of the cluster, which includes the pixels from the area outlined by the expert, is coloured red ant the rest of the clusters boundaries are given other unique colours.

142
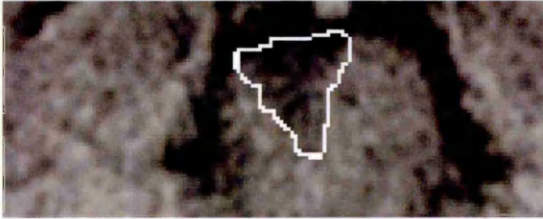
Figure 7.25 - Infarct outlined by the expert after evaluating the HCS process results.
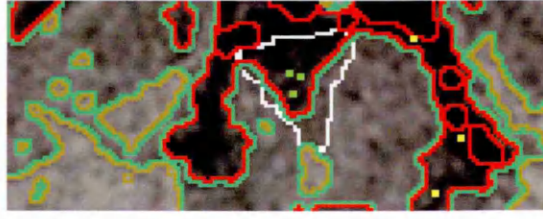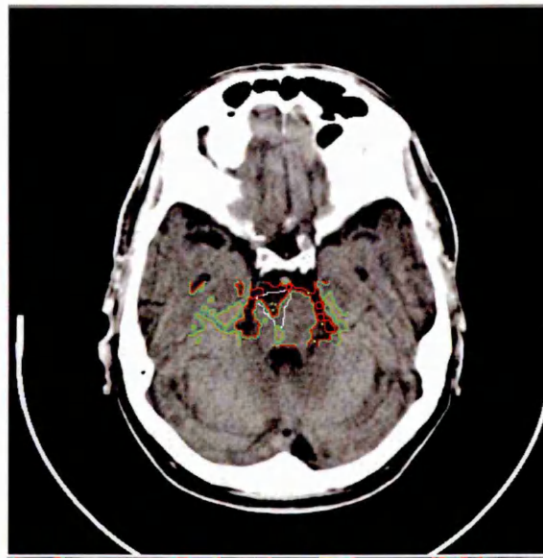
Figure 7.26 - Borders of the regions during an intermediate stage of the HCS process superimposed on the expert outlined image.

On inspecting Figure 7.26, the following two observations were made :

- HCS process did aid the expert in delineating the boundary of the infarct much more precisely. This could be inferred when one compares the earlier outline of the infarct by the expert, shown in Figure 7.21, with the one (see Figure 7.25) outlined by the expert after inspecting the HCS process segmented regions.

- When one compares the actual pixel values of some of the pixel locations within the infarct and the one outside the infarct, but identified as belonging to the infarct by the HCS process, it could be seen that they have exactly the same values.

  Table 7.1 lists the some of the pixel locations and their values. In Figure 7.27 the pixel locations listed in Table 7.1 are marked where correctly classified pixel locations are in Green and misclassified pixel locations are in Yellow.

Table 7.1

Coordinates of three of the pixels located inside and outside the infarct and their values.
(See Figure 7.30)

Pixel Location	Pixel Coordinates	Pixel value
Within the infarct **(Marked in Green)**	250, 284	1033
	249, 278	1036
	251, 278	1038
Outside the infarct **(Marked in Yellow)**	296, 297	1033
	289, 313	1036
	283, 268	1038
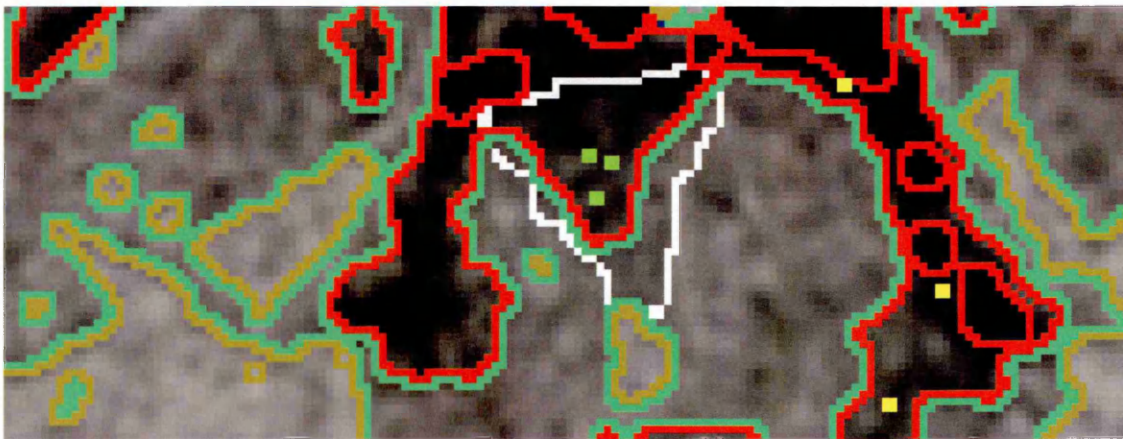
Figure 7.27 - Three of the pixel locations which were correctly classified, by the HCS process (marked in green) and three of the pixel locations which were misclassified (marked in yellow). Refer Table 7.1 for details.

7.5.3.2 Sub Acute Infarcts of Lentiform Nucleus

Figure 7.28 shows the locations of the infarcts on two different locations in the cross-section. Figure 7.29 shows the ROI chosen to enclose the two areas affected by the infarcts.

One of the main features of the HCS process is the evaluation of all the possible combinations of the regions, currently in the image, to find and merge the most similar regions (see Sections 4.3.4 and 4.4.1). Comparing all the possible combinations of regions, in an image, is CPU process intensive. However this was necessary in the medical image domain since similar tissue types could occur across the image interspersed by different tissue types. The image shown in Figure 7.28 demonstrates the need for comparing spatially disjoint regions since the diseased area had occurred in two different locations which were spatially disjoint.

Figure 7.28 - CT image of a section of the brain showing the infarct affected areas marked in white by the expert.
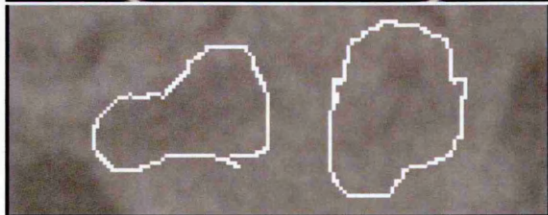
Figure 7.29 - The location and the size of the ROI enclosing the infarct affected areas.
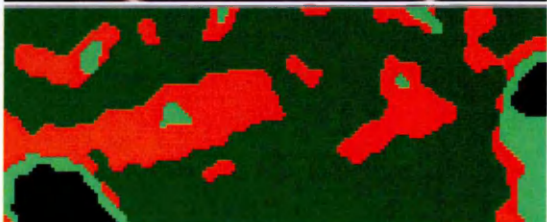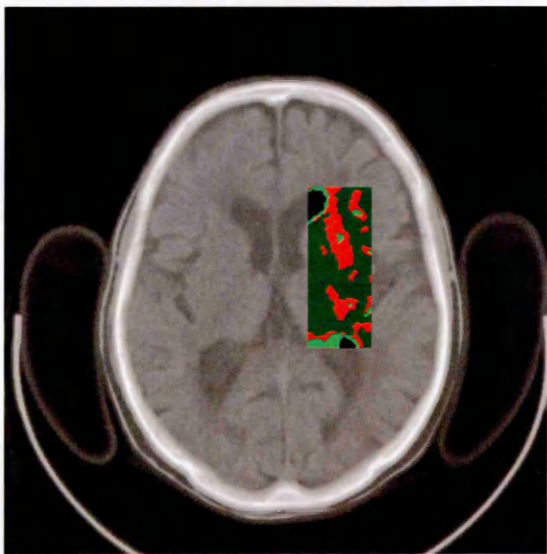
Figure 7.30 - Regions identified by the HCS process during an intermediate stage.
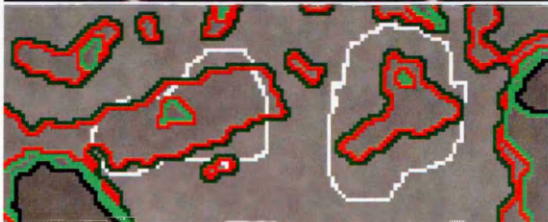
Figure 7.31 - The boundaries of the regions identified by the HCS.

145

Figure 7.30 shows four clusters segmented within the ROI by the HCS process during an intermediate stage. Figure 7.31 shows the borders of the four clusters superimposed on top of the infarct border outlined by the expert. From these it can be concluded that the areas affected by the infarct had been isolated by the HCS process into separate clusters and the two spatially disjoint areas, affected by the infarct were clustered as belonging to the same cluster.

7.5.3.3 Sub Acute Infarct in the Left Internal Capsule

Figure 7.32 shows the infarct affected area of the brain outlined in white by the expert. The image was processed within a ROI which enclosed the part of the image affected by the stroke. Figure 7.33 shows the location and size of the ROI chosen for the HCS processing.

Figure 7.32 - CT image of a section of the brain showing the infarct affected areas marked in white by the expert.
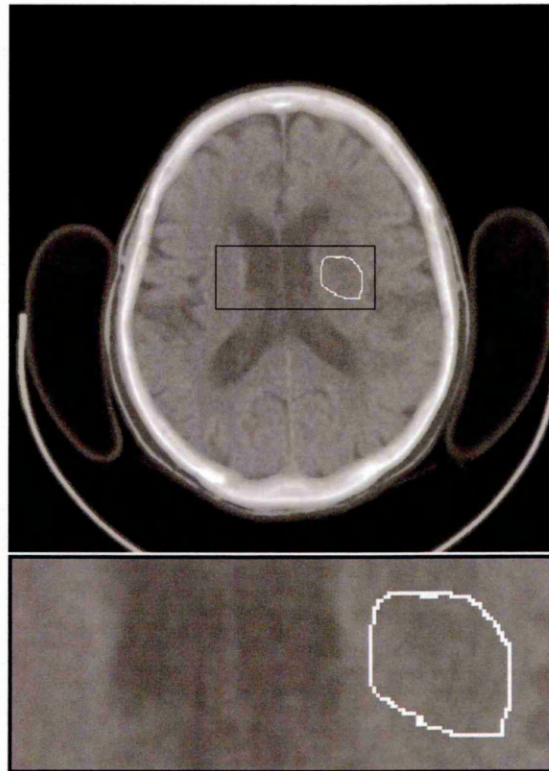
Figure 7.33 - The location and the size of the ROI enclosing the infarct.

Figure 7.34 shows the clusters segmented within the ROI by the HCS process during an intermediate stage. Figure 7.35 shows the borders of the five large clusters found. The cluster which includes pixels from the infarct affected area is coloured in Red; the rest of the clusters are given other unique colours. Figures 7.34 and 7.35 show that the infarct affected area had been segmented into a separate region by the HCS process.

146

There could be some misclassification but it would be rejected by the experts given the anatomical location of the misclassification. Since the expert had given only a rough estimate of the boundary of the infarct no exact validation of the segmentation process could possibly be done.
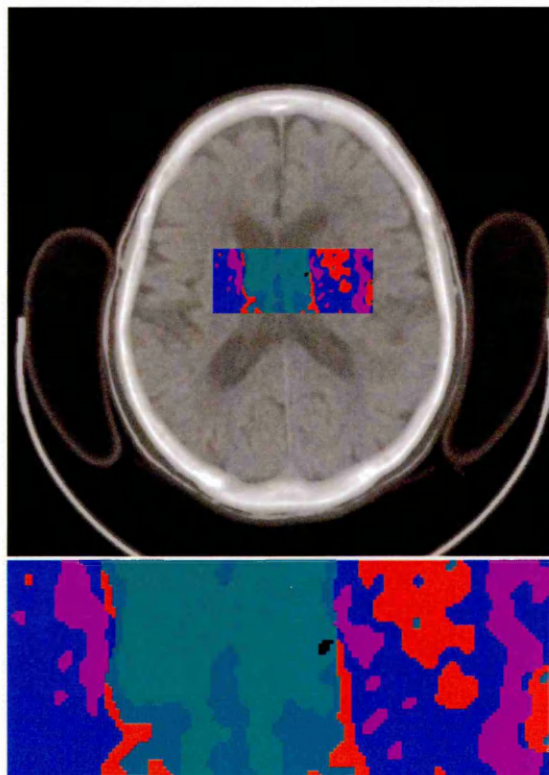
Figure 7.34 - Regions identified by the HCS process during an intermediate stage.
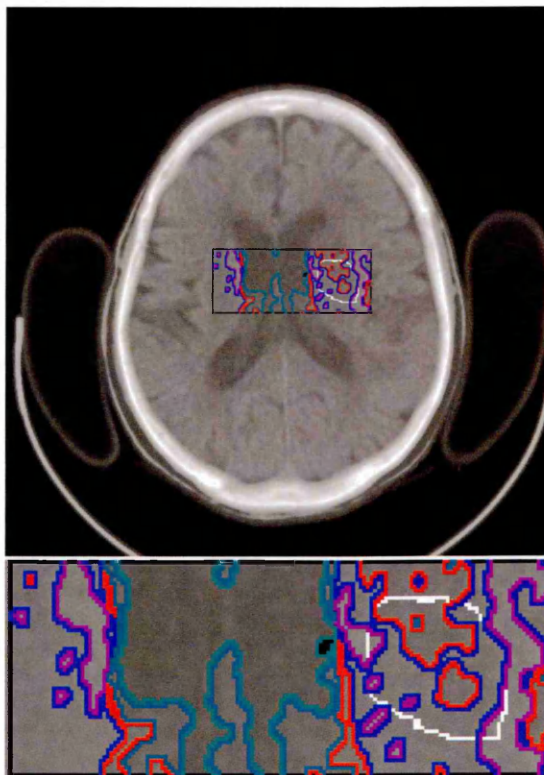
Figure 7.35 - The boundaries of the regions identified by the HCS.

7.5.4 Conclusion about the HCS Processing of CT Images

Because of issues such as spatial resolution, poor contrast, ill-defined boundaries, noise, or acquisition artefacts, segmentation is a difficult task and it is illusory to believe that it can be achieved by using gray-level information alone. A priori knowledge has to be used in the process, and so-called low-level processing algorithms have to be incorporated with higher level techniques such as deformable active models or atlas-based methods [Sonka and Fitzpatrick, 2000].

Given an image data, the HCS process will give consistently a set of segmentation results. HCS does not give a diagnosis. It is left for the human expert to make use of the segmentation results attained through HCS and incorporating his own expert knowledge to arrive upon a diagnosis. Thus the developed HCS process acts as a Computer Aided Detection tool.

Figure 7.36 - An Ultrasound image section.
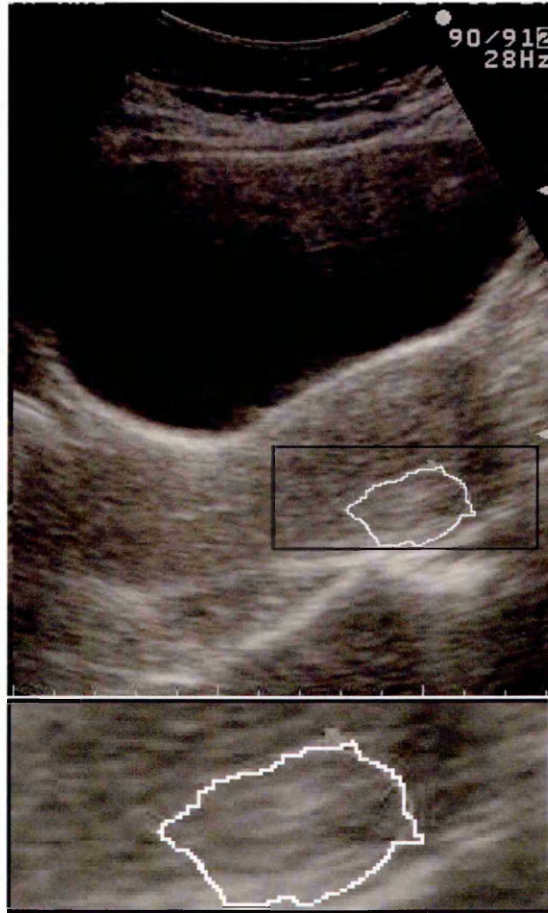
Figure 7.37 - Diseased area outlined in white and the ROI marked in black.

7.6 Highlighting Diseased Area in Ultrasound Images

Figure 7.36 shows the an Ultrasound image section of the Uterus. And image 7.37 shows the diseased area outlined in white by the sonologist. As shown in Figure 7.37 a ROI was marked to enclose the diseased area and the HCS was done within the ROI.

Figure 7.38 shows the clusters identified by the HCS process during an intermediate stage. There are three clusters coloured as Green, Blue and Yellow as shown in Figure 7.38. The cluster coloured as Blue contains the pixels from the area outlined as diseased by the sonologist. Figure 7.39 shows the boundaries of the three clusters and the diseased area outline coloured in Red.
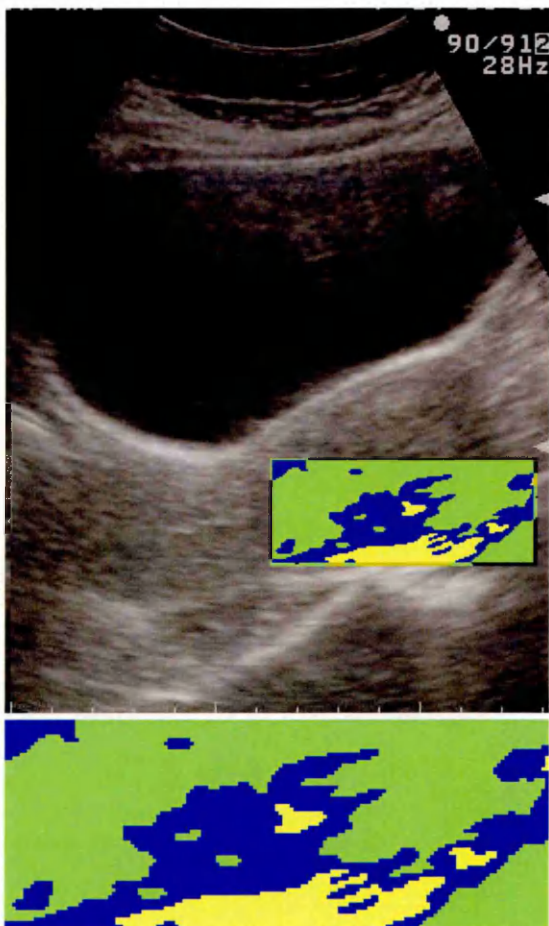
Figure 7.38 - Regions identified by the HCS process during an intermediate stage.
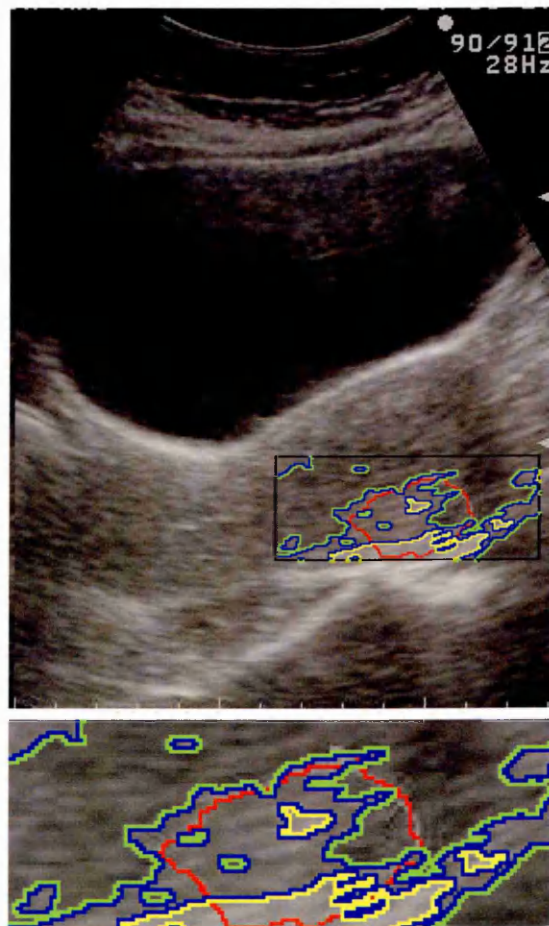
Figure 7.39 – Boundaries of the regions segmented by the HCS process during an intermediate stage.

7.6.1 Expert Opinion and Discussion

The segmentation results, shown in Figures 7.38 and 7.39 were sent to the Sonologist for critical comments, this is reproduced below :

- Looking at the original image only an expert sonologist would be able to pick up this abnormality.

- The program had delineated the diseased area very clearly as a separate region coloured Blue. As for the pixels outside the diseased area coloured Blue it could be differentiated by the physician as non diseased area as they were in the border of the Uterus. Therefore the program will be useful to differentiate diseased area in the case of border line pathology, where the sonologist will not be very sure of the diseased area.

- The region marked as Yellow within the diseased area gave the additional information that that area has got the core of the disease, and it was spreading out from that location.

149

The image data processed by the HCS programme was eight bit data. The original data captured by the Ultrasound machine was twelve bit data. The machine had the optional facility to store the original twelve bit data in DICOM format. But since that facility was optional the institute which provided the Ultrasound data did not have it in their machine. If the HCS process was provided with the original twelve bit data it might have segmented the diseased area much more precisely.

7.7 Summary

In this chapter the suitability of the HCS process to highlight dissimilar regions in medical images was investigated. The medical image data that was processed were of MRI, CT and Ultrasound modalities. To demonstrate the unsupervised capability of the HCS process the images of the different modalities were processed with the same set of parameters and with the same set of procedural steps (see Section 7.2 for details).

Summarising the results :
- HCS was successful in highlighting subtle changes in MRI T2 weighted images caused by stroke. The location of the abnormality highlighted by the HCS was confirmed by the diffusion weighted MRI scans (see Section 7.3 for details).
- The current study came to the conclusion that CT images, before contrast taking into effect, at hyperacute stage do not have any signal change to enable the HCS process to be able to isolate the stroke affected area from the healthy area (see Section 7.4 for details).
- The HCS ability to highlight infarcts in CT images was found to be mixed. If the infarct was well defined, the HCS was able to highlight it with precise border delineation. If the infarct was diffused, then HCS segmentation labeled some part of the image outside the infarct affected area as diseased (see Section 7.5 for details).
- The HCS ability to highlight diseased area in the Ultrasound images was quite good, even though it processed only eight bit data instead of the original twelve bit data.

Chapter 8

Overall Discussion, Conclusion and Further Work

8.1 Challenges and Objectives

Tissue characterization is a signal processing operation of extracting and presenting diagnostic information obtained from medical image data. Tissue characterization is essentially an inverse problem, where investigators ask what can be learned about a patient's state of health by analysing the relevant image data [Sonka and Fitzpatrick, 2000].

Even after years of research, tissue characterization methods are still not part of clinical practice. There are many reasons for this, but the primary ones are [Sonka and Fitzpatrick, 2000] :

- Tissue classifiers must be designed for specific diagnosis. This requires a multidisciplinary development team. Often, the initiative for this research is led by engineers and physicists who do not have the resources to discover and compensate for the sources of normal biological variability that can reduce diagnostic performance.
- Lack of accurate models of image signals.

To address the above issues the objectives of the current study were to :

- design a segmentation process which will be unsupervised and be completely data driven.
  This objective ensures that the developed process can be applied to any medical image modality without any prior information or training with equal success.
- design a segmentation process which will automatically generate a hierarchy of segmentation results.
  Satisfying this objective will ensure that the user is provided with a hierarchy of results to choose from. In situations where a one-off solution may not be successful, the user is given the option to choose the best possible solution from the hierarchy of results.

To address the problems outlined above the current study took the following approach :

- to develop methods which although they do not provide a diagnosis will augment the diagnostic present. This is achieved through highlighting the dissimilarity within an otherwise homogeneous part of the image. Dissimilarity, within an otherwise homogeneous part of the image, is usually related to the tissue abnormality in a medical image.

- to develop methods which do not use any prior information or model to detect the dissimilar regions within an image. Rather the dissimilar regions within an image are detected based on the information extracted from the current image data.

To develop the above methods and to provide a hierarchy of results, the current study implemented a agglomerative type of hierarchical clustering process [Legendre and Legendre, 2003]. Agglomerative hierarchical clustering is also known as the bottom-up method. The bottom-up method described in the literature usually suffers from a distorting phenomena, in which the cluster structures depend on the order in which the regions are considered for merging. This is because the most similar pairs of regions are found by comparing only those regions adjacent to one another. The process developed in this study avoided this problem by comparing all pairs of regions currently in the image to find the most similar regions for merging. This ensured that the designed process always yielded the same segmentation for any given dissimilarity threshold. A hierarchy of segmentation results was obtained by adopting a dynamic threshold for the allowable dissimilarity measure between merging regions. Comparing all the possible combinations of regions, in an image, is CPU process intensive. However, this comparison was necessary since similar tissue types could occur across the medical images interspersed by different tissue types.

Comparing all the regions, within an image, is a combinatorial problem which can easily overwhelm the computing power currently available. In this study a number of methods were devised to optimise this process. One of the main optimisation techniques implemented was to use concurrent programming techniques. Since the calculation of the dissimilarity between the regions are independent of each other it may be done in parallel.

8.2 Main Findings and Contributions of this Thesis

The main outcomes of the work are :

- Design of a segmentation process which is unsupervised and is completely data driven.

  This ensures that the segmentation process can be applied to any medical image modality, with equal success, without any prior information about the image data and without any need to train the segmentation process with the relevant image data (See Section 1.3). This was verified by the successful processing of images of different modalities with the same set of parameters and with the same set of procedural steps.

- Design of a segmentation process which can automatically generate a hierarchy of segmentation results.

- Development of a process by which the merging (*i.e.* clustering) of the most similar regions does not depend on the order in which the regions are evaluated for merging.

- Implementation of a merging process which is independent of the type of similarity measure used to compare the different regions in the image.

- Evaluation of the merging process to demonstrate the merging of spatially adjacent or disjoint similar regions.

- Development of a merging process which yields crisp border delineation between the regions.

- Implementation of a graphical user interface (GUI) to display the hierarchy of segmentation results based on the merge tree produced by the hierarchical clustering based segmentation.

8.3 Discussion of the Results

The results obtained by the Hierarchical Clustering based Segmentation (HCS) system, developed in this study, were compared with the results obtained by the Hierarchical image segmentation (HSEG) developed by NASA [Tilton NASA Case No. GSC 14,328] [Tilton, 2003].

HCS was compared with HSEG for the following reasons :

- HSEG (see Section 3.3.3) is one of the segmentation methods which is similar to HCS (see Section 3.4.1)
- One of the application domain of HSEG is to segment medical images and it has been licensed to Barton Medical Imaging to be used in its medical image analysis software product MED-SEG™ [Barton Medical Imaging].

Comparing the results of the HSEG with that of the results obtained by HCS (see Section 6.5 for details) it was found that the border pixel reclassification step implemented by the HCS process was the main differing step with that of the HSEG. It was also found that the HCS process with its border pixel reclassification step gave far better segmentation result when compared with HSEG.

8.4 Main Contributions of the Study

Dissimilarities in medical image data, within the same tissue type, might be due to pathological conditions. To highlight the gross or subtle dissimilarities and thus enhance the diagnostic power of the images, the following methods and processes were implemented in this study :

- Equal-probability quantizing [Haralick *et al.*, 1973] method to optimally display the wide range of medical image data values using only the 256 shades of gray available for display.
- Hierarchical clustering segmentation (HCS) process, developed in this study, that would automatically and consistently generate a hierarchy of segmentation results.

8.5 Assessment of the Performance of HCS in a Clinical Application

This current study is the only study, to the author's knowledge, that has been attempted to evaluate the possibility of identifying the stroke affected area in a T2 weighted MR image during the hyperacute stage (less than 24hrs) correlated with a Diffusion weighted MR image finding (see Section 7.3.2 for details).

The radiologist's assessment was that the HCS process was able to highlight the abnormal area correctly on the T2 weighted MR scan (confirmed by the Diffusion

weighted MR scans). He also observed that most physicians and possibility neuroradiologists could miss the signal changes on the T2 weighted scan (See Appendix 4 for the neuroradiologists assessment).

8.6 Possible application domain

The two main contributions of this study were a hierarchical clustering based segmentation process to highlight dissimilarities in medical images and the implementation of a GUI to optimally display medical images using equal-probability quantizing method.

8.6.1 Probable Usage of the HCS Process

The equal-probability method along with the GUI designed and implemented makes the hard to visualise diseased area more conspicuous. But to precisely outline the boundary of the diseased area the process which will be much more useful is the hierarchical clustering based segmentation (HCS) process developed. Precise estimation of regions of dissimilarity plays a crucial role in disease management for example in the treatment of stroke.

In their landmark study, Wintermark and co-workers were able to show that perfusion CT could with reasonable accuracy predict the final cerebral infarct size in acute stroke patients at the time of emergency evaluation [Kaste, 2004].

Roccatagliata *et al.* [2003] carried out a study to find if a quick, visual, freehand estimate of the size of ischemic lesions on CT cerebral blood volume (CBV) and cerebral blood flow (CBF) maps (in CT perfusion images) is sufficient to obviate the need for a more careful, thresholding approach to delineating abnormal regions. Specifically, they compared inter-observer variability in the detection of hypo-perfused CBF and CBV lesion areas, between using a "quick and dirty" approach, versus a more careful, methodical approach. They concluded that segmentation of ischemic regions on CBF maps by gross visual inspection is significantly more reliable than segmentation of CBV maps. Because CBV maps have inherently worse signal-to-noise ratio and infarct conspicuity than CBF maps, estimating the size of the "infarct core" may be facilitated by a more methodical thresholding approach to segmentation [Roccatagliata *et al.*, 2003].

It will be useful to evaluate the HCS process under clinical condition in segmenting and estimating the penumbra size and infarct size to evaluate potential recuperation ratio which may revolutionize the way stroke is treated [Kaste, 2004].

8.6.2 Probable Usage of the GUI to Optimally Display Medical Images

Lev *et al.* [1999] conducted a study to evaluate the advantage of viewing electronic copies of the CT image using variable window settings. They arrived upon the conclusion that in non-enhanced CT of the head, detection of ischemic brain parenchyma is facilitated by soft-copy (electronic copy) review with variable window width and centre level settings to accentuate the contrast between normal and edematous tissue.

The equal-probability method, along with the GUI, implemented in this study (see Section 5.3.1.2 for details), will facilitate detection of hard to visualise infarct condition. If this facility is tested in a clinical environment it could equal, if not better, that the study by Lev *et al.* [1999] observed in, *i.e.* a significant improvement in the diagnostic accuracy.

8.7 Further Work

Two methods have been implemented in this study *viz.* equal-probability quantising method, to optimally display 12 bit medical image data and the hierarchical clustering based segmentation process to highlight dissimilar regions in the medical images. Of these two methods the equal-probability quantising method, performs in real-time in the currently available hardware environment. But the HCS process took almost a month to produce a hierarchy of clusters for a region of interest size 140×140. The current hardware configuration, which can handle a maximum ROI size of 140×140, has a dual processor of each 1.6 MHz. clock speed and has 16 Gigabyte of main memory. Methods which yields a hierarchy of segmentation results are processing intensive. For example the software product MED-SEG™ [Barton Medical Imaging], which is based on NASA's RHSEG, uses a 60 node cluster to process images within a reasonable amount of time. Still RHSEG is suboptimal when compared to HCS developed in this study (see Section 6.5 for details).

The massive processing power required by HCS will be very soon available on a desktop environment. During September 2006 Intel announced that it has produced its first teraflop-on-a-chip. It is a eighty-core processor and each core, in Intel's prototype, clocks at 3.16GHz and communicates with each other through SRAM chips. Intel claims that this technology will be available within 5 years. To put this into perspective, the fastest public supercomputer in 1996 was the ASCI Red which featured over 4,500 compute nodes using 200MHz Pentium Pro processors and was the first computer to break the 1 teraflops barrier.

The current implementation of the HCS process was designed to run on a generic multi-processor environment. To utilise hardware specific facilities, like multi-core central processing unit, (CPU) the program need to be optimised to run on specific hardware environment.

Medical image data like CT and MRI inherently contain three dimensional information. The underlying three dimensional details of the anatomy can be easily recreated by stacking the two dimensional slices. One of the major challenges faced by the human interpretor of the medical images is the difficulty they face to visualise conditions which spans between slices. HCS can be very easily extended to process data in a three dimensional cube. This way HCS can fully utilise all the information currently available in the medical image data.

Appendix 1

Hydrogen exists in many molecules in the body. Water (consisting of two hydrogen atoms and one oxygen) comprises up to 70% of body weight. Hydrogen is also present in fat and most other tissues in the body. The varying molecular structures and the amount of hydrogen in various tissues effect how the protons behave in the external field. As an example, because of the total amount of hydrogen in water, it has one of the strongest net magnetization vectors relative to other tissues. Other structures and tissues within the body have less hydrogen concentration and become magnetized to a lesser extent. In other words, their net magnetization is less intense. The amount of mobile hydrogen protons that a given tissue possesses, relative to water (specifically CSF), is referred to as its spin density (proton density). This is the basis with which we begin to produce images using Magnetic Resonance. The hydrogen nucleus contains one proton and possesses a significant magnetic moment. In addition, hydrogen is very abundant in the human body. By placing the patient in a large external magnetic field, we magnetize the tissue (hydrogen), preparing it for the MR imaging process. [Faulkner]

The MRI system's most prominent component is a large magnet, and along with it are two sets of coils, the so-called gradient coils and radio frequency (RF) coils. An MRI image is a map of RF intensities emitted by tissues. This can be briefly explained as follows: the gradient coil is used to inject an out-of-phase pulse to perturb the aligned atoms away from the main magnetic field. As the atoms realign with the main field, they transmit energy back, which is detected by the RF coils which in turn generates an MRI image. [Suri *et al.*, 2002]

T1 is the longitudinal relaxation time. It indicates the time required for a substance to become magnetized after first being placed in a magnetic field or, alternatively, the time required to regain longitudinal magnetization following an RF pulse. T1 is determined by thermal interactions between the resonating protons and other protons and other magnetic nuclei in the magnetic environment or "lattice". These interactions allow the energy absorbed by the protons during resonance to be dispersed to other nuclei in the lattice.

All molecules have natural motions due to vibration, rotation, and translation. Smaller molecules like water generally move more rapidly, thus they have higher natural

158

frequencies. Larger molecules like proteins move more slowly. When water is held in hydration layers around a protein by hydrophilic side groups, its rapid motion slows considerably.

The T1 relaxation time reflects the relationship between the frequency of these molecular motions and the resonance (Larmor) frequency – which depends on the main magnetic field of the MR scanner. When the two are similar, T1 is short and recovery of magnetization is rapid; when they are different, T1 is long. The water molecule is small and moves too rapidly for efficient T1 relaxation, whereas large proteins move too slowly. Both have natural frequencies significantly different from the Larmor frequency and thus have long T1 relaxation times. Cholesterol, a medium-sized molecule, has natural frequencies close to those used for MR imaging and has a short T1 when it is in the liquid state. Thus the liquid cholesterol in craniopharyngiomas appears bright on T1-weighted images.

Water in the bulk phase (for example, CSF) has a long T1 relaxation time because the frequency of its natural motions is much higher than the range of Larmor frequencies used clinically. However, when this same CSF is forced out into the periventricular white matter (as interstitial edema due to ventricular obstruction) its T1 relaxation time is much shorter. The T1-shortening reflects the fact that water is now in hydration layers around the myelin protein rather than in the bulk phase. Proteinaceous solutions (such as abscesses and necrotic tumors) have a higher percentage of water in the hydration layer environment and thus have a shorter T1 when compared to "pure" aqueous solutions like CSF.

Subacute hemorrhage has a shorter T1 than brain tissue. This reflects the paramagnetic characteristics of the iron in methemoglobin. T1-shortening is produced by a dipole-dipole interaction between unpaired electrons on the paramagnetic iron and water protons in the solution. The short T1 allows subacute hemorrhage to recover longitudinal magnetization very quickly relative to brain. Thus, subacute hemorrhage will generally appear brighter than brain. The same dipole-dipole mechanism accounts for T1-shortening that is seen with the MRI contrast agent, gadolinium.

T2 is the "transverse" relaxation time. It is a measure of how long transverse magnetization would last in a perfectly uniform external magnetic field. Alternatively, it

159

is a measure of how long the resonating protons remain coherent or precess (rotate) "in phase" following a 90° RF pulse. T2 decay is due to magnetic interactions that occur between spinning protons. Unlike T1 interactions, T2 interactions do not involve a transfer of energy but only a change in phase, which leads to a loss of coherence.

T2 relaxation depends on the presence of static internal fields in the substance. These are generally due to protons on larger molecules. These stationary or slowly fluctuating magnetic fields create local regions of increased or decreased magnetic fields, depending on whether the protons align with or against the main magnetic field (as discussed in Fundamentals of MRI – Part I). Local field non-uniformities cause the protons to precess (rotate) at slightly different frequencies. Thus following the 90° pulse, the protons lose coherence and transverse magnetization is lost. This results in both T2* and T2 relaxation.

When paramagnetic substances are compartmentalized, they cause rapid loss of coherence and have a short T2* and T2. For example the magnetization induced inside a deoxygenated red blood cell is greater than in the plasma outside the red cell because the intracellular deoxyhemoglobin is paramagnetic. This compartmentalization of substances with different degrees of induced magnetization leads to magnetic non-uniformity with shortened T2*, causing the free induction decay (FID) to decay more rapidly. Since gradient echo images are essentially rephased FID images, this also leads to signal loss on gradient echo images. Thus acute and early subacute hemorrhage (containing deoxy and intracellular methemoglobin, respectively) appear dark on T2-weighted gradient echo images. The different magnetic field inside and outside red cells results in rapid dephasing of water protons diffusing across the red cell membrane in an acute hematoma with secondary T2-shortening and loss of signal.

As the natural motional frequency of the protons increases, T2 relaxation becomes less and less efficient and T2 prolongs. Rapidly fluctuating motions (such as in liquids) average out so there are no significant internal fields and there is a more uniform internal magnetic environment. The hydration-layer water in brain edema has a shorter T1 than bulk phase water like CSF, yet the motion of the protons in brain edema is not so slow that T2 relaxation is efficient, so T2 remains long. This accounts for the intense appearance of the vasogenic edema associated with brain tumors on T2-weighted MR images.

Spin Echo:

An MR pulsing sequence involves acquisition of multiple spin echo signals. For a 256 x 192 image (pixels in the frequency direction x pixels in the phase direction) with two excitations, 384 separate spin echoes are acquired. During the time between acquisitions, the longitudinal magnetization recovers or "relaxes" along the z-axis. Longitudinal recovery is identical to the process of initial magnetization when the body was first placed in the magnet. When the body is in the magnet, the "equilibrium state" is that of full magnetization. Therefore, longitudinal relaxation represents the recovery of magnetization along the z-axis, which occurs between spin echo acquisitions.

In the first step of a spin echo pulsing sequence, a 90° RF pulse flips the existing longitudinal magnetization from the z-axis 90° into the transverse xy-plane. Whenever transverse magnetization is present, it rotates at the Larmor frequency and induces an oscillating MR signal in a receiver coil (as discussed in Fundamentals of MRI – Part I). The magnitude of the transverse magnetization after the 90° pulse is essentially equal to the magnitude of the longitudinal magnetization which had recovered during the interval between 90^0 pulses. This interval is called the "repetition time" (TR) and is one of the programmable sequence parameters.

In the process of flipping the longitudinal magnetization 90° into the transverse orientation, the longitudinal component of magnetization is totally lost and must be allowed to recover before another signal can be generated. The amount of longitudinal magnetization that is recovered depends on the rate of recovery (T1) and the time allowed for recovery to occur, which is the TR.

The magnitude of the signal detected depends not only on longitudinal recovery between repetitions but also on how well the signal persists, or alternatively, on how slowly the transverse magnetization decays from its initial maximum value. This decay depends on the T2 of the substance. The amount of time allowed for decay to occur (the time between the initial 90° RF pulse and the detection of the spin echo) is called the echo delay time (TE) and is another programmable sequence parameter.

Mathematically the intensity (I) of the spin echo signal can be approximated:

$$I = N(H)f(v)(1 - e^{-TR/T1})e^{-TE/T2}$$

where N(H) is the NMR-visible, mobile proton density and f(v) is an unspecified function of flow. This equation indicates that the intensity of the MR signal increases as hydrogen density and T2 increase and as T1 decreases. It should also be noted that T1 and T2 influences are both subject to TR and TE, the programmable sequence parameters. Thus, the effect of the T1 and T2 relaxation times of the substance on signal intensity is subject to the specific values of TR and TE selected before the image is acquired. Only mobile protons, that is, those associated with liquids, return an NMR signal. Solids have very short T2s and thus have no significant NMR signal.

When considered in the most simplistic terms, the spin echo is a two-step process. The first step (longitudinal recovery) determines the starting intensity for the second step (transverse decay). The starting intensity reflects the relationship between T1 and TR and is ultimately limited by the proton density. The subsequent decay from this starting intensity reflects the relationship between T2 and TE. Consider the differentiation of brain tissue and CSF shown in. At TR = 0.5 seconds, the CSF signal starts to decay from a markedly decreased initial value. Despite the longer T2 of CSF, the intensity remains less than that of brain over the range of echo delay times shown. If the repetition time TR is lengthened to 2.0 seconds, the CSF signal starts to decay from a greater initial intensity and still decays more slowly than the signal from brain. Thus the two signals will become isointense at a TE of approximately 50 msec. With a longer TE, the CSF is more intense than brain.

The difference in T1 values between brain parenchyma (shorter T1) and CSF (longer T1) can be used to enhance contrast between the two. This is important when seeking abnormalities at the brain-CSF interface. A short TR time allows a shorter T1 substance (such as brain) to recover signal between repetitions to a much greater extent than a longer T1 substance (such as CSF). The contrast in short TR/short TE sequences is based primarily on differences in T1 and are called "T1-weighted" images. Note that substances with low values of T1 have the highest signal intensity on T1-weighted images.

As the TR is prolonged, all substances eventually recover full longitudinal magnetization between repetitions and the pixel intensity becomes dependent only upon proton density and is independent of T1. With short TE's, the effect of T2 decay is minimized and one is left with an image that depends primarily on differences in proton density, that is, a "proton density-weighted" image.

162

Substances with longer T2 times will generate stronger signals than substances with shorter T2 times, if both are acquired at the same TE and if proton density and T1 are comparable. When multiple spin echoes are acquired, the signal strength generally decreases as TE is lengthened due to increasing T2 decay. Increasing the echo delay time (TE) increases the differences in the T2 decay curves between substances, increasing the T2-weighting. Images obtained with a sufficiently long TR and TE such that the CSF is more intense than brain tissue are regarded as T2-weighted images.

A typical edematous or cystic lesion has a longer T1 and longer T2 than brain. On T1-weighted images, these lesions will appear dark (i.e. will have negative contrast). On T2-weighted images they appear bright and will thus have positive contrast. If a short TR/long TE sequence is inadvertently chosen, the tendencies towards positive and negative lesion contrast will cancel and the lesion may not be detected. In general, the strongest signal is detected from those substances with the highest proton densities (high water content), shortest T1 times (rapid recovery) and longest T2 times (slowest decay). The high signal from short T1 substances, such as liquid cholesterol, fat, subacute hemorrhage, and gadolinium enhanced brain tumor is enhanced on short TR/short TE images. The high signal from long T2 substances such as mucus, late subacute hemorrhage, and CSF is enhanced on long TR/long TE spin echo images. The weakest MR signals come from tissues with low proton density, long T1 values (slow recovery), short T2 values (rapid decay), and rapidly flowing blood. Air, dense calcification, and cortical bone have low mobile hydrogen density. Short T2 substances such as acute hemorrhage and early subacute hemorrhage have low signal on long TR/long TE images.

To summarize: the spin echo MR signal is greatest when the T1 is short and the T2 and proton density are high; it is decreased if the T1 is long and the T2 and proton density are low. The differentiation of lesions from normal tissues can be enhanced if one is aware of the differences in the relaxation times and selects the TR and TE times accordingly [Bradley].

Appendix 2

Local-Binary-Pattern-and-Contrast Distribution Feature (LBP-C)

LBP-C Distribution feature had been successfully used to segment textural images by Ojala and Pietikäinen [1999] The authors had compared the LBP-C Distribution feature with other texture measuring features like Grey-Level difference method and Law's Texture [Laws, 1980] method and have found that the LBP-C Distribution performs comparatively well in discriminating different types of textures [Ojala and Pietikäinen, 1999]. According to the authors, the major advantage of the LBP-C feature is that LBP and C are complementary features (derived from the same 3×3 neighbourhood area of a image) and using the pair of features, a two-dimensional distribution of the feature could be constructed for a given mask size (moving the 3×3 window within the mask). To compare two regions in an image, the two dimensional distributions from each region are compared with one another. According to Ojala and Pietikäinen [1999] a single texture measure cannot provide enough information about the amount and spatial structure of local feature. Better discrimination of textures should be obtained by considering joint occurrences of two or more features. Since one is comparing a two-dimensional distribution the measure is more discriminatory.

The LBP feature is found as follows (Figure A2.1) [Ojala and Pietikäinen, 1999]:
For a 3×3 neighbourhood in a image, the original pixel values are thresholded with the value of the centre pixel. Each of the pixels in the 3×3 neighbourhood is given a binomial weight whose value ranges from 1 to 128. The values of the pixels in the thresholded neighbourhood are multiplied by the weights given to the corresponding pixels resulting in a set of eight values ranging from 1 to 128. Finally, the eight values are summed up to obtain the LBP, for the 3×3 neighbourhood. The LBP value ranges from 0 to 256.

The Contrast feature is found as follows (Figure A2.1) [Ojala and Pietikäinen, 1999]:
In the thresholded neighbourhood, the Contrast feature is found by computing the difference of the average grey level of those pixels which are larger or equal to the centre pixel value, and those which are less than the centre pixel value. The Contrast value could range from a negative of (Maximum Pixel Value in the Image - 1) to Maximum Pixel Value in the Image.

6	5	2
7	6	1
9	3	7

Image pixel values

1	0	0
1	✕	0
1	0	1

Thresholded values

$2^0=1$	$2^1=2$	$2^2=4$
$2^3=8$	✕	$2^4=16$
$2^5=32$	$2^6=64$	$2^7=128$

Weight Matrix

1	0	0
8	✕	0
32	0	128

Thresholded values convolved by the weight matrix

LBP = 1 + 8 + 32 + 128 = 169
(Sum of the convolved values)

C = [(6 + 7 + 9 + 7)/4 - (5 + 2 + 1 + 3)/4] = 4.5
(Difference between average pixel values
higher and lower than the center pixel value)
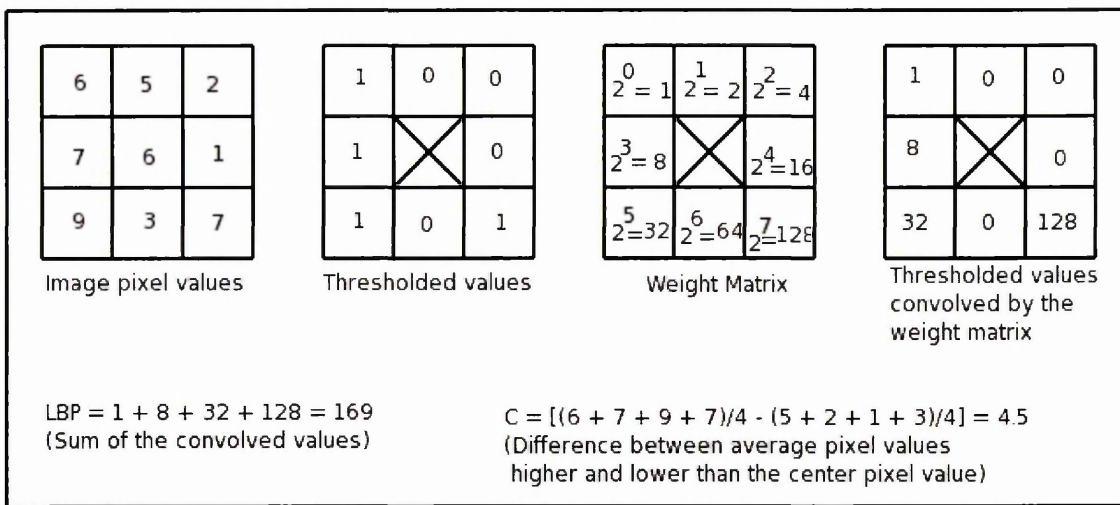
Figure A2.1
Local-Binary-Pattern and Contrast feature value calculation details for a sample 3×3
neighbourhood in a image.

To find the LBP-C Distribution the 3×3 neighbourhood is moved around a mask of given size (say 5x5) and for each overlapping position of the 3×3 neighbourhood the LBP-C pair is found and thus a LBP-C distribution is computed for the given mask size. The LBP/C distribution is approximated by a discrete two-dimensional histogram of size 256xb, where b is the number of bins for Contrast (C) [Ojala and Pietikäinen, 1999]. In their original paper Ojala and Pietikäinen [1999] had observed that choosing b is a trade-off between the discriminative power and the stability of the texture transform. If b is too small, the histogram will lack resolution and feature C will add very little discriminative information to the process. However, since the image region contains a finite number of pixels, it does not make sense to go to the other extreme, for then the histogram becomes sparse and unstable [Ojala and Pietikäinen, 1999]. The authors chose 8 bins for Contrast.

In this study, for the HCS based segmentation, the number of bins chosen were the actual number of possible Contrast values in the image as the value of b, (where b is the number of bins for Contrast) and this gives better results. And to compare the LBP/C distribution between two locations, in this study, the HCS process made use of the Bhattacharya measure [Aherne et al., 1997]. The Bhattacharya measure [Aherne et al., 1997] does not suffer from the problem of sparse histograms, unlike for Ojala and Pietikäinen [1999] who used the G-statistic [Sokal and Rohlf, 1987] for comparing the LBP/C distribution in their original work [Ojala and Pietikäinen, 1999].

Appendix 3

Correspondence from HSEG developer

From: James C. Tilton [tilton@backserv.gsfc.nasa.gov]

Sent: Mon 6/27/2005 3:51 PM

To: A.N.Selvan@shu.ac.uk

Subject: Follow-up on your questions

Dear Mr. Selvan,

I plan to release a new version of RHSEG by the end of this week, and would like to be sure your issues are addressed in the new version.

Would it be possible send me your experimental data, including ground truth? That way I can quickly determine the suitability of RHSEG for your application.

Thank you for your interest in RHSEG.

J. C. Tilton

From: James C. Tilton [tilton@backserv.gsfc.nasa.gov]

Sent: Wed 7/13/2005 10:51 PM

To: Selvan, Arul N

Subject: Re: Segmentation resuls regarding..

Attachments: NOTES.txt(1KB) Sheffield_University.tar.gz(1MB)

Dear Mr. Selvan,

Version 1.10 of my software will be released soon. I had promised to send you my results of processing your data as soon as Version 1.10 is released. I'm jumping the gun here by a couple days, but attached you will find my results.

You can probably view the results (after a fashion) with with your current version of HSEGViewer - but your current version of RHSEG will definitely NOT reproduce the results.

These results were produced using Version 1.10 of RHSEG and HSEGViewer, dated July 15, 2005.

I think you will see some very satisfactory segmentation results.

J. C. Tilton

Appendix 4

Neuroradiologist's evaluation

I have been going through all the processed images. My preliminary assessment is that the programme is able to pick up the abnormal area correctly on the T2 weighted scan (confirmed by the diffusion weighted scans). I would also like to mention that the signal changes seen on the T2 weighted scan, would be missed by most physicians and possibly neuroradiologists.

My concerns at this stage are

1. *Is the programme consistent. To answer this you could analysing the same area again*

2. *Is the programme picking up noise and by chance it is in the same location as the lesion. This could be checked by running the programme on other examples of similar lesions and by increasing the size of the area evaluated.*

CT is the primary imaging modality for the imaging of hyperacute stroke. CT scans in the hyperacute stage (less than three hours) are mostly normal or show very subtle changes. The treatment for strokes needs to be started in the hyperacute stage and therefore any process that can help identify a lesion would be very useful.

Going by the results so far on the T2, I would suggest running the programme on an example of CT scan of a hyperacute stroke. The example I have sent show no detectable abnormality.

References

1. Aherne, F. J., Thacker, A. N. and Rockett, I. P., 1997, "The Bhattacharya Metric as an Absolute Similarity Measure for Frequency Coded Data" Kybernetika Volume 32 Number 4, Pages 001-007.

2. Albertyn, L. E. and Brown, R. V., 1996, "Interpreting CT Head Scans A basic guide to image analysis". Churchill Livingstone, Medical division of Pearson Professional Limited New York First Edition.

3. Barnes, J. E., 1991, "Characteristics and control of contrast in CT", RadioGraphics, 12: 825–837.

4. Barton Medical Imaging http://www.bartron.ws/ (accessed June 1, 2007).

5. Beaulieu, J. and Goldberg, M., 1989, "Hierarchy in picture segmentation: A stepwise optimization approach", IEEE Transactions on Pattern Analysis and Machine Intelligence, Vol. 11, No. 2, Pages. 150-163.

6. Bhattacharya, U., Chaudhuri B. B., Parui S. K., 1997, "An MLP-based texture segmentation method without selecting a feature set" Image and Vision Computing 15 937-948.

7. Bihan, D. L., Mangin, J., Poupon, C., Clark, C., Pappata, S., Molko, N. and Chabriat, H., 2001, "Diffusion Tensor Imaging: Concepts and Applications", Journal of Magnetic Resonance Imaging, 13:534-546.

8. Bradley, G. W., "Fundamentals of MRI Part II", http://e-radiography.net/mrict/mri%20ct.htm.fundmri_2.htm (accessed May 27, 2007).

9. Brandt, E. M., Bohan, P. T., Kramer, A. L. and Fletcher, M. J., 1994, "Estimation of CSF, white and Gray Matter Volumes in Hydrocephalic children using Fuzzy Clustering of MR Images" Computerized Medical Imaging and Graphics, Vol. 18, No. 1 Pages 25-34.

10. Brink, J. A., 1999, "Liver Window Settings at Hepatic CT: Added Value or Marginal Cost?" Radiology 210, Pages 593-594.

11. Brown, R. G., 2004, "Engineering a Beowulf-style Compute Cluster", http://www.phy.duke.edu/~rgb/Beowulf/beowulf_book/beowulf_book/node1.html (accessed June 01, 2007)

12. Chabat, F., Y., Guang-Zhong and Hansell, M. D., 2003, "Obstructive Lung Diseases: Texture Classification for Differentiation at CT" Radiology, 228:871-877

13. Culebras, A; Kase, C. S; Masdeu, J. C; Fox, A. J; Bryan, R. N; Grossman, C. B; Lee, D. H; Adams, H. P; Thies, W; 1997, "Practice Guidelines for the Use of Imaging in Transient Ischemic Attacks and Acute Stroke - A Report of the Stroke Council, American Heart Association" Stroke, 28:1480-1497.

14. Faulkner, Wm., "Basic Principles of MRI",
http://e-radiography.net/mrict/Basic_MR.pdf (accessed May 27, 2007).

15. Fayad, L; Jin, Y.; Laine, A.F.; Berkmen, Y.; Pearson, G.; Freedman, B.; Van Heertum, R.; 2002 "Chest CT Window Settings with Multiscale Adaptive Histogram Equalization: Pilot Study", Radiology, 223(3),pp 845-852.

16. Frackowiak, R. S. J.; Ashburner, J. T.; Penny, W. D.; Zeki, S.; Friston, K. J.; Frith, C. D.; Dolan, R. J.; Price, C. J., 2003, "Human Brain Function", Academic Press, second edition.

17. Freixenet, J.; MuÜnoz, X.; Raba, D.; Mart, J.; and Cufi, X., 2002, "Yet Another Survey on Image Segmentation: Region and Boundary Information Integration" ECCV 2002, LNCS 2352, Pages 408 422, Springer- Berlin Heidelberg.

18. Fu, K. S.and Mui, J. K., 1981 "A survey on image segmentation", Pattern Recognition, Vol 13, Pages 3-16.

19. Gokcay, E. and Principe, C. J., 2002, "Information Theoretic Clustering" IEEE Transactions on Pattern and Machine Intelligence, Vol. 24, No. 2.

20. Gomori, J. M. and Steiner, I., 1987, "Non-linear CT windows", Computerized Radiology 11:21–27

21. Gonsalez, R. C, Richard, E. W., 1992, "Digital Image Processing", Addison Wesley.

22. Haralick, R. M., Shanmugam, K., Dinstein, I., 1973, "Tetural Features for Image Classification", IEEE Transactions in Systems, Man, and Cybernetics, Vol. SMC-3, No. 6, Pages 610-621.

23. Haralick, R. M., Shapiro, L., 1985, "Image Segmentation Techniques", Computer Vision, Graphics and Image Processing, 29, Pages 100-132.

24. Jin, Y., Laine, A. F., Berkmen, Y. M., *et al.* 2002, "Chest CT Window Settings with Multiscale Adaptive Histogram Equalization: Pilot Study", Radiology 223, Pages 845-852.

25. Johnson, C. D. 2003, "Hard- versus Soft-Copy Interpretation", Radiology 227, Pages 629-630.

26. Kaste, M.; 2004 "Reborn Workhorse, CT, Pulls the Wagon Toward Thrombolysis

Beyond 3 Hours", Stroke 35:357.

27. Kervrann, C. and Heitz, F. 1995, "A Markov Random Field Model-Based Approach to Unsupervised Texture Segmentation Using Local and Global Spatial Statistics", IEEE Transactions on Image Processing vol. 4. No 6.

28. László, N. G., Udupa, J. K. and Zhang, X. 2000, "New Variants of a Method of MRI Scale Standardization", IEEE Transactions on Medical Imaging Vol. 19, No. 2.

29. Laughlin, S. "Central nervous system imaging When is CT more appropriate than MRI?", 1998, Postgraduate Medicine, Vol. 104, N. 5.

30. Legendre, P. and Legendre, L., 2003, "Numerical Ecology". ISBN 0-444-89250-8 Elsevier.

31. Lev, M. H., Farkas, J., Gemmete, J. J. *et al.,* 1999, "Acute Stroke: Improved Nonenhanced CT Detection- Benefits of Soft-Copy Interpretation by using variable window width and center level settings", Radiology 213, Pages 150-155

32. Le Bihan, D., ois Mangin, J., Poupon, C., Clark, A. C., Pappata, S.; Molko, N. and Chabriat, H., 2001, "Diffusion Tensor Imaging: Concepts and Applications", Journal of Magnetic Resonance Imaging 13:534-546.

33. Le Bihan, D., Poupon, C., Amadon, A., Lethimonnier, F., 2006, "Artifacts and pitfalls in diffusion MRI," Journal of Magnetic Resonance Imaging Vol. 24, Issue 3, Pages 478 – 488.

34. Macovski, A., 1996,"Noise in MRI", Magnetic Resonance in Medicine, 36(3):494-7.

35. Makkat, S., Stadnik, T., Osteaux, M., 2003, "CT and MRI of Stroke: A Brief Review" Calicut Medical Journal; 1(1):e2.

36. Mayo-Smith, W. W., Gupta, H., Ridlen, M. S. *et al.,* 1999, "Detecting Hepatic Lesions: The Added Utility of CT Liver Window Settings", Radiology 210, Pages 601-604.

37. Miller, J. C., 2004, "CT and MR Imaging for Evaluation of Acute Stroke", Radiology Rounds, Vol. 2, Issue 10 October.

38. Mir, A. H., Hanmandu, M., Tandon, S. N., 1995 "Texture Analysis of CT Images" IEEE Engineering in Medicine and Biology Pages 781-786.

39. Moseley, M. E,. Cohen, Y., Mintorovitch, J., 1990, "Early detection of regional cerebral ischemic injury in cats: evaluation of diffusion and T2-weighted MRI and spectroscopy" Magnetic Resonance Medicine 14:330-346.

40. Nadler, M. and Smith, E. P., 1993 "Pattern Recognition Engineering" John Wiley and Sons inc.

41. Nichols, B.; Buttlar, D. and Farrell, J. P., 1996 "Pthreads Programming" O'Reilly & Associates, inc.

42. Nickels, M. K. and Hutchinson, S., 1997, "Texture image segmentation : returning multiple solutions" Image and Vision Computing 15 781-795.

43. Ojala, T., Pietikäinen, M. and Harwood, D., 1996, "A Comparative Study of Texture Measures with Classification Based on Feature Distributions". Pattern Recognition Vol. 29. No. 1. Pages 51-59.

44. Ojala, T.; Pietikäinen, M. 1999 "Unsupervised Texture Segmentation using Feature Distributions", Pattern Recognition 32 477-486.

45. Pal, N.; Pal, S., 1993 "A review on image segmentation techniques.," Pattern Recognition 26 1277-1294.

46. Parizel P. M, Makkat S., Van Miert E., Van Goethem J. W., van den Hauwe L, De Schepper A. M., 2001, "Intracranial hemorrhage: principles of CT and MRI interpretation" Eur Radiol; 11:1770-1783.

47. Press, W. H., Teukolsky, Saul A., Vetterling, W. T., Flannery, B. P., 2002, "Numerical Recipes in C The Art of Scientific Computing", Second Edition Cambridge university press.

48. Randen, T. and Husoy, J. H., 1999, "Filtering for Texture Classification: A Comparitive Study" IEEE Transactions on Pattern Analysis and Machine Intelligence, Vol. 21, No. 4.

49. Roccatagliata, L., Lev, M., Mehta, N., Koroshetz, W., Gonzalez, R., Schaefer, P., 2003, "Estimating the Size of Ischemic Regions on CT Perfusion Maps in Acute Stroke: Is Freehand Visual Segmentation Sufficient?" Radiological Society of North America, Scientific Papers.

50. Sankur B. and Sezgin M., 2004, "A survey over image thresholding techniques and quantitative performance evaluation" Journal of Electronic Imaging, 13(1): 146-165.

51. Sokal, R. R and Rohlf, F. J., 1987. "Introduction To Biostatistics" W.H. Freeman and company.

52. Sonka, M. and Fitzpatrick, J. M., 2000, "Handbook of Medical Imaging Volume 2 Medical Image Processing and Analysis", Published by SPIE-The international society for optical engineering.

53. Sonka, M.; Hlavac, V. and Boyle, R., 1993 "Image Processing, Analysis and Machine Vision", International Thompson Computer Press.

54. Sorensen, A. G., Buonanno, F. S., Gonzalez, R. G. *et al.*, 1996, "Hyperacute stroke: evaluation with combined multisection diffusion-weighted and hemodynamically weighted echo-planar MR imaging" Radiology; 199(2):391-401.

55. Suri, J. S., Setarehdan, K. S. and Singh, S., 2002, "Advanced Algorithmatic Approaches to Medical Image Segmenation" Springer-Verlag London Limited.

56. Tabb, M. T. and Ahuja, N., 1997, "Multiscale Image Segmentation by Integrated Edge and Region Detection" IEEE Transactions on Image Processing Vol. 6. No 5.

57. Tilton, J. C., 1999, "A Recursive PVM Implementation of an Image Segmentation Algorithm with Performance Results Comparing the HIVE and the Cray T3E," frontiers, Page 146, The 7th Symposium on the Frontiers of Massively Parallel Computation.

58. Tilton, J. C., 2003, "Hierarchical Image Segmentation" Online Journal of Space Communication Issue No. 3 Winter 2003 Research and Applications

59. Tilton, J. C. "Method for recursive hierarchical segmentation by region Growing and spectral clustering with a natural convergence criterion", Disclosure of Invention and New Technology: NASA Case No. GSC 14,328-1.

60. Turner, R., Le, B. D., Maier, J, *et al.*1990, "Echo-planar imaging of intravoxel incoherent motions," Radiology 177:407-414.

61. Warach S, Gaa J, Siewert B, *et al.*, 1995, "Acute human stroke studied by whole brain echo planar diffusion-weighted magnetic resonance imaging" Ann Neurol 37(2):231-41.

62. Warach, S. 2001 "Use of Diffusion and Perfusion Magnetic Resonance Imaging as a Tool in Acute Stroke Clinical Trials" Current Control Trials Cardiovascular Medicine 2:38-44.

63. Warfield, S. K., Westin, C, Guttmann, C. R. G., Albert, M., Jolesz, F. A. and Kikinis, R., 1999, "Fractional Segmentation of White Matter", Lecture Notes In Computer Science; Vol. 1679, Proceedings of the Second International Conference on Medical Image Computing and Computer-Assisted Intervention, Pages: 62 - 71.

64. Webb, A. R. 2002 "Statistical Pattern Recognition" Pages 278 – 283 John Wiley

and & Sons Ltd.

65. Zhang, J and Tan, T; 2002 "Brief review of invariant texture analysis methods" Pattern Recognition 35 735-747.

66. Zucker, S. W., 1976, "Region growing: Childhood and adolescence" Computer Graphics and Image Processing, Vol. 5, Pages 382-399.